Spring 2016

Enhanced bioactive scaffolds for bone tissue regeneration

Sonali Karnik

ENHANCED BIOACTIVE SCAFFOLDS FOR BONE TISSUE REGENERATION

by

Sonali Karnik M. Sc., M. S.

A Dissertation Presented in Partial Fulfillment
of the Requirements of the Degree
Doctor of Philosophy

COLLEGE OF ENGINEERING AND SCIENCES
LOUISIANA TECH UNIVERSITY

May 2016

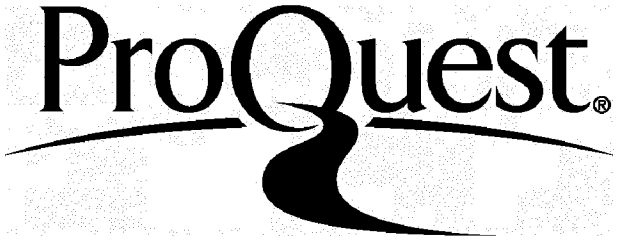

LOUISIANA TECH UNIVERSITY

THE GRADUATE SCHOOL

11/12/2015
Date

We hereby recommend that the dissertation prepared under our supervision by Sonali Karnik

entitled Enhanced Bioactive Scaffolds for Bone Tissue Regeneration

be accepted in partial fulfillment of the requirements for the Degree of Doctorate in Biomedical Engineering

David K Mills
Supervisor of Dissertation Research

Steve Day
Head of Department
BIOMEDICAL ENGINEERING
Department

Recommendation concurred in:

Advisory Committee

Approved:
Director of Graduate Studies

Approved:
Dean of the Graduate School

Hisham Hegab ISD
Dean of the College

GS Form 13a
(6/07)

ABSTRACT

Bone injuries are commonly termed as fractures and they vary in their severity and causes. If the fracture is severe and there is loss of bone, implant surgery is prescribed. The response to the implant depends on the patient's physiology and implant material. Sometimes, the compromised physiology and undesired implant reactions lead to post-surgical complications. [4, 5, 20, 28] Efforts have been directed towards the development of efficient implant materials to tackle the problem of post-surgical implant failure. [15, 19, 24, 28, 32]

The field of tissue engineering and regenerative medicine involves the use of cells to form a new tissue on bio-absorbable or inert scaffolds. [2, 32] One of the applications of this field is to regenerate the damaged or lost bone by using stem cells or osteoprogenitor cells on scaffolds that can integrate in the host tissue without causing any harmful side effects. [2, 32] A variety of natural, synthetic materials and their combinations have been used to regenerate the damaged bone tissue. [2, 19, 30, 32, 43]

Growth factors have been supplied to progenitor cells to trigger a sequence of metabolic pathways leading to cellular proliferation, differentiation and to enhance their functionality. [56, 57] The challenge persists to supply these proteins, in the range of nano or even picograms, and in a sustained fashion over a period of time. A delivery system has yet to be developed that would mimic the body's inherent mechanism of

delivering the growth factor molecules in the required amount to the target organ or tissue.

Titanium is the most preferred metal for orthopedic and orthodontic implants. [28, 46, 48] Even though it has better osteogenic properties as compared to other metals and alloys, it still has drawbacks like poor integration into the surrounding host tissue leading to bone resorption and implant failure. [20, 28, 35] It also faces the problem of post-surgical infections that contributes to the implant failure. [26, 37]

The focus of this dissertation was to design and develop novel implant materials for coating titanium to improve its biological properties. These natural and/or semi-synthetic materials improved cellular adhesion, biological response to the scaffolds and prevented growth of bacteria when they were enhanced with growth factor and anti-infective loaded nanotubes. The implant materials showed promise when tested *in vitro* for cell proliferation, differentiation and bacterial growth inhibition.

APPROVAL FOR SCHOLARLY DISSEMINATION

The author grants to the Prescott Memorial Library of Louisiana Tech University the right to reproduce, by appropriate methods, upon request, any or all portions of this Dissertation. It is understood that "proper request" consists of the agreement, on the part of the requesting party, that said reproduction is for his personal use and that subsequent reproduction will not occur without written approval of the author of this Dissertation. Further, any portions of the Dissertation used in books, papers, and other works must be appropriately referenced to this Dissertation.

Finally, the author of this Dissertation reserves the right to publish freely, in the literature, at any time, any or all portions of this Dissertation.

Author Sylvania

Date 05/02/2016

DEDICATION

This dissertation is dedicated to my father, Late Mr. Jayant Karnik, whose faith in my dream to be a researcher has been a pillar of strength so far. It is also dedicated to my maternal uncle, Mr. Dilip Tamhane, who encouraged my curious nature and love of science. Lastly and most importantly, to my mother, Mrs. Sushama J. Karnik, whose support and love has been a driving force in my life.

TABLE OF CONTENTS

LIST OF TABLES

LIST OF FIGURES

ACKNOWLEDGEMENTS

I would like to express my immense gratitude towards my mentor and guide, Dr. David K. Mills, for defining my doctoral dissertation. I thank him for his constant support, encouragement and guidance throughout my doctoral degree. Working under his guidance has helped me learn a lot on both professional and academic levels. I would also like to thank my advisory committee members Drs. Mark DeCoster, Steven Jones, Jamie Newman, and Teresa Murray for their help during my ongoing research. I would like to mention Dr. Alfred Gunasekaran for his timely help in electron microscopy imaging and Dr. Rebecca Giorno for her assistance in bacterial studies. I wish to thank Dr. James Spaulding for training me in tissue embedding and sectioning techniques and Dr. Sven Eklund for his support and expertise in conducting anodization experiments on titanium.

I would like to mention here my heartfelt thanks to my fellow lab members and friends, especially Miss Yangyang Luo, Mr. Udaybhanu Murthy Jammalamadaka, and Mr. Karthik Tappa for helping and supporting me throughout the projects and testing times. I would like to thank Miss Bharati Belwalkar for her help in statistical analyses for the projects and the resulting manuscripts. I would like to mention my special thanks to Mr. Reid Grimes for his help and expertise in anodization of titanium and to Mr. Chris Boyer, Mr. Jeff Ambrose, Dr. Jeff Weisman, and Mr. Lin Sun with whom I conducted the combined studies for the scaffolds and other project collaborations.

I would also like to acknowledge all the professors who helped me gain knowledge during the course of Master's and Doctoral degrees and my friends from Louisiana Tech University who are a family to me.

CHAPTER 1

INTRODUCTION AND BACKGROUND

The National Ambulatory Medical Care Survey and the American Academy of Orthopedic Surgeons estimate that in the United States annually over 6.8 million cases of bone injuries are brought to medical attention. [4, 5] The cause of these bone injuries varies from trauma in young individuals to osteoporosis or a combination of both in old aged patients. [17] Depending upon the severity of the injury and the patient's physiological condition, the treatment can vary from immobilizing the bone in a cast or surgical implants. [17] Response to the treatments, especially in case of implants, varies depending upon the patient physiology and the type of implant material. Most of the implant materials available commercially have some drawbacks and can cause painful complications in the patients post-surgery.

The field of orthopedic and orthodontic tissue engineering and regenerative medicine directs its efforts to develop novel materials that can be used to improve the implant materials. In order to design better implants and develop improved scaffolds, we need to understand bone injuries, bone regeneration, the current treatments and their drawbacks. The following sections in this chapter explain in detail the skeletal system, anatomy and physiology of bone and summarize the current treatments and their limitations.

1.1 Skeletal Tissue System and Bone

Skeletal tissues are involved with the prime purpose of providing support to the body, protection to the vital organs, and locomotion. This is achieved by well-coordinated and concerted actions of various tissues within the skeletal and nervous system. The major components of the skeletal tissue system are bones, muscles, cartilage, ligaments and tendons. The following subsections explain bone anatomy, the types of bone, and its cellular components.

1.1.1 Bone

Bone is a connective tissue consisting of organic and inorganic components. The organic components of bone include an extracellular matrix and three types of cells; osteoblasts, osteocytes and osteoclasts. The inorganic part of the bone consists of minerals including calcium, phosphorous and magnesium which act as the body's reservoir of these salts. Bone has a vascular supply in the form of a network of arteries, veins and capillaries as well as lymphatic vessels. Bone also contains marrow in its stroma or inner hollow space which is a reservoir of stem cells that houses hemopoeitic cells as well as skeletal tissue cells. [21, 34, 44] Bone is a rigid organ but is also dynamic in nature and is able to regenerate as old bone disintegrates and a new one is formed. The mechanism of constantly replacing old bone with a new one is achieved by bone progenitor cells, and osteoblasts which lay new foundations and the old bone is resorbed by bone resorptive cells, called osteoclasts. Osteoclasts release metalloproteases which digest the old bone minerals in the matrix, giving way to new bone formation. [23, 47] Figure 1-1 shows bone anatomy in detail.

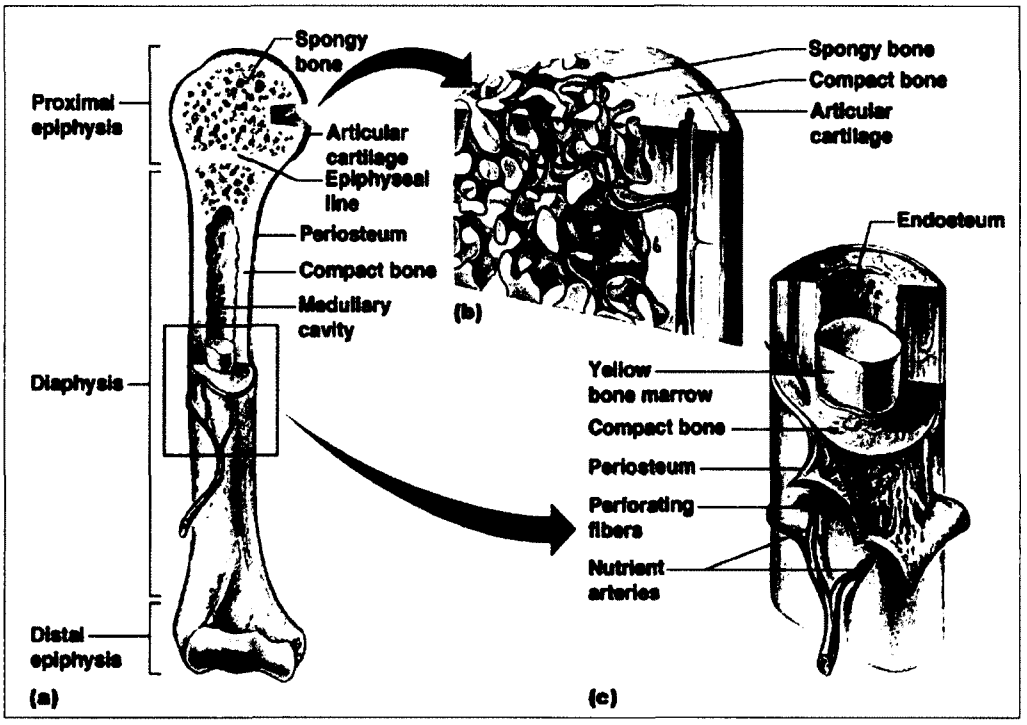

Figure 1-1. Graphical Representation of the Bone Anatomy. [18]

1.1.2 Types of Bones

Based on the length, bones can be classified into five types: long, short, flat, sesamoid and irregular. The characteristics and examples of the five types are as follows:

1. Long Bone: Long bones have a shaft which is longer in length than width. The articular surfaces of the long bones (epiphyses) are rounded and covered mostly with articular cartilage. The middle long and slender region (diaphyses) is made up of compact bone. However, the rounded articulating part is made of spongy, cancellous bone, e.g. femur, humerus and tibia. [21, 23, 34 , 44, 47]
2. Short Bone: Short bones can be said to have a cubic shape and have mostly spongy bone surrounded by a thin layer of compact bone. Examples of short bones are the small bones of ankles and wrists. [21, 23, 34 , 44, 47]

3. Flat Bone: Flat bones are curved and thin. They consist of two layers of thin compact bone and a thin layer of spongy bone in between. They are found in the skull and sternum. [21, 23, 34 , 44, 47]
4. Sesamoid Bone: Bones embedded in tendons are called sesamoid bones and are found in the articular joints like the knee joint. They resemble short bones in their shape and carry out the function of holding the tendon away from the bone and increasing the muscle leverage. An example of the sesamoid bone is the patella in the knee joint. [21, 23, 34 , 44, 47]
5. Irregular Bone: Any bone not fitting into the above categories is classified as irregular bone. As the name suggests, these bones have irregular shapes. They are spongy bones surrounded by a thin mass of compact bone and are found in the vertebral column, pelvic girdle and in the skull. [21, 23, 34 , 44, 47]

1.1.3 Cellular Components of Bones

Bone consists of three types of cells: osteoblasts, osteocytes, and osteoclasts. These cells originate in the bone marrow present in the medullary cavity. [16, 23, 47]

1. Osteoblasts: Osteoblasts, like other skeletal tissue cells, are derived from the mesenchymal stem cells present in the bone marrow. They are also called bone progenitor cells as they form the new bone matrix. A variety of growth factors play in concert with each other to differentiate the osteoblasts and secretion of bone matrix. [16, 23, 47]
2. Osteocytes: Osteoblasts on maturation are called osteocytes. These cells are metabolically less active than osteoblasts but help maintain the bone matrix. They are found in small cavities in the bone mineral matrix secreted by them,

called lacunae and form a network of cytoplasmic processes called canaliculi. [16, 23,47]

3. Osteoclasts: Osteoclasts are large motile macrophages present in the bone matrix and are involved in resorption of old bone matrix. Osteoclasts originate from the hematopoietic stem cells like other macrophages, have a monocytic lineage and inherit the property of phagocytosis. They play an important role in calcium homeostasis. [16, 23,47]

1.2 Bone Injuries and Tissue Repair

Bone injuries are generally called fractures and have various causes. [23, 47, 51] Bone can fracture due to high impact or stress as in the case of trauma or a low impact or stress as in cases of osteoporosis, bone cancer, and osteogenesis imperfecta. [9, 23, 47, 51] When bone fracture is caused due to pathological causes such as cancer, osteoporosis, or osteogenesis imperfecta; it is termed a pathological fracture.

The tissue repair and regeneration process in bone depends on the patient's physiological condition and age. [9, 51] Disorders like diabetes mellitus, osteoarthritis, and other pathologies complicate and delay the process of tissue repair. [9, 51] Bone healing is also slow in older patients as compared to younger patients. [9, 51]

Tissue repair in bone involves a sequence of events that uses stem cells, osteoprogenitor cells and various molecular triggers responsible for stimulating migration of these cells and their differentiation. The events of bone tissue repair can be summarized as follows and are depicted pictorially in Figure 1-2:

1. Reactive phase (Hematoma formation): Initial inflammatory response and secretion of cytokines and growth factors. The secretion of cytokines and growth factors signal the progenitor cells to migrate to the site of injury.
2. Reparative phase (Soft and Hard Callus formation): Proliferation of the progenitor cells that will replace the damaged tissue.
3. Remodeling phase: Differentiation of proliferated progenitor cells forming a new tissue that will be functional just like the old tissue. [9, 16, 47, 51]

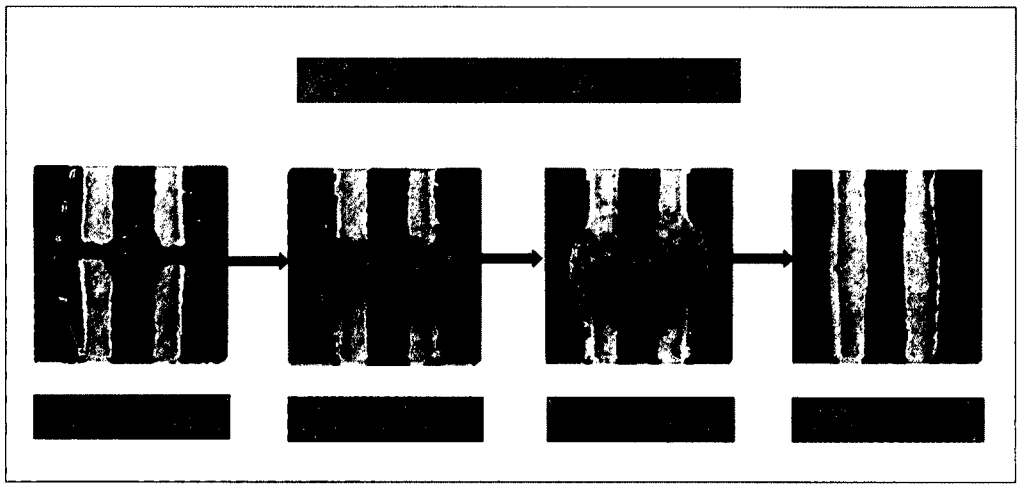

Figure 1-2. Graphical Representation of Phases of Bone Healing. [3]

1.3 Current Treatment Modalities

A variety of treatment modalities are used to assist the natural repair and regeneration response of the body. In cases where the response is hindered due to patients' physiological state or complexity of the injury, natural or artificial implants are used. The treatment also involves use of pain killers, physiotherapeutics and other assistive drugs. [14]

In severe cases of fractures where the gap between the broken bones is large and the bone structure becomes unstable, surgery is prescribed to stabilize the bones. Metal implants (titanium plates and/or screws) are used to hold the bones in place. [14, 51] In extreme trauma, compromised physiological condition and/ or old age, the surgery can be a complicated procedure and healing can be problematic. [51] For convenience, the implant materials discussed in this dissertation are broadly categorized as having a biological and non-biological origin. The implant materials and their limitations are described in the sections below.

1.3.1 Biological Implants

The implants that are derived from biological materials or are composed of biological materials are categorized as biological implants. These types of implants include biological tissues, decellularized tissue matrix, and materials isolated and purified from the tissues of organisms. [36, 46] Focusing on the orthopedic and orthodontic implants, the biological orthopedic and orthodontic implants are bone grafts. Depending on the origin of bone grafts, they are further categorized into autografts and allografts.

1.3.1.1 *Autografts.* Autografts are derived from the same individual who needs the implant. [46] The bone is usually taken from the iliac crest, spine, or ribs. The process of surgically removing the graft from a healthy donor site is called harvesting. This type of implant procedure is performed in the spine fusion surgery. [46] Autograft poses risks such as donor site morbidity, infection, chronic pain at the site of harvesting, and nerve injury during the harvesting procedure. [33, 46] Bone autografts are employed less in recent times due to development of better alternative methods. [15, 56]

1.3.1.2 *Allografts.* Allografts are harvested from cadavers by a tissue bank. Allografts have drawbacks such as lower chances of bone fusion, risk of disease transmission, and undesirable immune response to the graft by the host tissue. [15, 56]

1.3.2 Non-Biological Implants

The implants that are composed of materials having synthetic, inorganic or non-biological origin are categorized as non-biological implants. The non-biological orthopedic and orthodontic implants are metal implants and polymer implants. Their nature and limitations are described in detail below.

1.3.2.1 *Metal implants.* The most commonly used metals or metal alloys for implants are stainless steel, vitallium (cobalt – chromium alloy), and titanium. [28] Due to corrosion after implantation, stainless steel has been replaced by vitallium and titanium. [28] In the recent years, titanium has become a popular choice as metal implant material. Titanium implants are made of either pure titanium or as an alloy of titanium with vanadium and aluminum.

While titanium as an implant material has virtues such as good osteointegration compared to other metals, is less corrosive because of the oxide layer forming on the surface of the metal, and produces less scatter during Computational Tomography Scan (CT Scan) and Magnetic Resonance Imaging (MRI), recently it has been linked with undesirable immune response in some patients. [53] Titanium implants also have high failure rates due to post-surgical infections. [49]

1.3.2.2 *Polymer implants.* Polymer implants are used widely for both bone and soft tissue reconstruction. [19] Polymers are long chains of repeating monomers forming macromolecules attaining high molecular weights. The most commonly used

biomaterial polymers are polymethylmethacrylate, silicone, polyethylene, polypropylene, nylon, and poly-ε-caprolactone. [19]

Silastic implants (elastic silicone implants) have severe side effects like capsule formation and contracture. [19, 43] Silicone implants in arthroplasty cause silicone synovitis. [43] Complications related to polymethylmethacrylate are cause by the high setting temperatures and an exothermic reaction, which leads to bone necrosis. Polymethylmethacrylate can also cause tissue toxicity due to the presence of unbound monomer, methyl methacrylate. [27] Other polymer materials lack the tensile and compressive strength of the natural tissue and do not integrate well with the tissue. [30]

1.4 Clinical Need for Improved Implant Materials

Drawbacks in commercially available metal implant materials range from mild immune reactions, such as allergies, to more severe consequences, such as bone resorption. [49, 53] Commercially available polymers need significant improvements with respect to their tissue integration potential and mechanical properties. [27, 30, 43]

Implant materials are needed that are tissue integrative, biodegradable, immunocompatible, and similar in mechanical properties to the natural tissue. These implants should help the regeneration of the damaged tissue and should either exist in the body inertly after the healing process is complete or should be resorbed in the body as non-toxic or excreted out.

CHAPTER 2

TISSUE ENGINEERING AND ENHANCED MATERIALS IN REGENERATIVE MEDICINE

Tissue engineering is an emerging field that combines the use of cells, engineering, and materials along with suitable biochemical and physicochemical cues to improve or replace the biological functions. [32] Natural tissues require a specific biological and mechanical structure to perform their regular functions. Due to either injury or organic failure the natural tissue might lose its structural integrity and fail to perform its natural function. [32] Tissue engineering attempts to regenerate the damaged tissue and restore its functionality.

The term regenerative medicine even though used in relation to tissue engineering is focused on the use of the stem cells or progenitor cells to repair or replace the damaged tissue. [2, 32] The damaged tissue is repaired using a scaffold based approach. [2, 32] A suitable biomaterial is selected and seeded with either differentiated cells, stem cells or progenitor cells. These cells are guided by mechanical and /or biochemical signals. Once the cells adhere to and populate the scaffold under the influence of mechanical andor biochemical signals, they differentiate and produce the extracellular matrix. Depending on the type of the cells and tissue, the cells will produce the marker molecules and regenerate the damaged tissue. [2, 32, 54]

Bone injuries, as discussed in the earlier chapter, are commonly referred to as fractures. Depending upon the severity of the injury and patient physiology, the treatment may involve simple and common procedures like immobilization of the bone by application of casts or surgical procedures to fix the bone internally using metal plates and screws. [4, 5, 17] Commercially available materials used for the fixative and reparative bone surgeries have drawbacks that are discussed in detail in the previous chapter. [24] Recent advances in the field of tissue engineering and regenerative medicine have made it possible to design bioactive polymers that bridge the gap between natural tissue and artificial implant materials. [2, 32, 54] These polymers can be either of natural, synthetic or composite in origin. By applying engineering principles and modifying the material properties of these implant materials we can incorporate bioactive molecules in their mesh networks. [54] This approach can be used for *in situ* delivery of the bioactive molecules reducing the risks to other systemic organs.

Depending on their design and the placement of the cells, the enhanced and engineered biomaterials can then be used either as an assistive tool for the body's natural regenerative process to accelerate the healing of injury, or to compensate for the loss of regenerative potential due to compromised physiology. These biomaterials can also be used to improve the performance of the implants. The biomaterials should have good osteointegration and osteoconduction for the implant to succeed. These materials also should possess mechanical strength comparable to the native tissue.

Most of the polymers that are used for bone tissue regeneration lack material strength and the metal implants lack the porosity and osteointegrative properties. If the polymer composites are used in combination with metal implants, both the materials can

compensate for the missing properties. Addition of nanoparticles for sustained delivery of bioactive molecules and surface modification can make the bioengineered scaffolds desirable to the cells. With modified surface properties and secretion of bioactive molecules the new nanoenhanced composites hold promise to fulfill at least some of the important criteria of good implant materials.

2.1 Rationale Behind the Three Integrated Projects

This chapter describes the three integrated and interrelated projects that focus on the repair of the damaged bone tissue by applying principles of tissue engineering and regenerative medicine. The interrelated projects make use of the enhanced bioactive scaffolds as a base or a template for the progenitor cells to lay a foundation of new tissue to replace the damaged bone tissue. In these projects, hydrogels were made from natural organic and inorganic substances through polymer crosslinking. These hydrogels enhanced with nanoparticles were used as *in situ* delivery vehicles for the bioactive molecules.

The nanoparticles, namely halloysites, would contain the bioactive molecule of choice. Since the bioactive molecules would be contained inside the nanoparticles and hydrogels would hold the nanoparticles in their mesh network, the release would be sustained and extended when compared to the release from the hydrogels alone. With this scheme of design, the hydrogels can be modified for their function by changing the bioactive molecule loaded inside the halloysites.

If the progenitor cells are the target, growth factors like BMP 2, 4, and 6 can be used to improve the cellular response of the cells encapsulated in the hydrogel mesh

network. This design can be used to deliver cells with a package of boosters for differentiation at the site of injury.

The construct with the progenitor cells encapsulated in the hydrogels would aid the damaged tissue which might have lost its potential for repair if the body has compromised physiology. If the objective is to attract the stem and progenitor cells to the site of injury, the hydrogels enhanced with growth factor loaded halloysites can be used. The secreted growth factors would act as a biochemical signal to attract the cells to the site of injury. The nanoenhanced hydrogels can be used to coat the surface of metal implants especially titanium, to improve cellular response, integration into host tissue, and to prevent microbial growth on the implant surface. The titanium metal surface can be modified by anodization to increase its surface roughness and to improve the osteogenic response. Figure 2-1 illustrates the rationale behind the three interrelated projects. Sections 2.2, 2.3, and 2.4 describe the projects in detail.

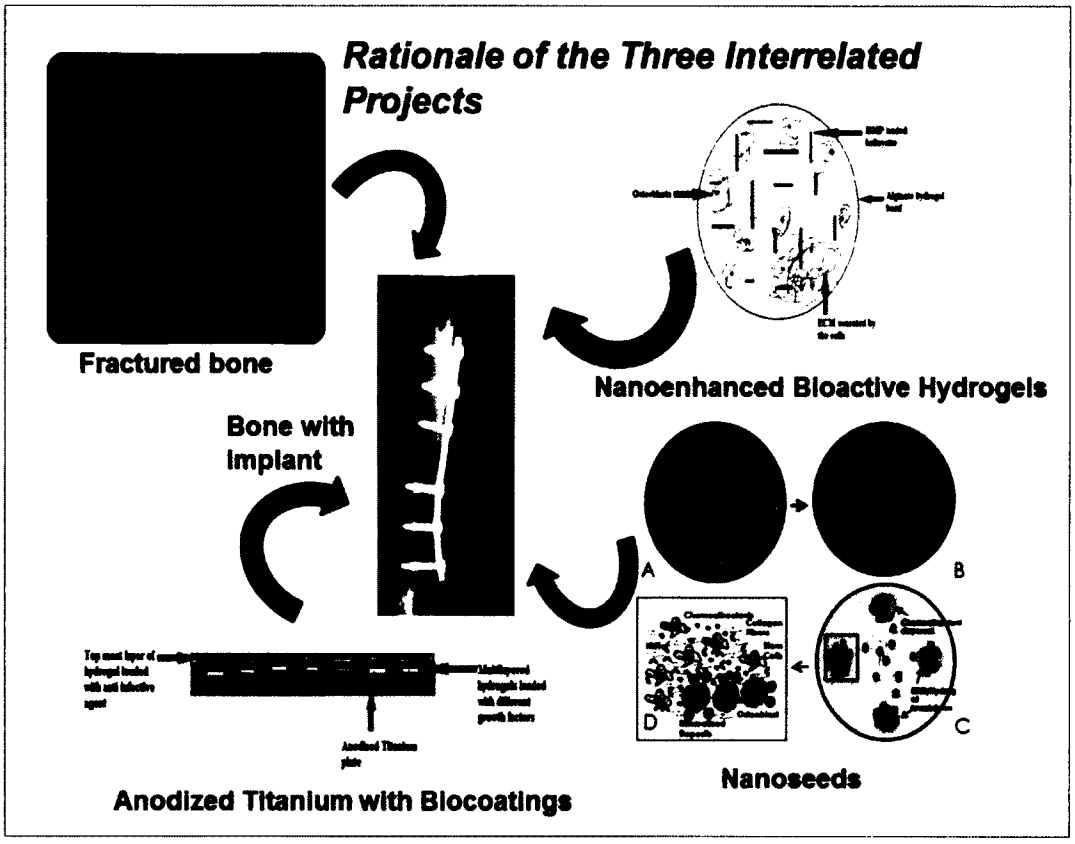

Figure 2-1. Graphical representation of the rationale behind the three interrelated projects. [10, 11]

2.2 Nanoenhanced Bioactive Hydrogels

The term hydrogel was used in 1894 for the first time in literature. [42] Hydrogels are made of network of polymer chains that are hydrophilic in nature, hydrogels have water as their dispersion medium and 90% of their weight is water. [41] This property of hydrogels makes them very flexible and similar to natural tissue. [41] Hydrogels are commonly used as scaffold materials in tissue engineering. The mesh network of the hydrogels mimics the 3D environment of the natural tissue making them ideal for cellular growth and response. [41, 55]

Hydrogels can be made from natural or synthetic materials depending on the application. In tissue engineering, both the natural as well as synthetic materials are used

for making hydrogels, e.g. natural materials like alginic acid, chitosan, hyaluronic acid, collagen, agarose and synthetic materials like polyvinyl alcohol, polyacrylamides, silicone, etc. [41, 55]

In the first of the three interrelated projects, hydrogels were made from natural and synthetic materials through polymer crosslinking. The materials used were alginate, chitosan and calcium phosphate. Alginate and chitosan are FDA approved and biphasic calcium phosphate is commonly used as an alternative in bone grafts. The hydrogels contained embedded halloysites doped with bone morphogenic proteins.

Previous work on alginate-HNT scaffolds doped with BMP 2 showed promising results using the cell line ATCC 7F2 CRL 12557 mouse osteoblasts. The work was continued with BMP 4 and 6 loaded HNTs on the cell line ATCC 7F2 CRL 12557 mouse osteoblasts. The cell lines, ATCC CRL 2593 MC3T3 E1 subclone 4, a mouse pre-osteoblast cell line and ATCC CRL 2623, a mouse mesenchymal stromal cell line were also tested on the hydrogels with BMP 2 loaded halloysites. The composite hydrogels composed of alginate-chitosan and alginate-calcium phosphate were tested for their biological and mechanical properties. These nanoenhanced bioactive hydrogels can find application in implant coatings as well as stand-alone filler materials for bone regeneration. Figure 2-2 shows the graphical representation of the concept of the nanoenhanced bioactive hydrogels.

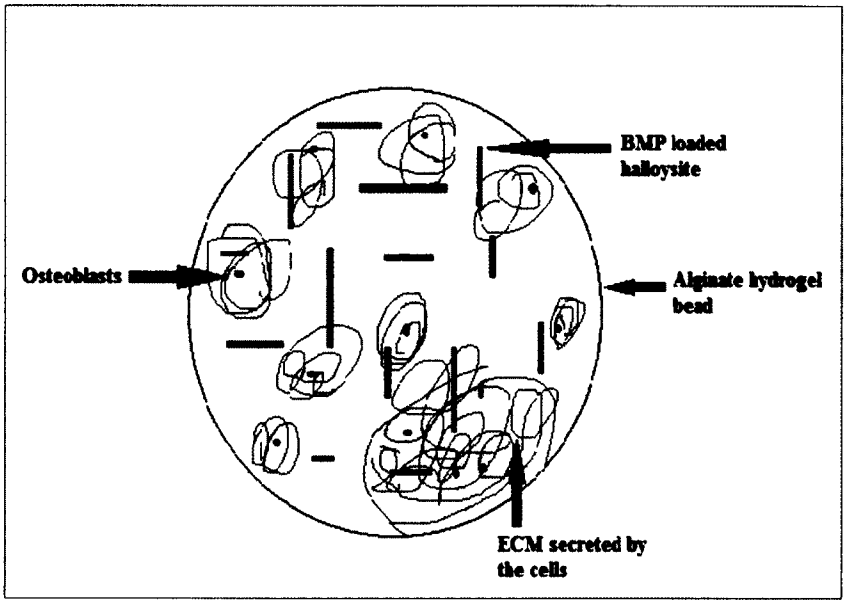

Figure 2-2. Graphical representation of the concept of nanoenhanced bioactive hydrogels.

2.3 Nanoseeds

The objective of this study was to investigate the potential of BMP 2 loaded into halloysites as a chemoattractant agent to actively recruit cells into the damaged tissue and thus advance tissue healing and repair. The principal goal of this research was to develop a novel nanocomposite, a *Nanoseed* composed of halloysite clay nanotubes (HNTs) nanoparticle composites, doped with osteogenic chemoattractants and inserted within biocompatible hydrogels (alginate, calcium phosphate or chitosan). The hydrogel construct was termed a *Nanoseed* because of the nanotubes that were incorporated into the hydrogels' mesh network. Nanoseeds, containing the chemoattractant BMP 2 loaded HNTs, were placed on the collagen gel matrix with bone progenitor cell reservoirs. These constructs were then assessed for their ability to actively recruit osteoprogenitor cells to

produce a bone matrix. The experimental design and the concept of *Nanoseed* are illustrated in Figure 2-3.

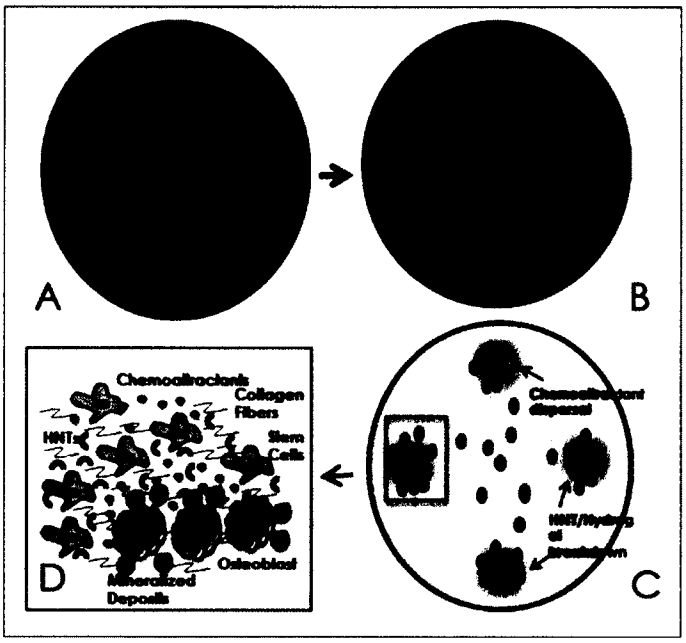

Figure 2-3. The experimental design and the concept of *Nanoseed*.

2.4 Hydrogel Biocoatings for Titanium Implants

Post-surgical infections are a major reason for the metal implant failures. [20] Titanium, a favored choice for metal implants, faces the problem of bacterial biofilm formation leading to its failure. [37] There are studies on coating the surfaces of the metal implants with anti-microbial coatings, but these coatings could not prevent the formation of bacterial film. [26] The major reason for the failure of anti-microbial coatings is the failure to release the anti-microbial drugs in a controlled and sustained manner. [26, 39, 52] The coatings either broke down early in the body's internal environment or failed to release the drug. [39, 52]

In the hydrogel biocoating project, there are two major goals: the first is to prevent the formation of bacterial films and the second is to make the surface of the titanium favorable to the bone cells for attachment and proliferation. Calcium phosphate bone cement has been used in combination with alginate and chitosan and enhanced these hydrogels with anti-microbial agent loaded halloysites. Gentamicin Sulfate (GS) was used as the anti-microbial agent because of its heat stability, wide use in the orthopedic surgeries and its effectiveness against the gram negative strains of bacteria. [8, 38] To achieve better surface for cellular response, the titanium surface was modified by anodization.

The hydrogel biocoatings were tested for their effectiveness in achieving a controlled and sustained release of the drug as well as their ability to inhibit the bacterium. Anodization was done by acid etching using Hydrofluoric acid (HF) as the electrolyte. The surface morphology of the anodized titanium was studied by scanning electron microscopy. The anodized titanium was also tested to check if it retained its osteogenicity by examining the deposition of hydroxyapatite crystals by treating it with simulated body fluid. The graphical representation of the concept of hydrogel coatings for anodized titanium is shown in the Figure 2-4.

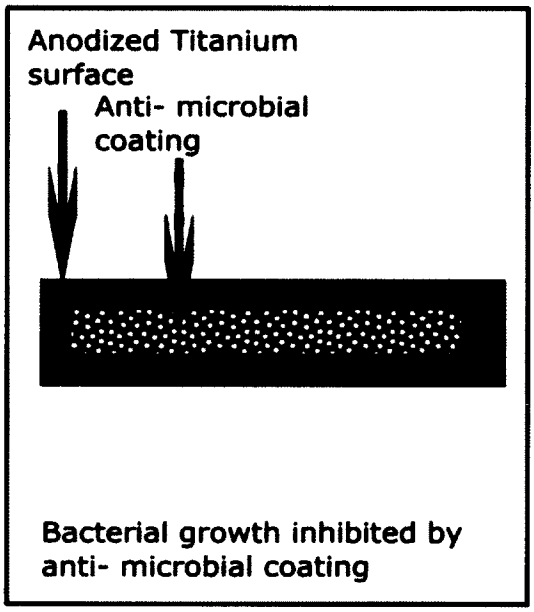

Figure 2-4. Graphical representation of the concept of hydrogel coatings for anodized titanium.

2.5 Objectives of the Projects

The basic objective of all the three projects is to design scaffolds that are cytocompatible, tissue integrative, tissue conductive, and would resemble native tissue in their material properties. The detailed objectives of the individual projects are listed below:

1. To design bioactive enhanced hydrogels with growth factor molecules loaded in them to improve the cellular response and surface morphology.
2. To obtain a sustained and extended release of growth factors and anti-infectives from the nanoparticles and hydrogels enhanced with nanoparticles.
3. To check the surface and other material properties of the hydrogels enhanced with nanoparticles.

4. To investigate if the nanoenhanced hydrogels act as a chemoattractant to the progenitor cells.
5. To anodize titanium and investigate its surface properties with respect to osteogenicity.
6. To design anti-infective hydrogels that would inhibit microbial growth and can be used to coat anodize titanium.

CHAPTER 3

INSTRUMENTATION AND METHODS

The current chapter details the instrumentation and methods used for scaffold preparation, material characterization of the scaffolds, and the response of different cell types to the scaffolds.

3.1 Instruments

Instruments form an important means of investigating a variety of scaffold properties. The following subsections detail the instruments used in the current dissertation. The instruments and the types of data they produced are detailed below.

3.1.1 HITACHI S 4800 Field Emission-Scanning Electron Microscope and EDX

HITACHI S 4800 Scanning Electron Microscope (FE-SEM) was used to image the hydrogel and titanium metal surfaces. The high magnification attained by the FE-SEM allowed a close comparison of the surface morphologies of the hydrogels and titanium (anodized and non-anodized). This comparison helped in the assessment of the surface properties and in predicting the behavior of the scaffolds in simulated body conditions. Figure 3-1 shows HITACHI S 4800 FE-SEM at the Institute of Micromanufacturing, Louisiana Tech University, Ruston (IfM).

Figure 3-1. HITACHI S 4800 FE-SEM at Institute of Micromanufacturing, Louisiana Tech University. [12]

3.1.2 NOVA e2000 B. E. T. Surface Area and Pore Size Analyzer

Brunnauer-Emmett-Teller or B. E. T Surface Area and Pore Size analysis works on the principle of physical adsorption of gas molecules on the surface of solid materials. [31] This theory by Brunnauer-Emmett-Teller is based on the Langmuir theory which assumes that the adsorbate, in this case an inert gas, behaves as an ideal gas under isothermal conditions and its partial pressure is directly proportional to its volume adsorbed on the solid surface. [31, 40]

NOVA e2000 Surface Area and Pore Size Analyzer works on the B. E. T. principle and can measure surface area and pore size of the sample using the helium void volume method. For our hydrogel samples, we have used the Langmuir method of plotting the isotherm. But the instrument, NOVA e2000, can perform other types of

computational analyses such as V-t method, DR method, etc. Figure 3-2 shows NOVA e2000 Surface Area and Pore Size Analyzer at IfM.

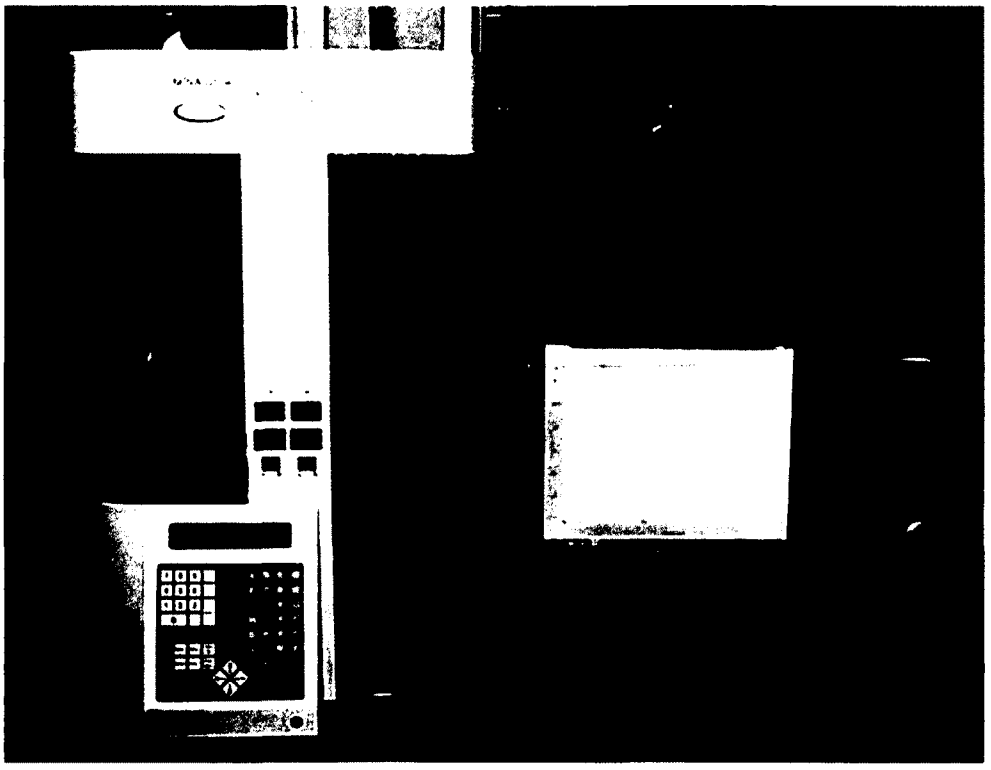

Figure 3-2. NOVA e2000 Surface Area and Pore Size Analyzer at Institute of Micrmanufacturing, Louisiana Tech University. [1]

3.1.3 NANODROP 2000 Spectrophotometer

NANODROP 2000 from Thermo Scientific is a UV-VIS spectrophotometer which uses only 1 µl of the sample for DNA, RNA, Protein, and other assays for biochemical analyses. This instrument also analyzes the samples within few minutes. Either a cuvette (for dilute samples) or the pedestal can be used for the analyses of the samples and the results can be obtained in the form of graphs on the software that is linked to the instrument. [6]

NANODROP 2000 spectrophotometer was used to measure the samples from the release study samples as well as the histochemical analyses. NANODROP 2000 used for

this research was located in the common second floor lab in the Biomedical Engineering building, Louisiana Tech University. Figure 3-3 shows Thermo Scientific NANODROP 2000 spectrophotometer.

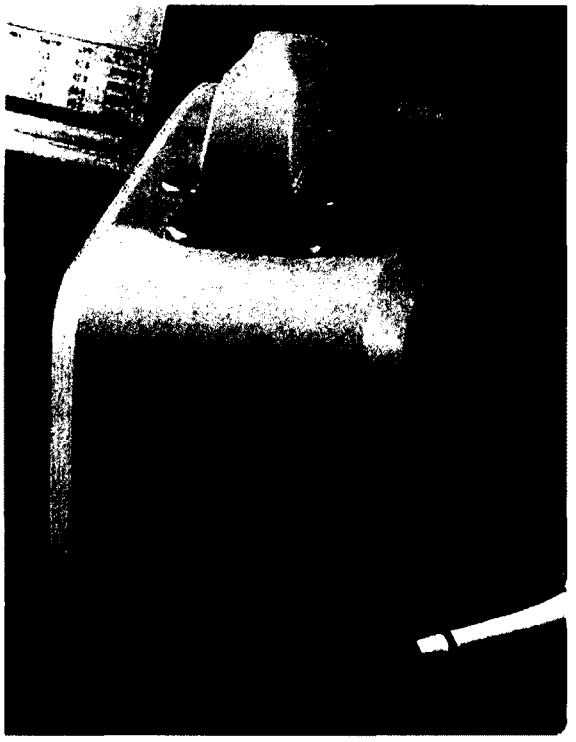

Figure 3-3. Thermo Scientific NANODROP 2000 spectrophotometer

3.1.4 Olympus BX51 Fluorescent Microscope

The Olympus BX51 fluorescent microscope images cells live or in the fixed state. It has filters for different fluorescent dyes such as DAPI, Alexa Fluor Red, FITC, and TRITC. This microscope can also image the cells in phase contrast mode when the UV lamp is turned off. The images are captured in high definition and can be taken at 10X, 20X or 40X magnifications.

For visualizing the cells stained with different histochemical stains and fluorescent dyes we used 10X and 20X magnifications. The scaffolds and the seeded cells were also imaged on the phase contrast mode. Figure 3-4 shows Olympus BX51

epifluorescence microscope in the microscopy lab in the Biomedical Engineering Building.

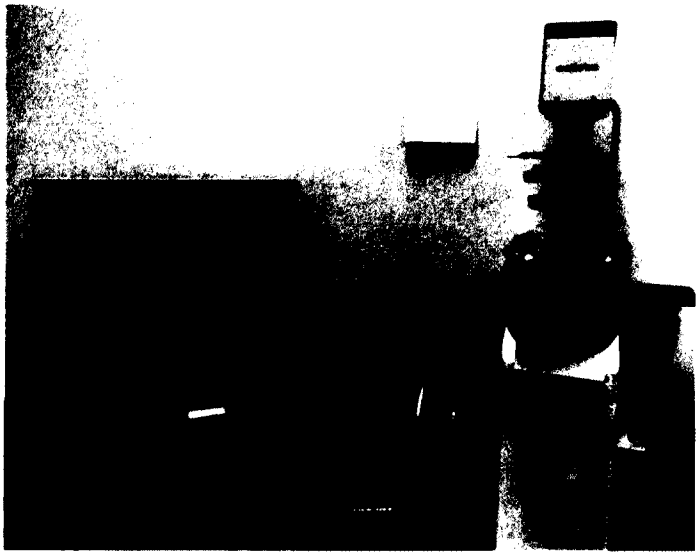

Figure 3-4. Olympus BX51 epifluorescence microscope in BME microscopy lab, Louisiana Tech University.

3.1.5 LABCONCO Lyophilizer

Lyophilizer freeze dries the samples under low temperature and vacuum. This method of drying preserves most of the structural details of the samples, especially, hydrogels. For electron microscopy, the samples need to be dry and if hydrogels are dried under vacuum at room temperature their structure collapses turning the hydrogel beads into powder. Lyophilizer uses temperatures as low as −20 °C retaining the structural features while at the same time drying the samples.

The hydrogel samples were frozen at −20 °C overnight and then subjected to vacuum conditions in the LABCONCO lyophilizer. The process was carried out for 36 hours. The samples obtained were stored at room temperature under dry conditions. Figure 3-5 shows the LABCONCO lyophilizer located in Biomedical Engineering building Room 151.

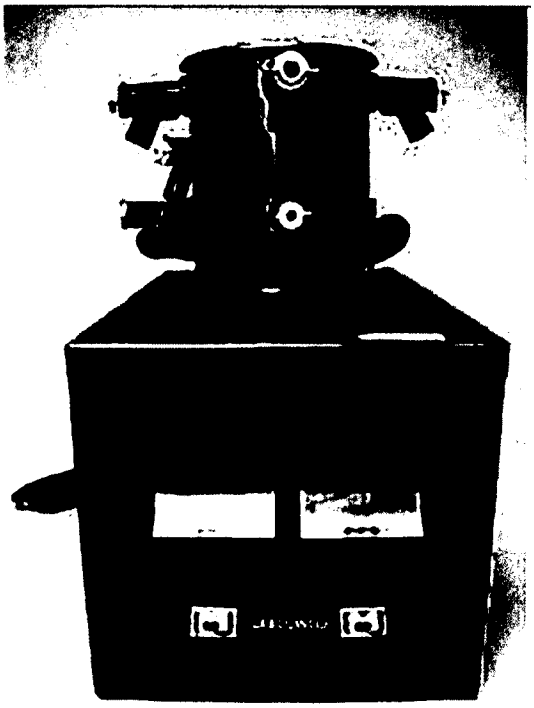

Figure 3-5. LABCONCO lyophilizer in BME 151, Louisiana Tech University.

3.1.6 Absorbance Microplate Reader

The principle of absorbance microplate reader is similar to that of spectrophotometer the only difference being the stage on which the samples are mounted for analyses. Absorbance microplate reader utilizes a stage that can read 96 well plates or similar plates that are used for cell culture and ELISA studies.

For the quantification of released bioactive molecules in the release profile studies using ELISA, Phenix LT-4000 absorbance microplate reader was used. The assays were done in a 96 well plate specially treated for ELISA. Figure 3-6 shows Phenix LT-4000 absorbance microplate reader in Biomedical Engineering building Room 238.

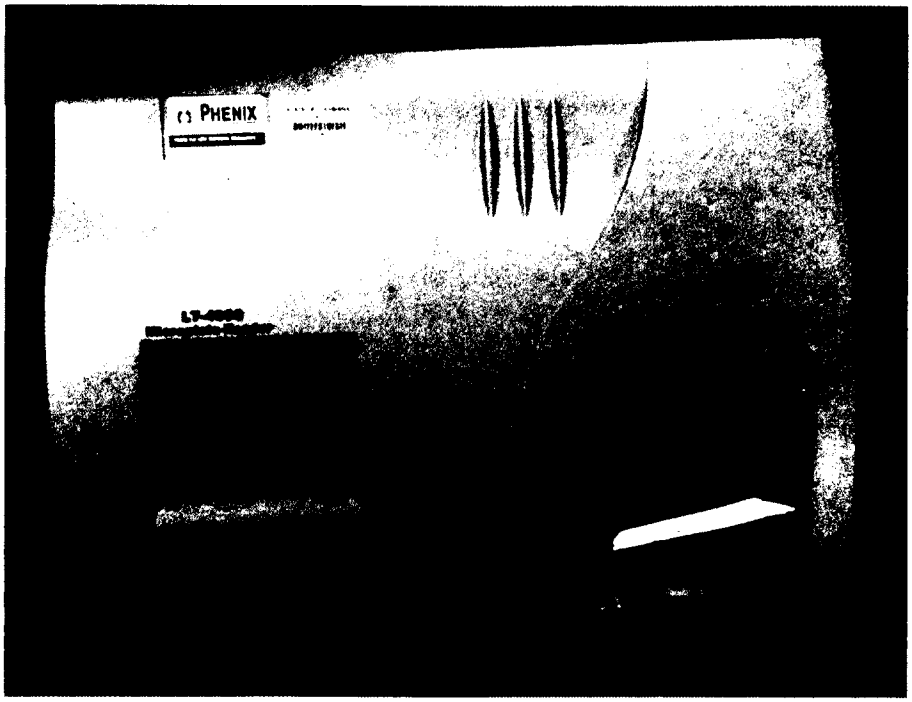

Figure 3-6: Phenix LT-4000 absorbance microplate reader in BME 238, Louisiana Tech University.

3.1.7 Anodization Set-Up

Anodization uses the metal to be coated and etched as an anode. The method used in this research for etching on the surface of titanium is acid etching. Hydrofluoric Acid (HA) was used as an etchant and titanium metal sheet (polished manually with alumina) was used as an anode. Oure platinum electrode was used as cathode. A voltage of 1 V was applied with a current of 10 amps. Figure 3-7 shows the anodization set up in Carson-Taylor Hall Room 316.

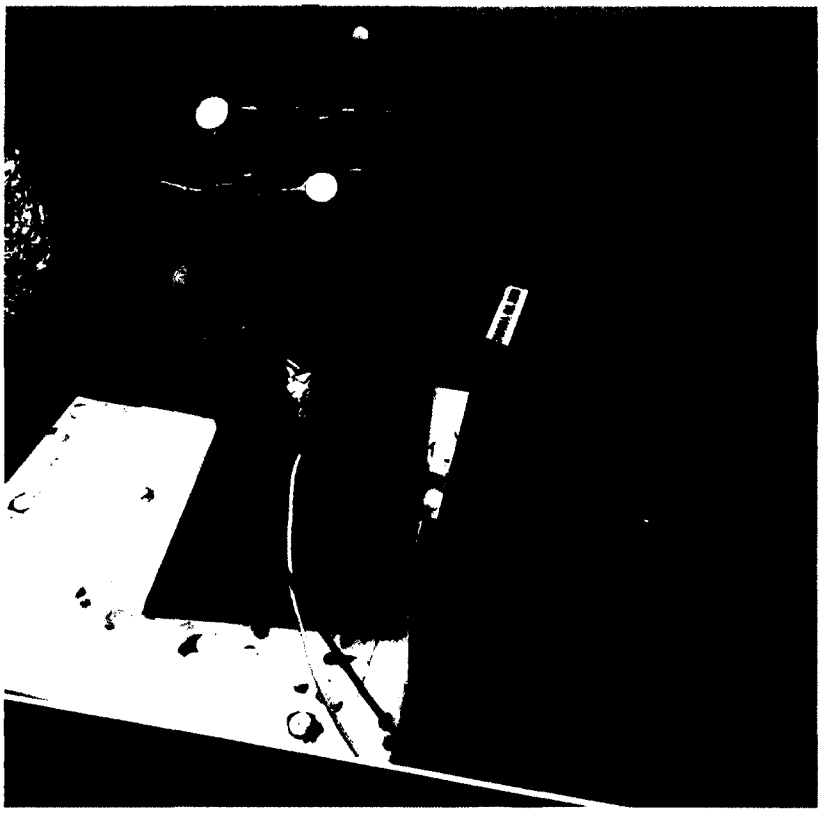

Figure 3-7. Anodization set-up at Carson-Taylor Hall room 316, Louisiana Tech University.

3.2 Methods

Detailed in the following sub-sections are the methods used to construct the scaffolds, prepare samples for various analyses and biochemical assays used for determination of the cellular response to the scaffolds.

3.2.1 Preparation of Hydrogels

Hydrogels are formed by crosslinking monomers into long interlinked polymers. They have a mesh like network that can be attributed to the chemistry of their bonds. Hydrogels can hold large amounts of water molecules in their structure giving them their name.

In current research, calcium alginate hydrogel forms the base of all the hydrogel composites. Sodium alginate 2% w/v was reverse crosslinked with 1% w/v calcium

chloride. The hydrogel composites consisted of the following materials in specific concentrations are shown in Table 1.

Table 1: Materials in specific concentrations used for hydrogel composites

Alginate Only	2% w/v sodium alginate	1% w/v calcium chloride			
Alginate + HNTs	2% w/v sodium alginate	1% w/v calcium chloride	1% w/v HNTs		
Alginate + TTCP	2% w/v sodium alginate	1% w/v calcium chloride		0.33 gm TTCP per 1 ml alginate solution	
Alginate + TTCP + HNTs	2% w/v sodium alginate	1% w/v calcium chloride	1% w/v HNTs	0.33 gm TTCP per 1 ml alginate solution	
Alginate + TTCP + Chitosan	2% w/v sodium alginate	1% w/v calcium chloride		0.167 gm TTCP per 1 ml alginate solution	3.33 mg Chitosan lactate per 1 ml alginate solution
Alginate + TTCP + Chitosan + HNTs	2% w/v sodium alginate	1% w/v calcium chloride	1% w/v HNTs	0.167 gm TTCP per 1 ml alginate solution	3.33 mg Chitosan lactate per 1 ml alginate solution

3.2.2 Vacuum Loading of Halloysite

HNTs were loaded with bioactive molecules like growth factors and anti-microbial agents. The basic process of vacuum loading remained the same, with the concentrations differing according to the molecule of interest. For sterilizing them, the

HNTs were spread onto a parchment paper piece and kept under the UV light for 45 minutes. Throughout the loading process aseptic conditions were maintained.

3.2.2.1 *Loading HNTs with Growth Factors.* Bone Morphogenetic Proteins 2, 4, and 6 were obtained from ProSpec Militany, Tel Aviv, Israel. A stock solution of the respective growth factors was prepared as per the manufacturer's instructions. A dilution of the concentration 10 µg/ml was prepared from the stock solution for all the three growth factors. All the solutions were made from sterile diluents and under aseptic conditions.

After sterilization under the UV light, the HNTs were sonicated for 15 minutes with the prepared growth factor solutions. The final concentration of HNTs to the growth factor solution is 50 mg HNTs in 10 ml of 10 µg/ ml growth factor solution. This solution was then kept in vacuum chamber under sterile conditions for 24 hours with intermittent vacuum applied to it. After 24 hours, the HNTs were separated by centrifugation and then washed in distilled water to remove traces of growth factors sticking on the outer surface of the tubes. After washing, the loaded HNTs were dried in vacuum and stored at 4 °C.

3.2.2.2 *Loading HNTs with Anti-Microbial Agent.* The anti-microbial agent used in the current research, Gentamicin Sulfate (GS), was obtained from Sigma-Aldrich, St. Louis, MO. A solution of 60 mg/ ml was prepared in autoclaved water. To the 10 ml of 60 mg/ml solution of GS 50 mg HNTs were added and sonicated for 15 minutes under sterile conditions. This solution was then kept in vacuum chamber under sterile conditions for 24 hours with intermittent vacuum applied to it. After 24 hours, the HNTs were separated by centrifugation and then washed in distilled water to remove

traces of growth factors *sticking on the outer surface of the tubes. After washing, the loaded HNTs were dried in vacuum and stored at* 4 °*C.*

3.2.3 Sample Preparation for FE-SEM

Lyophilization is a process where the sample is subjected to rapid drying under frigid and vacuum conditions. This is done to retain the structural details but to remove water molecules from the sample. FE-SEM requires the samples to be dry to obtain high magnification and high resolution images.

To lyophilize, the hydrogels were subjected to -20 °C temperature overnight before starting the process. This prevents the hydrogel structure and pores from collapsing under extreme low pressure. After freezing the samples, they were attached to the docks provided for the glass beaker and the vacuum was started. The process usually completes in 24 hours but the samples were kept running in the lyophilizer for 36 hours to ensure that they have no moisture.

3.2.4 Coating 12 Well Plates with Collagen Type I Gels

The cell migration experiments in the project 'Nanoseeds' required a gel matrix to hold the hydrogel constructs in place away from the cell reservoir. Collagen type I gel was the best suited option as it is the basic component of any tissue's extra cellular matrix. This gel would mimic the conditions found in the natural tissue. The cell culture 12 well plates were coated with collagen type I to obtain the gel matrix.

Rat tail type I collagen was obtained from GIBCO, Life Technologies and the collagen gel was prepared as per the procedure and formulae provided by the manufacturer.

3.2.5 Cell Assays

Biochemical assays quantify the cellular response to the scaffolds and in turn can give us an idea about how the scaffolds behave *in vitro.*

3.2.5.1 *Trypan Blue Cell Count for Seeding Density.* To fix the concentration of seeding the cells on to the scaffolds, we needed to quantify the number of cells in one T25 cell culture flask at 80% confluence. To calculate the amount of cells present in the flask, Trypan Blue cell viability method was used.

Cell suspension (1 ml) was taken from a passage 2, 80% confluent T25 flask and 0.1 ml of 0.4 % v/v Trypan Blue solution was added to it. A hemocytometer was used to determine the number of live and dead cells. If the cells take up the dye, they are non-viable and vice versa. Under a 10 X magnification of the light microscope, the total number of cells and number of blue cells are counted in a hemocytometer. The number of viable cells is calculated as follows:

% viable cells = [1.00 – (No. of Blue Cells / Total number of cells)] X 100

Cells/ ml cell suspension = No. of Viable cells X 10^4 X 1.1

3.2.5.2 *NucBlue Fluorescent Staining.* NucBlue Live Ready Probes fluorescent stain, Life Technologies, Thermo Fisher (Grand Island, NY) works on the same principle as the DAPI stain. It is a cell permeant nuclear dye that emits blue fluorescence when bound to the DNA. The staining procedure was carried out as per the manufacturer's instructions. Three drops of the dye were added per ml of the cell suspension and incubated for 20 minutes protected from the light. The cells were visualized under Olympus fluorescence microscope under the DAPI filter.

Results are not shown in Section 5.3 as the dye faded after Day 3 and the Days 1 and 3 figures were not sufficient to suggest the migration of cells form the cell reservoir towards hydrogel 'Nanoseeds'. The histochemical staining with Alcian Blue and Von Kossa were more conclusive to show the migration and differentiation of the cells towards the hydrogel 'Nanoseeds'.

3.2.5.3 *Alcian Blue Staining.* Alcian Blue stains the acidic mucopolysaccharides of the ECM blue and helps to visualize the otherwise fuzzy ECM. This assay helps to assess the ECM production on the scaffolds or in response to them.

The fixed cells or the constructs with the cells were washed with HBSS and then stained with 0.5%v/v Alcian Blue stain from Electron Microscopy Inc. for 20 minutes. The cells and the constructs were visualized under 10 and 20 X magnification of Olympus Light microscope.

3.2.5.4 *Picrosirius Red Staining.* Picrosirius Red stain helps to visualize the collagen secretion by the cells when they are forming ECM. Collagen, especially type I, is a major component of ECM of a majority of the tissues in the body. Picrosirius Red stains collagen red, revealing the extent of ECM production and differentiation of the cells.

The fixed cells or the constructs with the cells were washed with HBSS and then stained with Picrosirius Red, Polysciences Inc. (Warrington, PA) solution A for two minutes and then in solution B for 60 minutes. After 60 minutes, solution B was removed and solution C was added and kept for two minutes. After the staining was completed, the excess stain was washed with distilled water. The collagen secretion was visualized under Olympus light microscope at 10 and 20 X magnification.

3.2.5.5 *Von Kossa Staining.* Von Kossa stain utilizes the reaction between 3% v/v silver nitrate solution and the phosphate group of calcium phosphate or hydroxyapatite molecules to visualize the calcium phosphate synthesis by the cells after differentiation. Bone progenitor cells produce calcium phosphate as a result of differentiating into the mature osteocytes. Calcium phosphate is the major inorganic content of bone.

The fixed cells or the constructs with the cells were washed with HBSS and then 3% v/v silver nitrate solution from Polysciences Inc. (Warrington, PA) was added to the wells. The solution and the constructs were the placed under UV light for 15 minutes. After 15 minutes, the solution was discarded and the constructs washed with distilled water twice and 5% v/v sodium thiosulfate solution was added to the constructs to remove traces of unreacted silver nitrate. The constructs were then washed with distilled water twice. The black or brown stained phosphate deposits were visualized under Olympus BX51 brightfield microscope at 10 or 20X magnification.

3.2.6 Release Profile Study

The release profiles of bioactive agents were studied in simulated physiological conditions. Release profiles of the bioactive molecules were obtained from both loaded HNTS and hydrogels enhanced with loaded HNTs. The loaded HNTs or the hydrogel beads enhanced with loaded HNTs were suspended in sterile Hank's Balanced Salt Solution (HBSS) and put on a rocker platform for uniform agitation. Samples were taken and stored in sterile tubes at 4 °C for further analysis. All the release profile experiments were performed at room temperature.

For growth factor release profile (BMP 2), the samples were collected at 24 hours and 7 days. The concentration was determined by performing ELISA on the stored

samples. The samples were brought to room temperature before performing the assay. The ELISA kits were custom made Quantikine kits for BMP 2 and obtained from R&D systems (Minneapolis, MN). The readings were taken on the absorbance plate reader. The concentration of the released BMP 2 at a particular time point was estimated by plotting standard curves of the known BMP 2 standards and finding the corresponding values of the concentration for a particular optical density reading.

The release profile for GS was carried out using similar method of agitation and sample collection. The samples were collected at 24 and 36 hours and stored at 4 °C. The method for estimating the concentration was OPTA colorimetric analysis. The readings were taken on UV/VIS NANODROP spectrophotometer. The concentration of released GS was estimated by plotting standard curves of known concentration standards of GS and finding the corresponding values of the concentration for a particular optical density reading.

3.2.7 Bacterial Inhibition Study

Bacterial inhibition study was done to assess the efficiency of GS when loaded in HNTs and encapsulated in hydrogels. Muller-Hinton LB agar plates were prepared as per the standard procedure and aseptic conditions were maintained throughout the study. DH5α strain of *E. coli* was used to study the effect of anti-infective agent by studying the formation of growth inhibition zone on the agar plates. A negative control plate had a lawn of bacteria growing without any anti-infective agent. Positive control plate had GS standard disc placed on the bacterial culture. The experimental plates had different compositions of hydrogels with and without the anti-infective agent GS. The study was

conducted for 24 hours and the plates checked for the formation growth inhibition zones around the hydrogel constructs indicating the effectiveness of the anti-infective agent.

CHAPTER 4

NANOENHANCED BIOACTIVE HYDROGELS

4.1 Introduction

In the field of regenerative medicine, research efforts are directed at the development of scaffolds that are biocompatible and that assist in the body's native regenerative response. Hydrogels are a commonly used scaffold. Hydrogels have been used extensively to deliver a wide variety of bioactive agents. [41, 55] Alginate is a FDA approved material, commonly used in drug delivery, cell and enzyme encapsulation. [13, 58] One of the challenges faced by the hydrogels is the release of biomolecules in extremely low amounts and in a sustained manner. [58]

To achieve this objective, the HNTs were loaded with growth factors like BMP 2, 4 and 6. HNTs are cylindrical in their structure with concentric layers of aluminosilicate and have a lumen which is charged. [7] This unique structure of the HNTs makes them suitable for loading a variety of charged molecules. [22] Previous studies on the HNTs have shown that they can be used to deliver bioactive molecules like anti-infective agents, proteins, etc. in a sustained manner. [22, 29]

The hypothesis of this project was that HNTs would provide a sustained release of the growth factors and would improve the material and biological properties of the calcium alginate hydrogels.

4.2 Materials and Methods

All the plastic wares, such as, syringes, centrifuge tubes, microcentrifuge tubes, 12 well plates, pipettes, etc. were purchased from Mid Scientific, St. Louis, MO. Cell culture media, buffers, and serum were purchased from Life Technologies, Grand Island, NY. Sodium citrate, sodium chloride, calcium chloride, sodium alginate, and HNTs were obtained from Sigma-Aldrich, St. Louis, MO. BMPs (BMP 2, 4, and 6) were purchased from Prospec (Rehovat, Israel). Preosteoblast cell line MC3T3 subclone E1 (ATCC CRL 2593) was obtained from ATCC, Manassas, VA. BMP 2 Quantikine ELISA Kit was obtained from R&D Systems, MN.

4.2.1 Cell Culture, Cell Seeding and Preparation of the Constructs

Preosteoblast cell line was the model used to study *in vitro* cellular response to the nanoenhanced hydrogels. This cell line exhibits osteoblast differentiation once supplied with ascorbic acid and after differentiation their behavior is similar to that of the calvarial osteoblasts. [50] Standard aseptic cell culture protocols were followed to proliferate, passage and dissociate the cells in sterile cell culture grade plasticware.

For encapsulation, after detaching them from the flasks, the cells were suspended in Sterile HBSS. After centrifugation, the cell pellet was isolated and then resuspended in fresh HBSS. The seeding density was determined by hemocytometer and tryphan blue solution. The procedure is described briefly in Section 3.2.5.1. The seeding density used was 1 X 10^6 cells / bead.

For preparation of the hydrogel beads, all the solutions, such as, 2% w/v sodium alginate, 1% w/v calcium chloride, and HNTs (before loading) were sterilized. The HNTs were sterilized under UV for 45 minutes and the solutions were prepared in autoclaved

reverse osmosis (RO) water. To ensure that the solutions have no contaminants, they were sterile filtered through 0.45 μm syringe filters. The HNTs were loaded as mentioned in Section 3.2.2.1.

The cells that were suspended in sterile HBSS were carefully dispersed in the 2% w/v sodium alginate solution. Cell culture plastic 24 well plates were set up with 1% w/v calcium chloride solution. The set up comprised of five groups: control group # 1, control group # 2, experimental group # 1: BMP 2, experimental group # 2: BMP 4, and experimental group # 3: BMP 6. The sodium alginate+ cells solution was dropped carefully using sterile 27-G syringes in the respective wells.

4.2.2 Sample Fixation and Histochemical Analyses

The samples were made in triplicates and the experiment was performed twice to check for the reproducibility of results. The hydrogels were formed instantaneously but the beads were kept in the calcium chloride solution for about 15 minutes to ensure complete gelation. After 15 minutes, the beads were washed twice with sterile HBSS and complete α-MEM was added as the growth medium for the cells.

The samples were fixed on days 0, 1, 3, 7, 14, and 21 and biochemical and histochemical analyses were performed. The detailed procedures for Alcian Blue, Picrosirius Red, and Von Kossa Staining are provided in Sections 3.2.5.3, 3.2.5.4, and 3.2.5.5, respectively.

4.2.3 Release Profile Study for BMP 2

Release profile study for BMP 2 was done to understand the elution of the protein from HNTs. As the amount of the protein that would be eluted fell in the ranges of nanograms and pictograms, custom made ELISA kits were used. The Quantikine ELISA

kits from R&D systems can estimate the amount of BMP 2 as low as 50 picograms. The details of the sample collection and overall procedure are provided in the Section 3.2.6.

4.2.4 FE-SEM Imaging and Material Testing

To visualize if the addition of HNTs had any effect on the surface morphology of the hydrogels, FE-SEM imaging was performed on lyophilized hydrogel samples. The Lyophilization protocol is detailed in Section 3.2.3.

The material properties such as porosity, and surface area were analyzed using BET method. The sample preparation was simple for BET Surface area and pore size analyzer (NOVA e2000). The hydrogels were dried on Whatman No. 1 filter paper till the excess water was drained. After partial drying, the initial weights of sample (respective hydrogel types) were recorded. The degassing step was skipped as the hydrogels char at temperatures as high as 300 °C. Langmuir method of plotting isotherm was used to analyze the results. The principle behind BET NOVA e2000 surface area and pore size analyzer is described in detail in Section 3.1.2.

4.3 Results and Discussion

This section represents the results and their discussion from the experiments mentioned in Section 4.2.

4.3.1 Histochemical Analysis

The results of histochemical analysis of the hydrogels enhanced with BMP 2, 4, and 6 were compared to the previously obtained histochemical analysis results of the hydrogels enhanced with BMP 2 loaded HNTs from the thesis, Bioactive Hydrogels for TMJ Repair. [29] The comparison was done to investigate the potential of HNTs loaded with growth factors as an *in situ* drug delivery vehicle and also to test the primary

hypothesis of this project, that is, the addition of growth factor loaded HNTs improves the biological and material properties of hydrogels.

4.3.1.1 *Alcian Blue staining*. The Alcian Blue assay was performed to visualize the amount of acidic ECM mucopolysaccharides. Alcian Blue stains the acidic mucopolysaccharides, found in the extracellular matrix produced by the differentiating cells, blue indicating the extent of ECM production. Figures 4-1 to 4-4 show Alcian Blue staining of the alginate hydrogels enhanced with BMP 2, 4, and 6 loaded HNTs with osteoblasts encapsulated in them. Figure 4-1 (A-F) shows Day 0 Alcian Blue staining of the alginate hydrogels with BMP 2, 4, and 6 loaded HNTs. The Alcian Blue staining was performed on fixed hydrogel beads on days 0, 1, 3, 7, 14, and 21. The figures are representative and only days 0, 7, 14 and 21 are shown in this dissertation as they show the progression of ECM production after cellular differentiation in the different experimental groups of hydrogels with growth factors and HNTs.

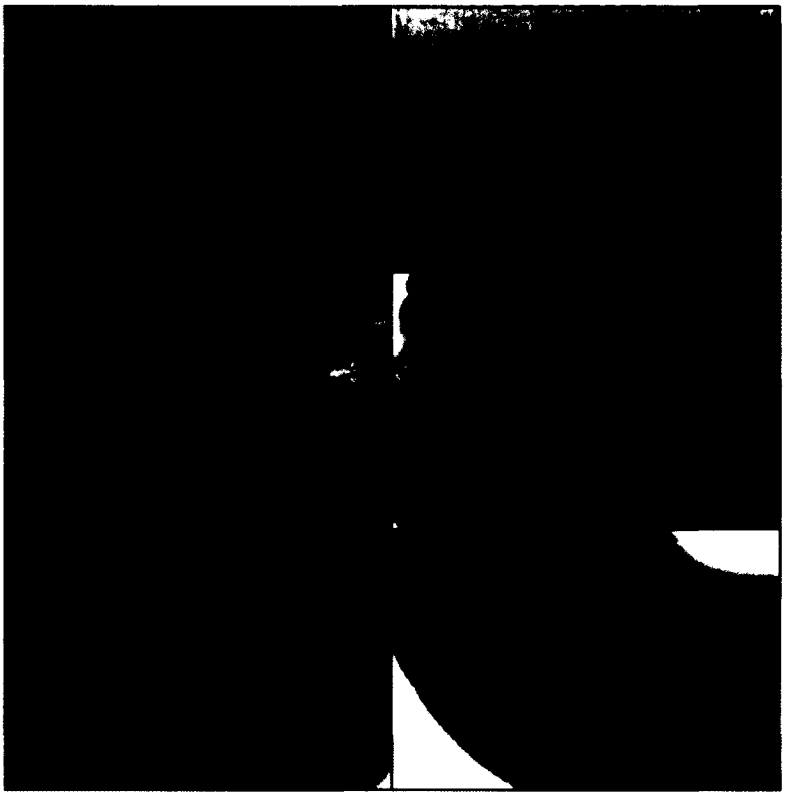

Figure 4-1. Alcian Blue staining Day 0 A) Control 1 Alginate-only B) Control 2 Alginate + HNTs C) Experimental 1 Alginate+ HNTs+ BMP 2 D) Experimental 2 Alginate+ HNTs+ BMP 2 with 0.4M Ascorbate E) Experimental 3 Alginate+ HNTs+ BMP 4 F) Experimental 4 Alginate+ HNTs+ BMP 6.

In Figure 4-1, A) and B) are controls with alginate hydrogels without HNTs as in A and without growth factors as in B. Figures 4-1 C), D), E), and F) show alginate+ HNTs+ BMP 2, alginate+ HNTs+ BMP 2 with 0.4 M ascorbate added to the medium, alginate+ HNTs+ BMP 4 and alginate+ HNTs+ BMP 6, respectively. Day 0 staining was done after 8 hours of osteoblast encapsulation with the hydrogels. The images show that C and D have more proliferating cells as seen by the pink Hematoxylin stained nuclei. Images E and F are comparable to the controls in A and B. No pink stained masses were visible in the images A, B, E, and F. This suggests that proliferation was slower in these hydrogels as compared to the images in C and D after 8 hours of cell encapsulation. Figure 4-2 (A-F) shows Alcian Blue on Day 7.

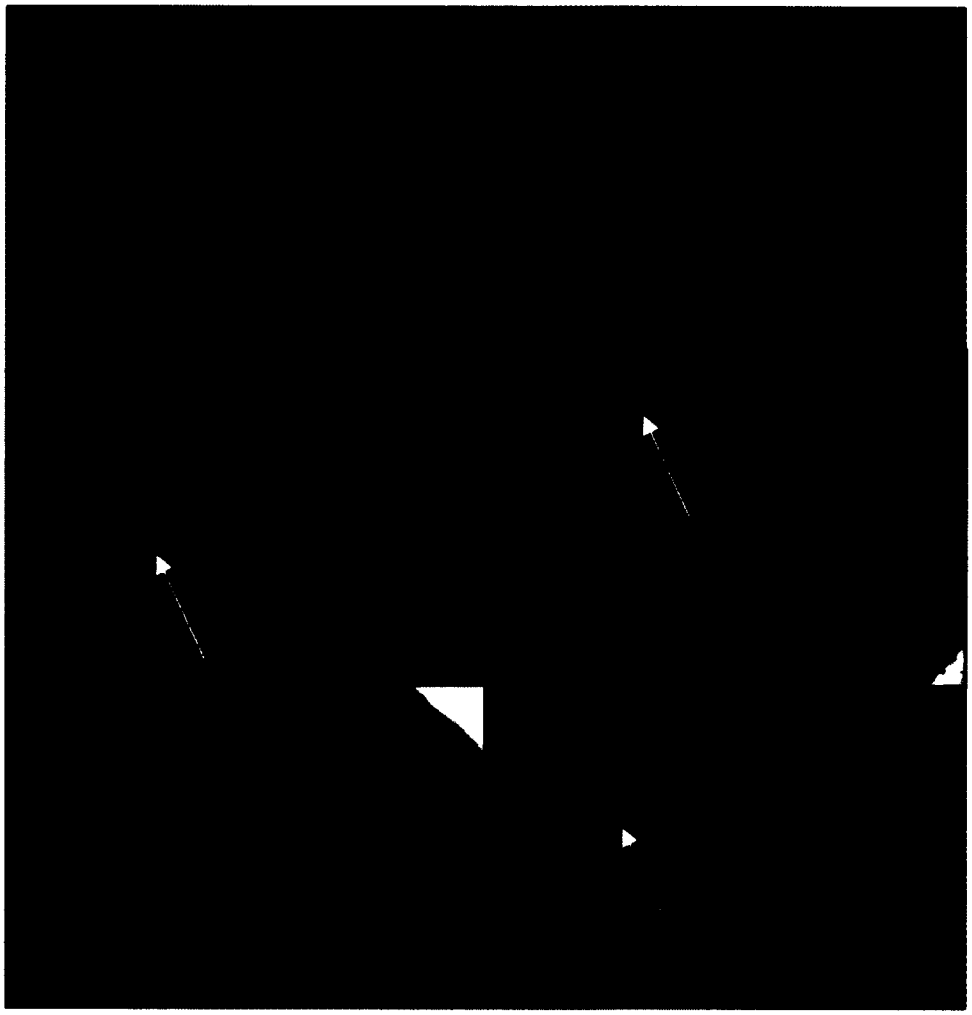

Figure 4-2. Alcian Blue staining Day 7 A) Control 1 Alginate-only B) Control 2 Alginate + HNTs C) Experimental 1 Alginate+ HNTs+ BMP 2 D) Experimental 2 Alginate+ HNTs+ BMP 2 with 0.4M Ascorbate E) Experimental 3 Alginate+ HNTs+ BMP 4 F) Experimental 4 Alginate+ HNTs+ BMP 6.

In Figure 4-2, controls A and B show less to no deep stained islands or patches of differentiated cells. The staining looks lighter in the controls A and B unlike the experimental groups (C-F). Experimental groups #1 and #2 (C and D) show pink and blue areas with deep pink stained islands or patches of differentiating cells shown by the arrows. Experimental groups #3 and #4 (E and F) show deeply stained hydrogels suggesting that the ECM produced was more and evenly spread than the rest of groups. E and F also show some dark pink spots or deeply stained patches which are cells

concentrated in these areas shown by arrows. A comparison of the images, C, D, E, and F with the controls A and B, suggests that the experimental groups performed better with respect to the ECM production (which is suggestive of cellular differentiation) by Day 7. The images E and F when compared to C and D show prominent dark patches of cells surrounded by ECM mucopolysachharides that is evenly spread throughout the hydrogels suggesting that experimental groups #3 and #4 performed better with to respect to ECM production than experimental groups #1 and #2. Figure 4-3 (A-F) shows Alcian Blue staining on Day 14.

Figure 4-3. Alcian Blue staining Day 14 A) Control 1 Alginate-only B) Control 2 Alginate + HNTs C) Experimental 1 Alginate+ HNTs+ BMP 2 D) Experimental 2 Alginate+ HNTs+ BMP 2 with 0.4M Ascorbate E) Experimental 3 Alginate+ HNTs+ BMP 4 F) Experimental 4 Alginate+ HNTs+ BMP 6.

In Figure 4-3, controls A and B show light pink (cells) and blue regions (stained ECM) suggesting differentiating cells surrounded by the ECM they secrete. The staining is lighter than the experimental groups #1-#4 (images C-F). The experimental groups #1 and #2 (C and D) show dark pink patches shown by arrows (differentiating osteoblasts) surrounded by dark blue regions of dense ECM mucopolysachharides. The experimental groups #3 and #4 (E and F) show larger dark pink or purple patches of the differentiating cells surrounded by dark blue stained ECM mucopolysachharides. The images in Figure 4-3 (A-F) show that even though the controls (A and B) have started showing blue stained ECM, it is much lighter than the experimental groups #1-#4 (C-F). The experimental groups #3 and #4 (E and F) show darker and deeper blue stained hydrogels than the experimental #1 and #2 (C and D) suggesting more ECM is produced in these hydrogels than the other on Day 14. Figure 4-4 (A-F) shows Alcian Blue staining on Day 21.

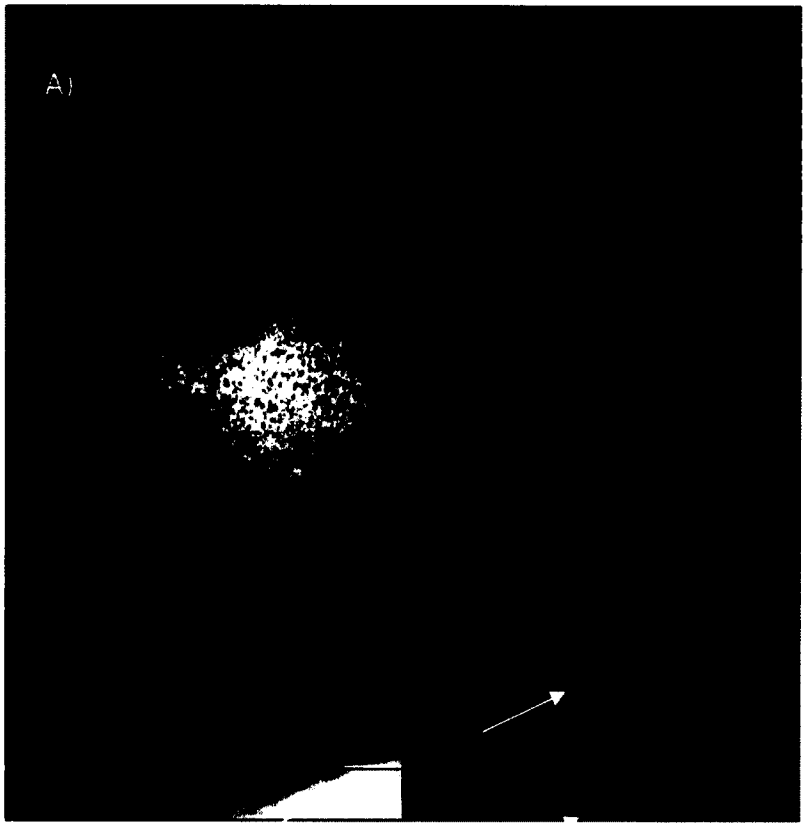

Figure 4-4. Alcian Blue staining Day 21 A) Control 1 Alginate-only B) Control 2 Alginate + HNTs C) Experimental 1 Alginate+ HNTs+ BMP 2 D) Experimental 2 Alginate+ HNTs+ BMP 2 with 0.4M Ascorbate E) Experimental 3 Alginate+ HNTs+ BMP 4 F) Experimental 4 Alginate+ HNTs+ BMP 6.

In Figure 4-4, controls A and B show deep pink or purple patches of cells surrounded by ECM stained in blue. The experimental groups #1-#4 (C-F) show deeper pink stained regions and dark blue stained regions of ECM as compared to the controls A and B. The experimental groups #1 and #2 (C and D) show the dark pink or purple regions of cells, shown by arrows, surrounded by blue colored region of ECM produced by these cells. The experimental groups #3 and #4 (E and F) show dark patches of cells, shown by arrows, surrounded by deep blue stained ECM. The images E and F show hydrogels stained blue and no differentiable pink regions because the ECM mucopolysachharides are denser than the other groups.

If the images of the experimental groups #1-#4 (C-F) from day 0 to Day 21 are compared, experimental groups #3 and #4 (E and F) show deep blue stained hydrogels from day 0 to Day 21 suggesting that the hydrogels with BMP 4 and 6 loaded HNTs perform better with respect to the early onset of ECM production by the differentiating cells. The experimental group 2 (D) showed more deep pink patches of the cells on Day 7 and the trend continues till Day 21. The deep pink patches are surrounded by deep blue stained regions of ECM mucopolysachharides, well defined on days 14 and 21. This suggests that hydrogels with BMP 2 loaded HNTs combined with 0.4 M ascorbate in growth medium enhanced cellular proliferation and differentiation.

The control 2 with alginate+ HNTs and no growth factors (B) showed no enhancement of cellular responses in the hydrogels on days 0 to 21 suggesting that halloysite, alone, would not enhance the cellular responses in these hydrogels. To achieve enhanced cellular response for nanoenhanced hydrogels, the HNTs should be loaded with osteogenic growth factors such as the ones used in this project, namely, BMP 2 ,4, and 6.

The observations made by visual qualitative analysis of the Alcian Blue stained sections of hydrogels can be further ascertained by image analysis done by Image J software. The representative images of Controls 1 & 2 and the experimental groups E1, E 3, and E4 for days 0 and 21 are given in Figure 4-5 to 4-15. Figure 4-5 shows RGB peaks for alginate-only hydrogel control (C1) for day 0.

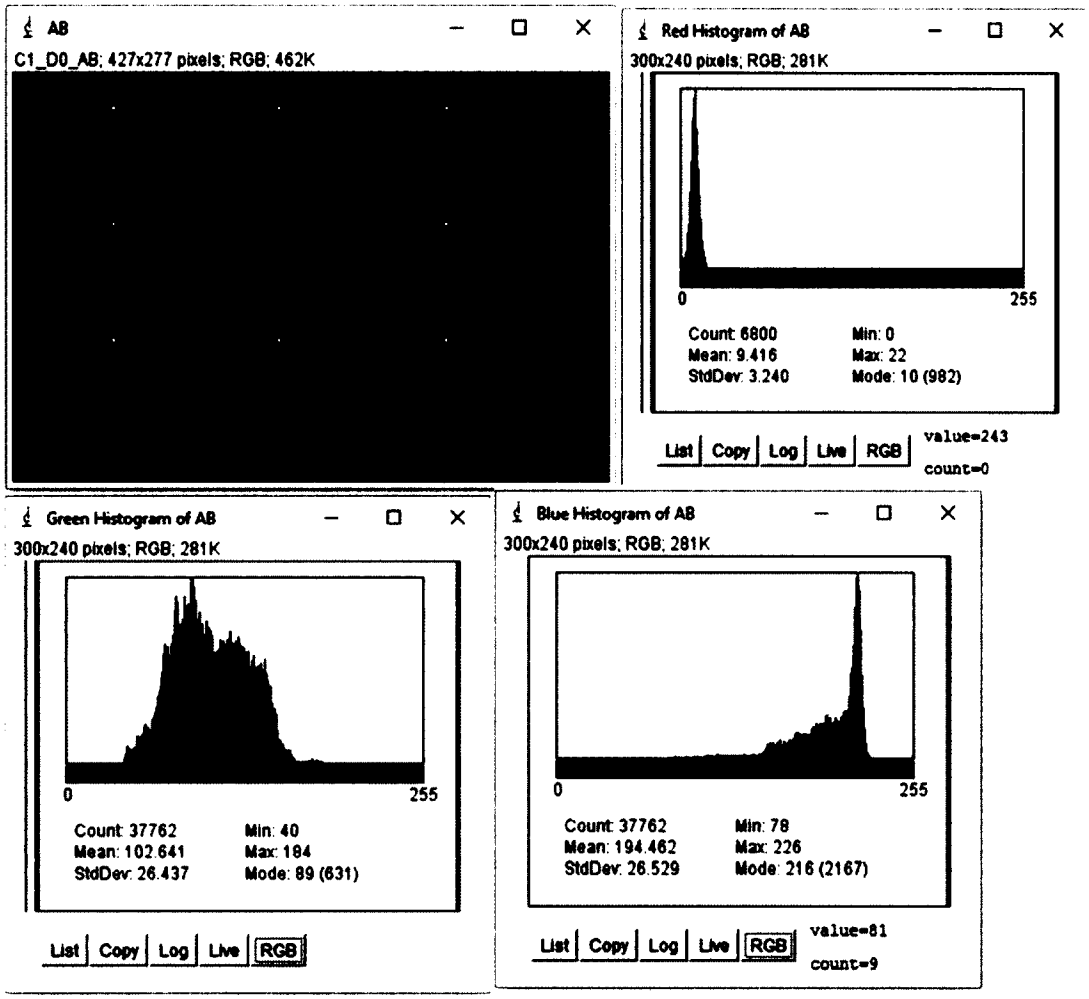

Figure 4-5. Image analysis for Alcian Blue staining Control 1 Day 0.

Figure 4-5 shows the RGB peaks for Alcian Blue staining for control 1 on day 0. The intensity for Blue and Red is towards the value 255 which is for white color. It implies that the Blue and Red are less intense in the given region of interest. This supports the observation from the qualitative visual analysis of the histological staining earlier suggesting less cell proliferation and low ECM production in the control 1 on day 0. Figure 4-6 shows RGB peaks for alginate-only hydrogel control (C1) for Day 21.

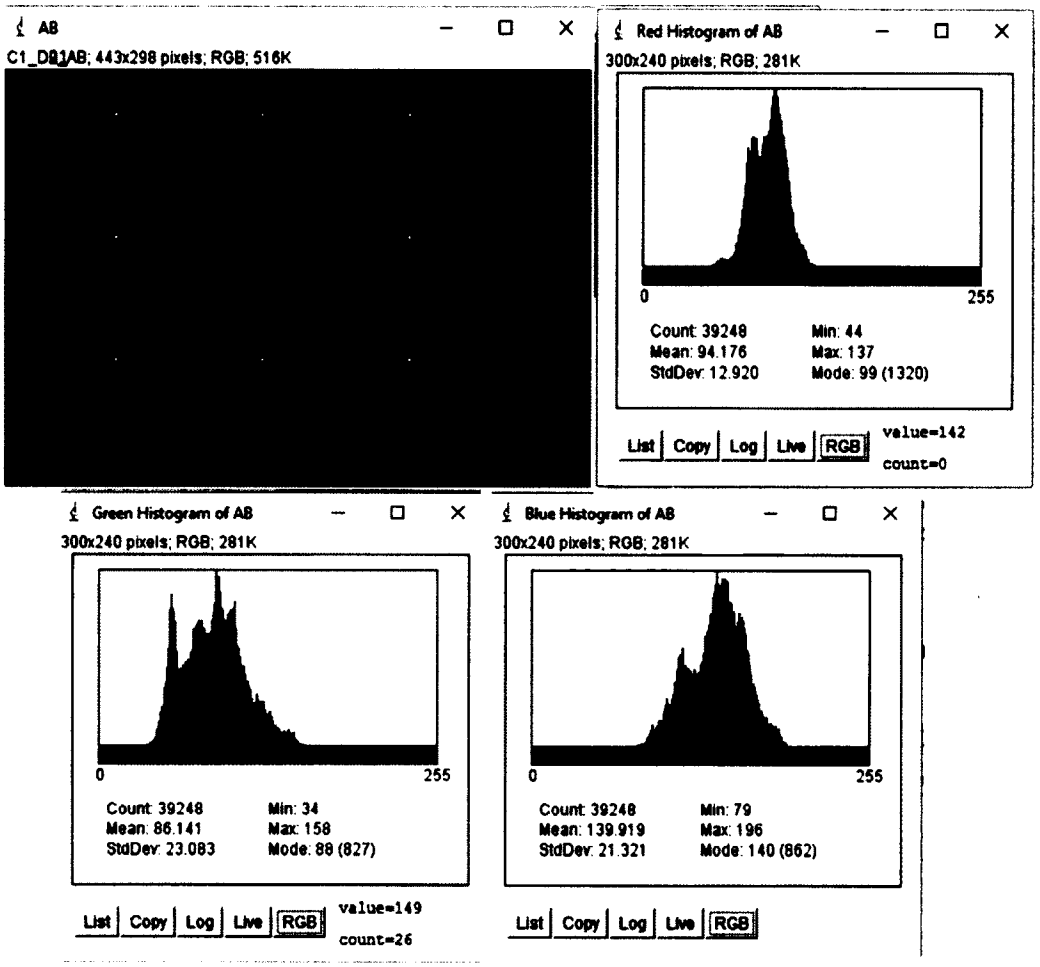

Figure 4-6. Image analysis for Alcian Blue staining Control 1 Day 21.

Figure 4-6 shows RGB peaks for Alcian Blue staining for control 1 on Day 21. The intensity for Blue falls in the range between the values 0 which is for Black and 255 which is for white color. This suggests that there is some production of ECM in the hydrogel matrix as observed in the earlier section on the histological analysis. The intensity for red falls near black suggesting more intense red staining indicating presence of proliferated cells. This observation supports the observations in the previous section suggesting that alginate-only hydrogels showed more cellular proliferation by Day 21 and very little ECM production. Figure 4-7 shows RGB peaks for alginate + HNTs hydrogel control (C2) for day 0.

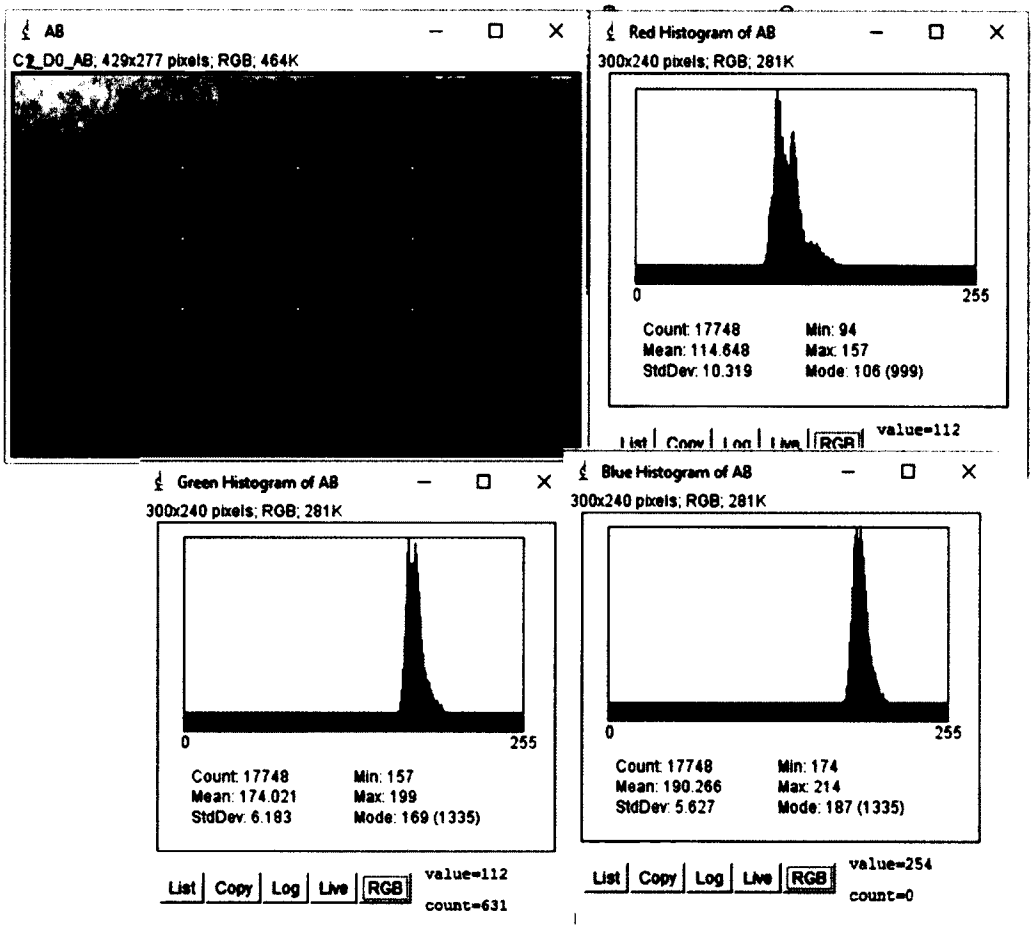

Figure 4-7. Image analysis for Alcian Blue staining Control 2 Day 0.

Figure 4-7 shows the RGB peaks for Alcian Blue staining for control 2 on day 0. The red color has intensity falling midway between the values for black color (0) and white color (255). Green and blue have intensities closer to white color suggesting a less intense staining. This suggests that the Red color is more intense in the region of interest suggesting more cell proliferation. This supports the observations in the previous section that control 2 has more cell proliferation and less ECM production. Figure 4-8 shows RGB peaks for alginate + HNTs hydrogel control (C2) for Day 21.

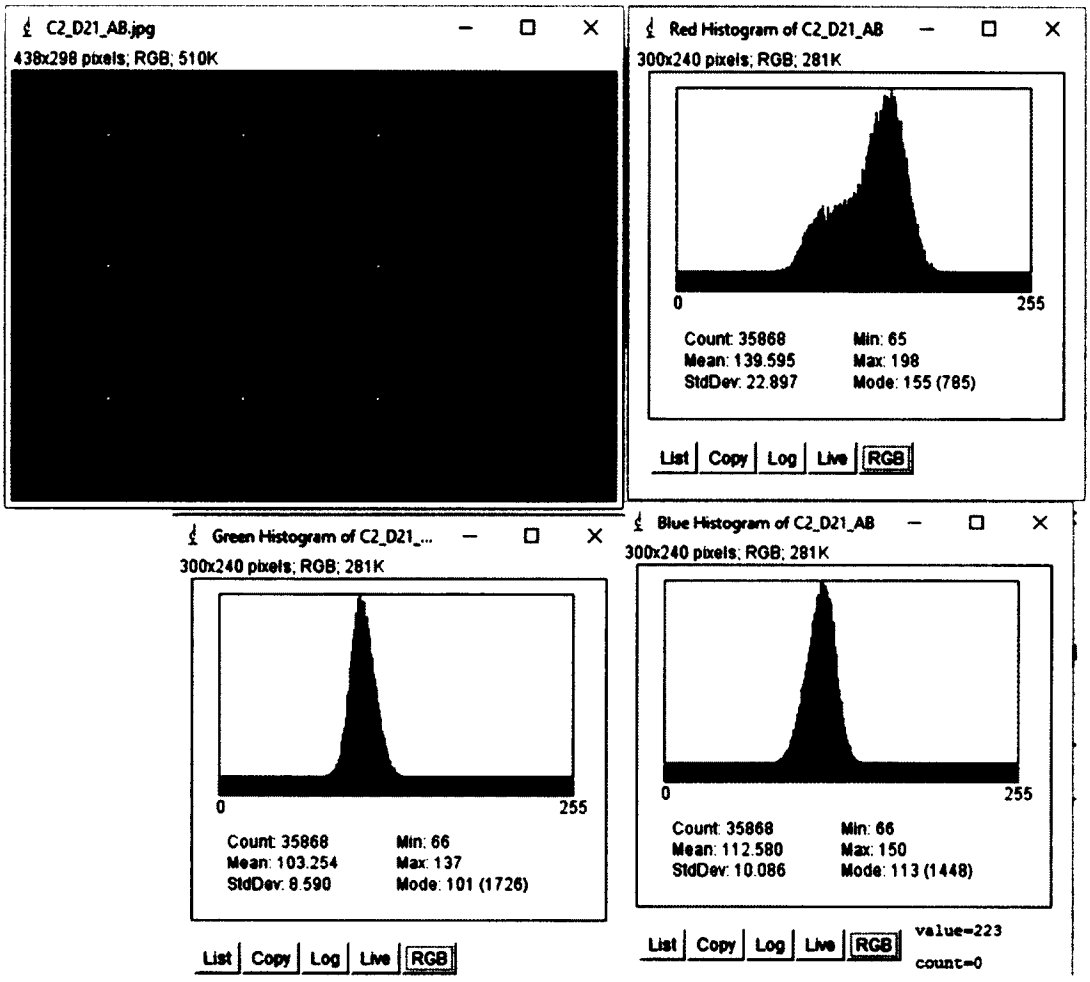

Figure 4-8. Image analysis for Alcian Blue staining Control 2 Day 21.

Figure 4-8 shows Alcian Blue staining for control 2 on Day 21. The red color shows intensity ranging over a broad range of values lying midway between the values for black (0) and white (255). This suggests that there is increased cell proliferation seen in the region of interest. The blue and green colors have intensity values at the midway but more towards black. This suggests that there is slight increase in the ECM production from day 0. This is supported by the observations in the earlier section suggesting that when compared to control 1 and day 0 there was slight increase in ECM production in

control 2 on Day 21. Figure 4-9 shows RGB peaks for Alginate + HNTs + BMP 2 hydrogel experimental (E1) for day 0.

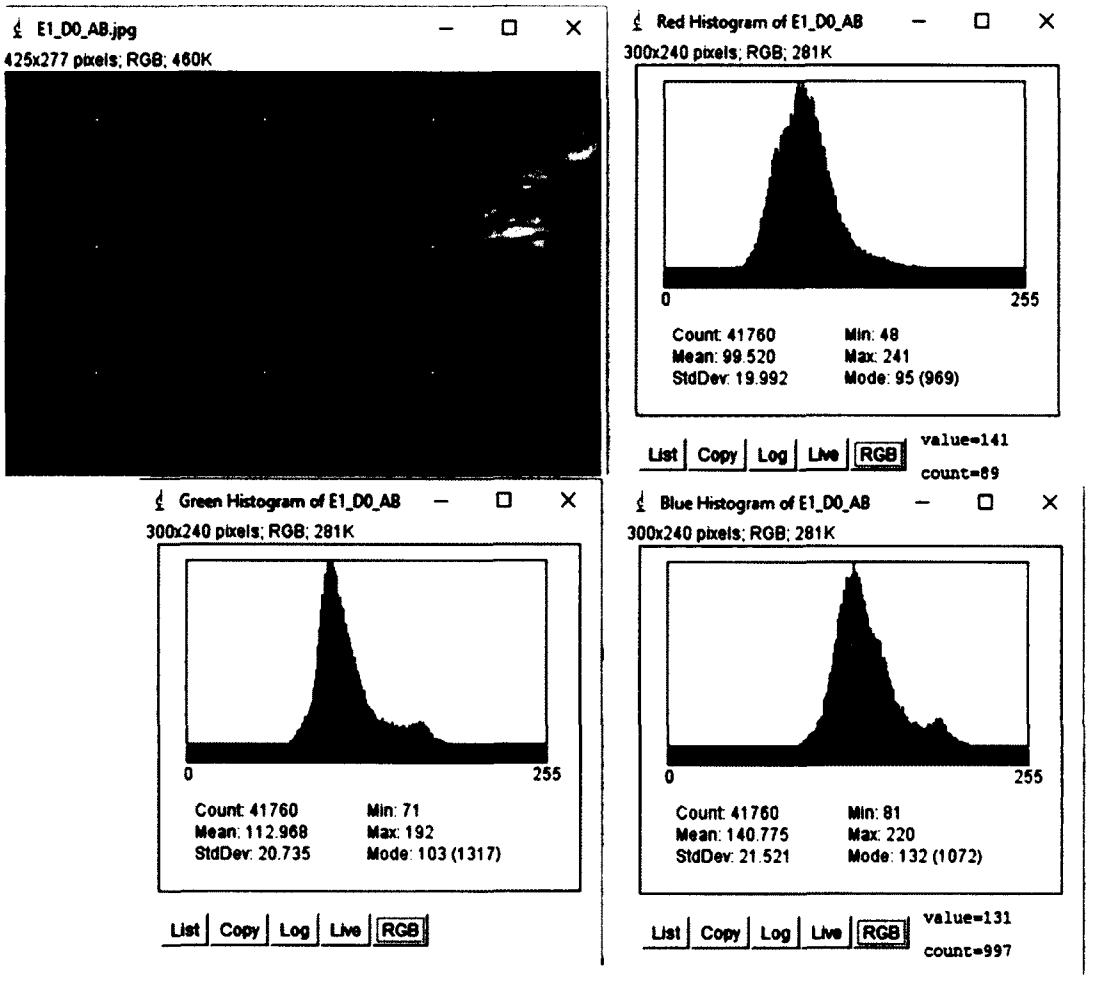

Figure 4-9. Image analysis for Alcian Blue staining Experimental 1 Day 0.

Figure 4-9 shows RGB peaks for Alcian Blue staining of experimental 1 on day 0. All the three colors show peaks that are well pronounced and lie slightly towards black. This suggests that there is fair amount of cell proliferation and some ECM production in the experimental 1 on day 0. This observation is also substantiated in the earlier section. Figure 4-10 shows RGB peaks for alginate + HNTs + BMP 2 hydrogel experimental (E1) for Day 21.

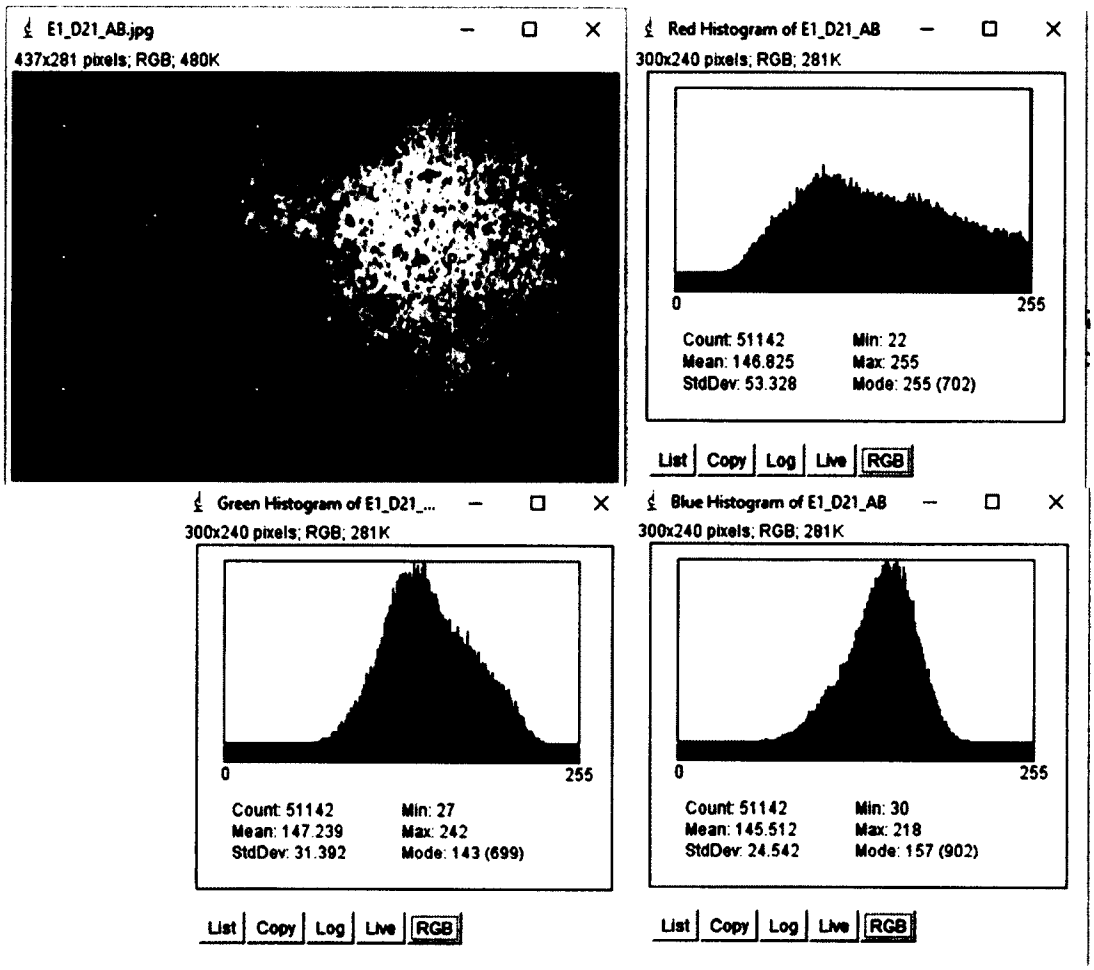

Figure 4-10. Image analysis for Alcian Blue staining Experimental 1 Day 21.

Figure 4-10 shows RGB peaks for Alcian Blue staining for experimental 1 on Day 21. All the three colors show broad range of values for intensities. Especially red that ranges from value near black (0) to white (255). This suggests that there is more cell proliferation as well as ECM production suggested by the intense staining in red and blue. Figure 4-11 shows RGB peaks for alginate + HNTs + BMP 4 hydrogel experimental (E3) for day 0.

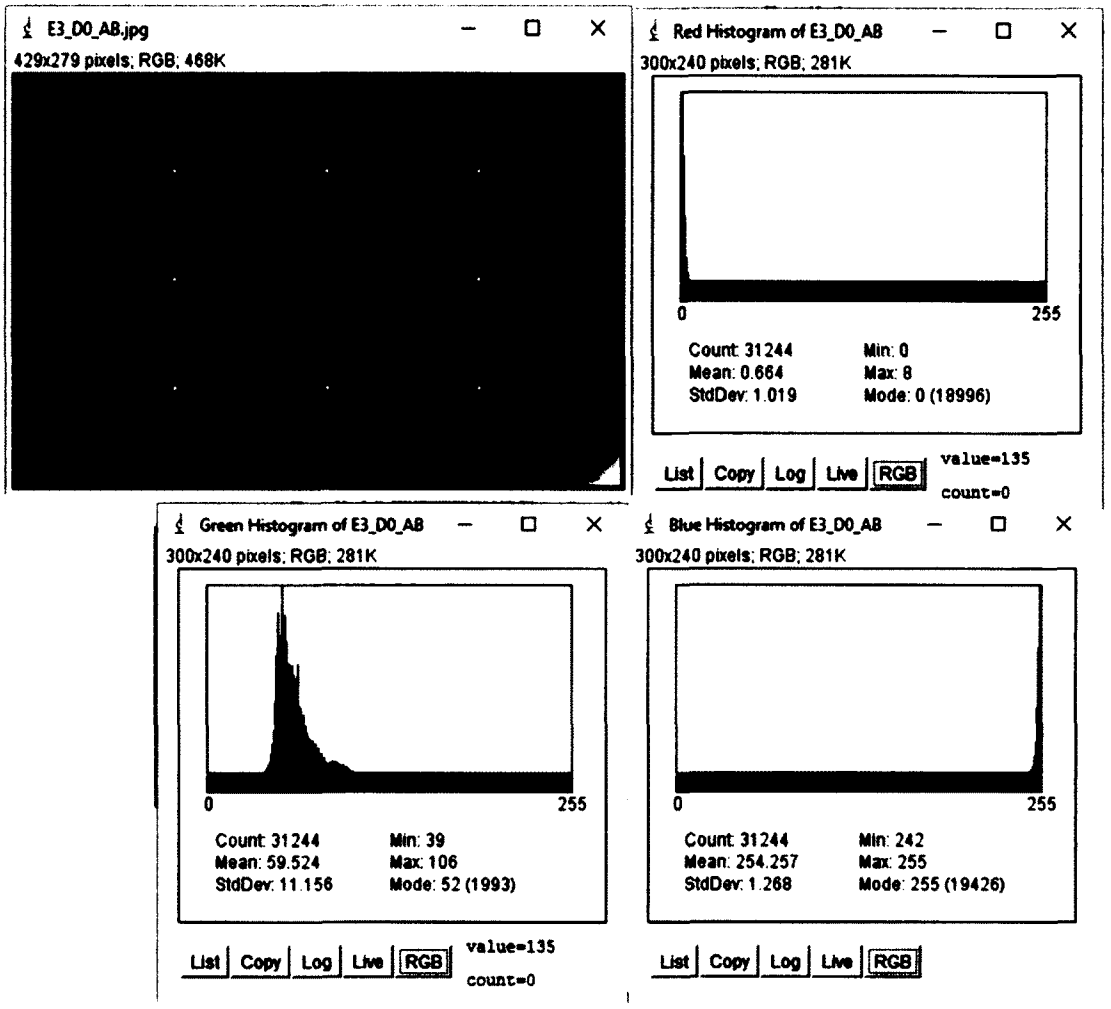

Figure 4-11. Image analysis for Alcian Blue staining Experimental 3 Day 0.

Figure 4-11 shows RGB peaks for Alcian Blue staining for experimental 3 on day 0. There is an intense red staining suggested by the sharp red peak falling on the value 0 for black color. There is very less intense blue color suggested by the blue peak lying on the value 255 for white color. This suggests that there is cell proliferation but little to no ECM production. Figure 4-12 shows RGB peaks for alginate + HNTs + BMP 4 hydrogel experimental (E3) for Day 21.

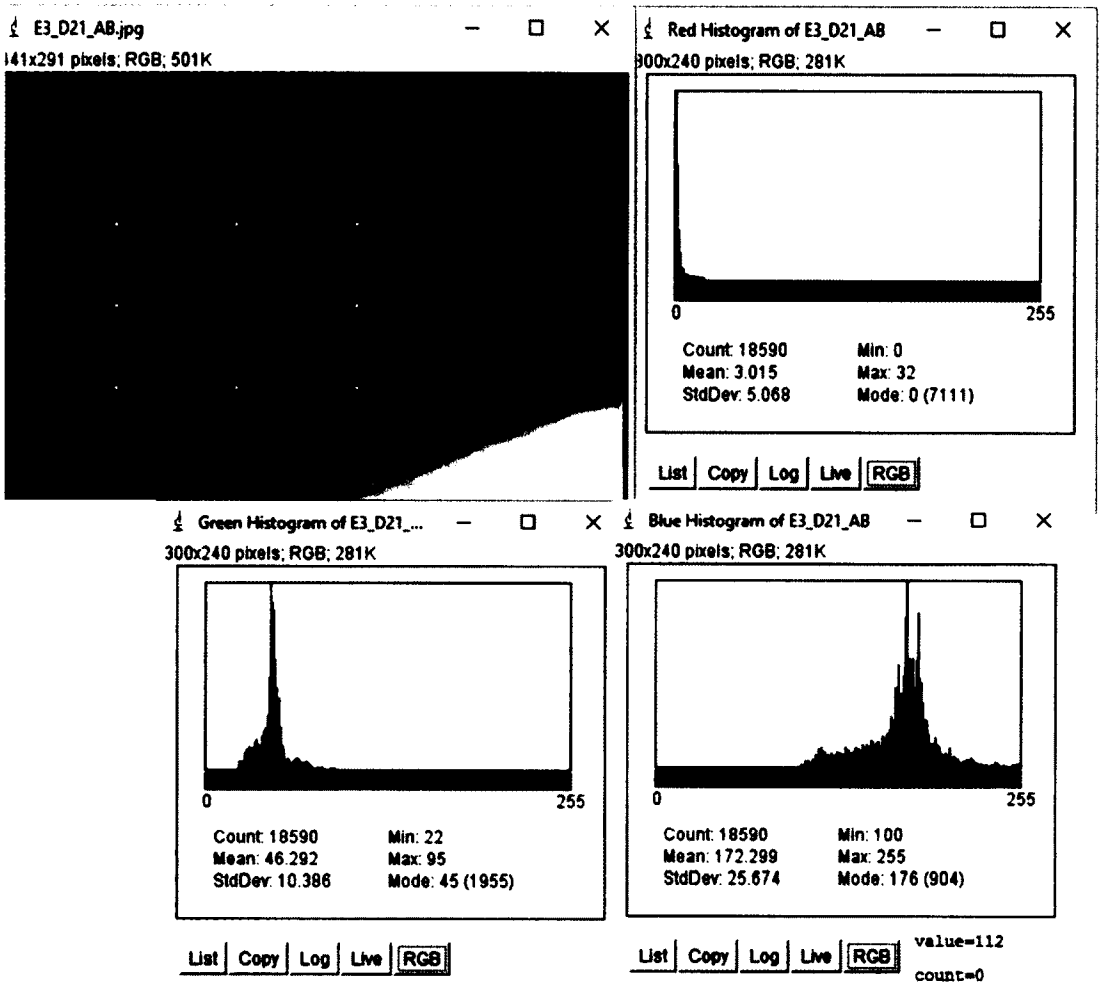

Figure 4-12. Image analysis for Alcian Blue staining Experimental 3 Day 21.

Figure 4-12 shows RGB peaks for Alcian Blue staining for experimental 3 on Day 21. As seen in the graph for red color the peak shows intense red staining suggesting a high cell proliferation. The blue color also has intensity increased from day 0 suggesting increased ECM production. These observations are supported by the observations made in the previous section that the ECM production increased as the days progressed in experimental 3. Figure 4-13 shows RGB peaks for alginate + HNTs + BMP62 hydrogel experimental (E4) for day 0.

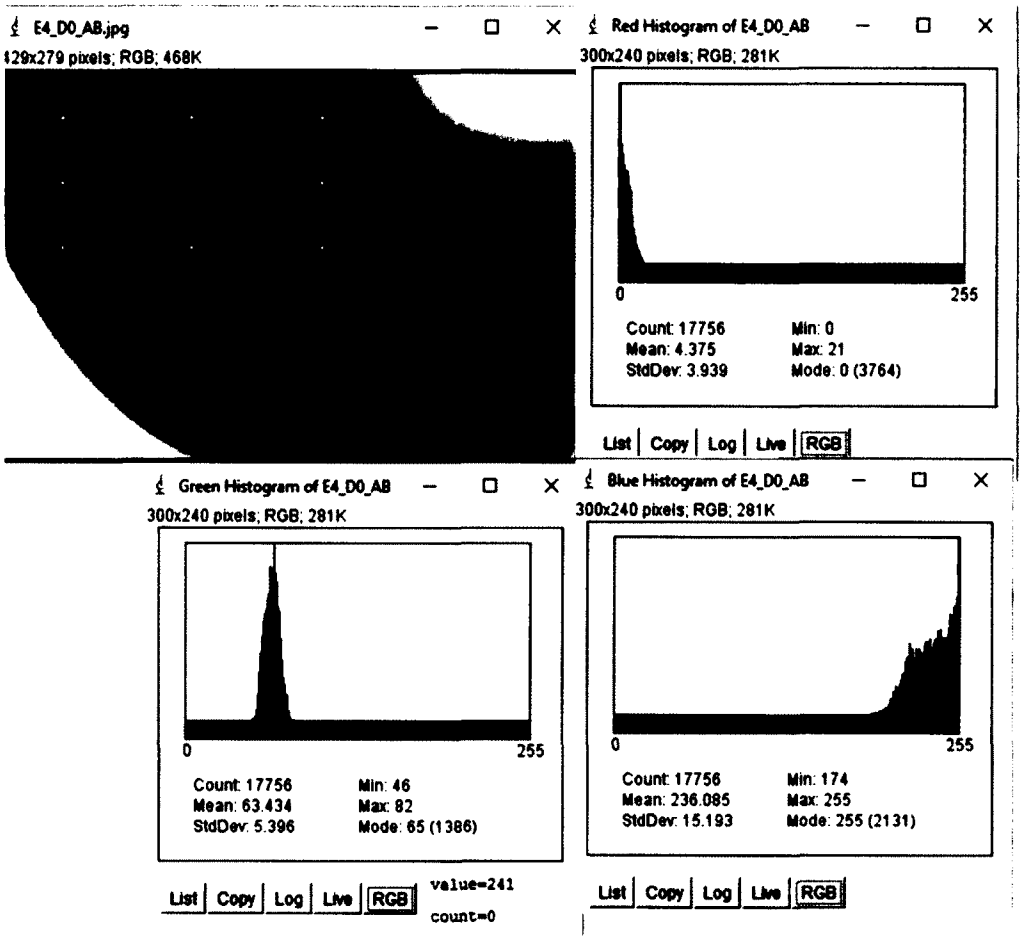

Figure 4-13. Image analysis for Alcian Blue staining Experimental 4 Day 0.

Figure 4-13 shows RGB peaks for Alcian Blue staining for experimental 4 on day 0. Red has more intense staining in the region of interest suggesting high cell proliferation and blue has very less intensity suggesting little ECM production on day 0. This observation is supported in the previous section which showed little ECM production in the experimental 4 on day 0. Figure 4-14 shows RGB peaks for alginate + HNTs + BMP62 hydrogel experimental (E4) for Day 21.

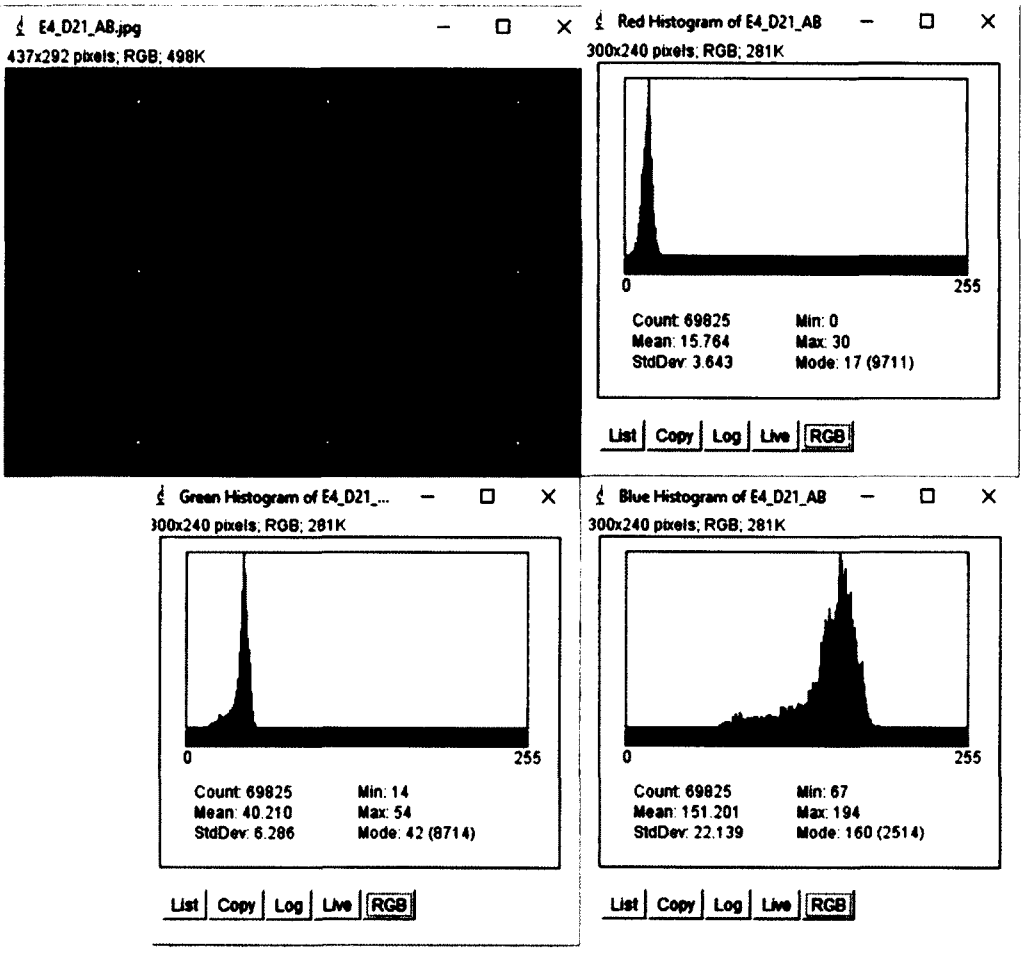

Figure 4-14. Image analysis for Alcian Blue staining Experimental 4 Day 21.

Figure 4-14 shows RGB peaks for Alcian Blue staining for experimental 4 on Day 21. The red has intense staining but it has reduced since day 0 and the intensity for blue has increased suggesting retardation in the cell proliferation and increase in ECM production supported by the observations in the previous section suggesting an increase in the ECM production since day 0 in experimental 4.

These representative image analysis results support the earlier observations made suggesting that the addition of HNTs and BMPs 2, 4, and 6 improved ECM production and emhanced cellular differentiation in these constructs when compared to the controls 1 and 2 form days 0 to 21.

4.3.1.2 *Picrosirius Red staining.* The Picrosirius Red staining helps to visualize the collagen secreted by the differentiating cells as a result of laying foundation of the new tissue. Collagen is the most abundant substance in connective tissues. [45] It gives the tissues their elasticity and maintains their structural integrity. [45] Figures 4-5 to 4-8 show the Picrosirius Red staining of the alginate hydrogels enhanced with BMP 2, 4, and 6 loaded HNTs with osteoblasts encapsulated in them for days 0, 7, 14, and 21. The figures are representative and show the days that highlight the trend of progression of differentiation and production of collagen as a part of new tissue formation. Figure 4-15 (A-F) shows the Picrosirius Red staining for day 0.

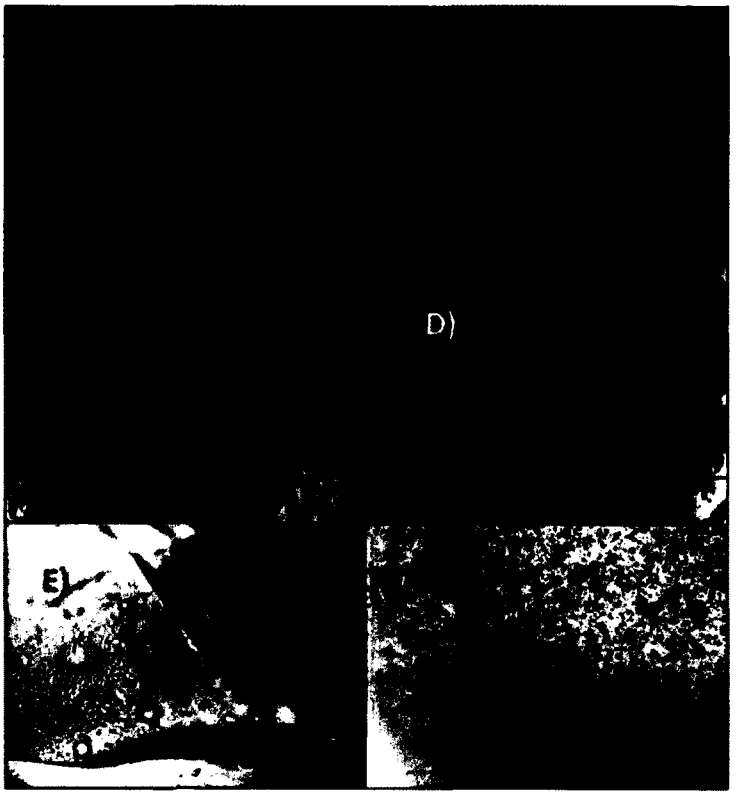

Figure 4-15. Picrosirius Red staining Day 0 A) Control 1 Alginate-only B) Control 2 Alginate + HNTs C) Experimental 1 Alginate+ HNTs+ BMP 2 D) Experimental 2 Alginate+ HNTs+ BMP 2 with 0.4M Ascorbate E) Experimental 3 Alginate+ HNTs+ BMP 4 F) Experimental 4 Alginate+ HNTs+ BMP 6.

In Figure 4-15, Controls 1 and 2 (A and B) show dark spots of cells. Control 2 (B) shows deeper staining as compared to control 1 (A). Experimental groups 1, 2, 3, and 4 (C-F) show dark patches of cells surrounded by red stained gel matrix containing collagen. Experimental 2 (D), shows larger cell patches suggesting that more cells proliferated compared to the other experimental groups, (C, E, and F). The experimental groups 1 and 2 show deep red staining suggesting that the collagen secretion was more compared to the experimental groups 3 and 4 (E and F). Figure 4-16 (A-F) shows Picrosirius Red staining for Day 7.

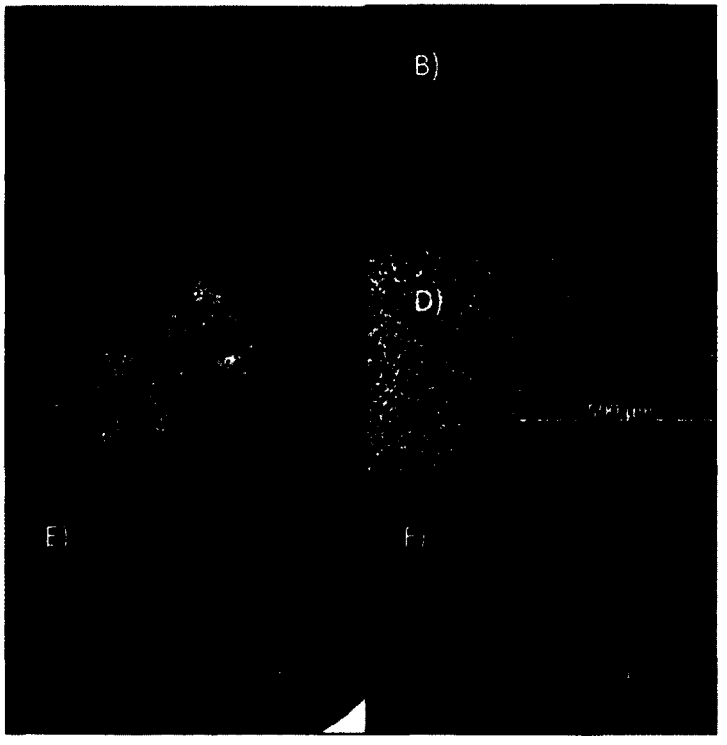

Figure 4-16. Picrosirius Red staining Day 7 A) Control 1 Alginate-only B) Control 2 Alginate + HNTs C) Experimental 1 Alginate+ HNTs+ BMP 2 D) Experimental 2 Alginate+ HNTs+ BMP 2 with 0.4M Ascorbate E) Experimental 3 Alginate+ HNTs+ BMP 4 F) Experimental 4 Alginate+ HNTs+ BMP 6.

In Figure 4-16, Controls 1 and 2 (A and B) show dark spots of proliferated cells and collagen which is stained in red. The amount of collagen that is produced by the cells

is more compared to Day 0. Experimental groups #1, 2, 3, and 4 (C-F) show more proliferation of the cells as dark patches are more numerous compared to Day 0. Experimental groups #2, 3, and 4 (D, E, and F) show deeper staining with Picrosirius Red suggesting more collagen production as the days advance. The staining of the experimental groups #2, #3, and #4 (D, E, and F) is darker than the controls indicating that the hydrogels with BMP 2 and ascorbate, BMP 4 and BMP 6 were performing better with respect to collagen secretion against the controls. Figure 4-17 (A-F) shows Picrosirius Red staining for Day 14.

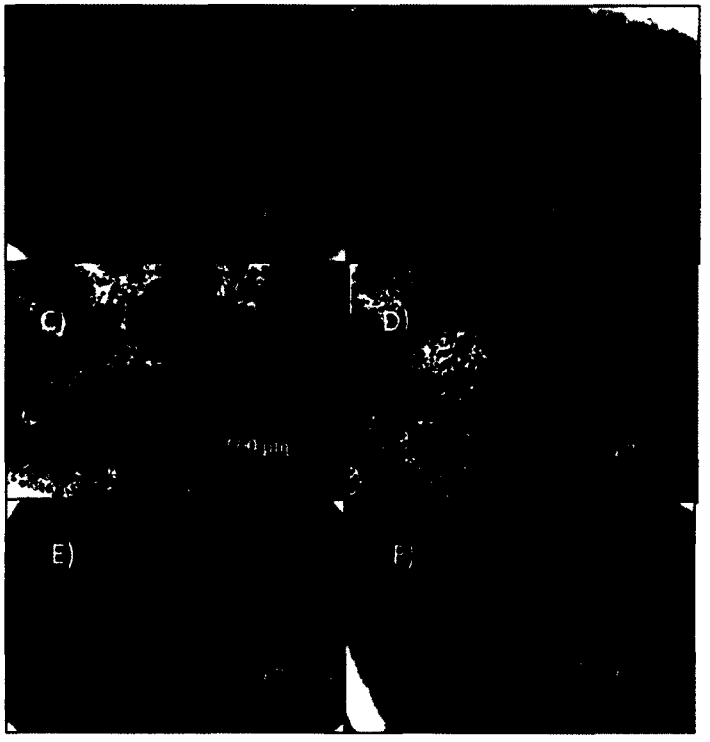

Figure 4-17. Picrosirius Red staining Day 14 A) Control 1 Alginate-only B) Control 2 Alginate+ HNTs C) Experimental 1 Alginate+ HNTs+ BMP 2 D) Experimental 2 Alginate+ HNTs+ BMP 2 with 0.4M Ascorbate E) Experimental 3 Alginate+ HNTs+ BMP 4 F) Experimental 4 Alginate+ HNTs+ BMP 6.

In Figure 4-17, controls 1 and 2 (A and B) show deep red staining compared to days 0 and 7. The experimental groups #1, #2, #3, and #4 (C-F) show deeper staining

with experimental groups #3 and #4 (E and F) showing a uniform and dark staining. This suggests that as the days progressed, collagen production increased with collagen secretion being more uniformly distributed in experimental groups #3 and #4 (E and F). Experimental groups #1 and #2 (C and D) show more dark patches of cell compared to group #3 and #4 (E and F). Based on the deep stained gel matrix in experimental groups #3 and# 4, it can be inferred that the cell patches were not visible because of larger amounts of collagen being produced by the differentiating cells. Figure 4-18 shows Picrosirius Red staining for Day 21.

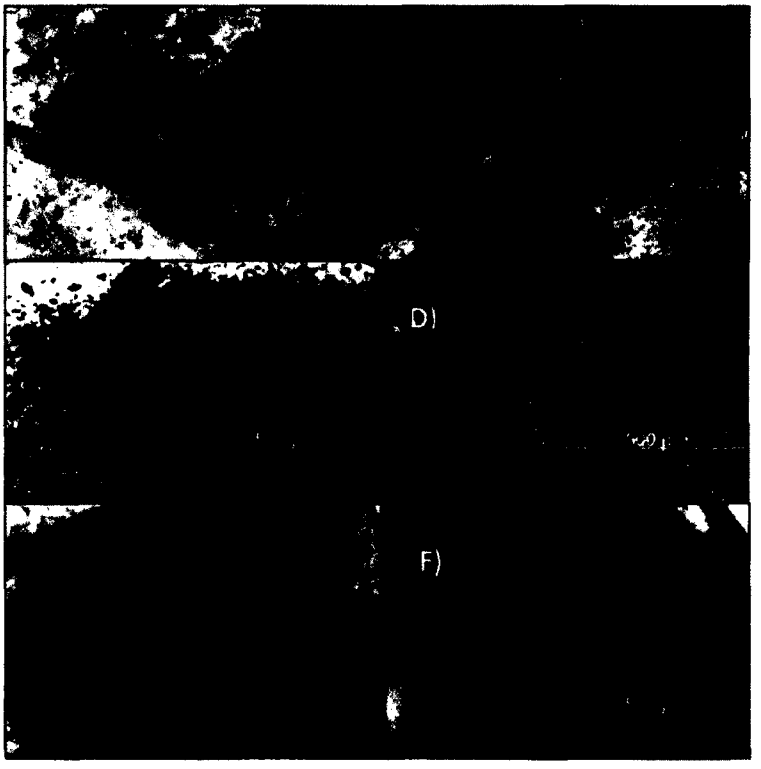

Figure 4-18. Picrosirius Red staining Day 21 A) Control 1 Alginate-only B) Control 2 Alginate + HNTs C) Experimental 1 Alginate+ HNTs+ BMP 2 D) Experimental 2 Alginate+ HNTs+ BMP 2 with 0.4M Ascorbate E) Experimental 3 Alginate+ HNTs+ BMP 4 F) Experimental 4 Alginate+ HNTs+ BMP 6.

In Figure 4-18, controls 1 and 2 (A and B) show lighter staining compared to experimental groups #1-#4 (C-F). A comparison of all the groups reveals that the collagen production is at its peak on Day 7. The experimental group #4 (F) shows the most collagen amongst all the groups (A-E) on Day 21. All the experimental groups show large cell patches surrounded by collagen they produced.

Comparison of the experimental groups #1-#4 (C-F) with controls 1 and 2 (A and B) throughout all days, suggests that there was a marked difference in the cellular response with respect to collagen production by the experimental groups. The cellular proliferation and differentiation was more compared to the experimental groups on all days except Day 7. The difference in the collagen production by the experimental groups throughout the 21-day period might be the influence of the growth factors (BMP 2, 4, and 6) loaded in HNTs. There was also an early onset of collagen production on Day 0 (8 hours after cellular encapsulation in the hydrogels) in the experimental groups suggesting collagen production starts early in the hydrogels with growth factor loaded HNTs against the controls. This may be important as it would trigger faster bone regeneration by enhanced and early cell differentiation response.

The observations made by visual qualitative analysis of the Picrosirius Red stained sections of hydrogels can be further ascertained by image analysis done by Image J software. The representative images of Controls 1 & 2 and the experimental groups E1, E 3, and E4 for days 0 and 21 are given in Figure 4-19 to 4-28. Figure 4-19 shows RGB peaks for alginate-only hydrogel control (C1) for day 0.

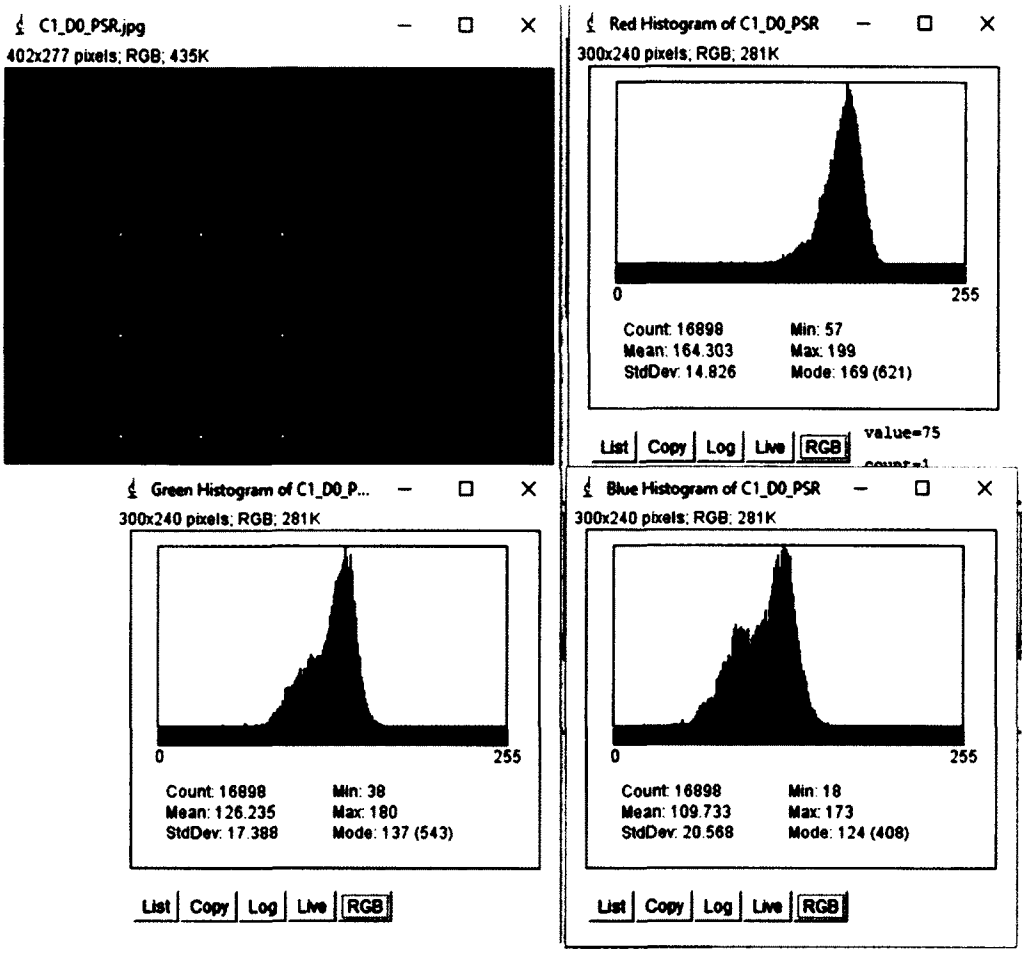

Figure 4-19. Image analysis for Picrosirius Red staining for Control 1 Day 0.

Figure 4-19 shows RGB peaks for Picrosirius Red staining for control 1 on day 0. The intensity for red color is less as can be seen in the graph for red color. The colors green and blue show intensities of similar values suggesting that not much red stain present in the region of interest which means that the collagen production is very less. This is expected on day 0 of the staining and is also supported in the observations made in the earlier sections. Figure 4-20 shows RGB peaks for alginate-only hydrogel control (C1) for Day 21.

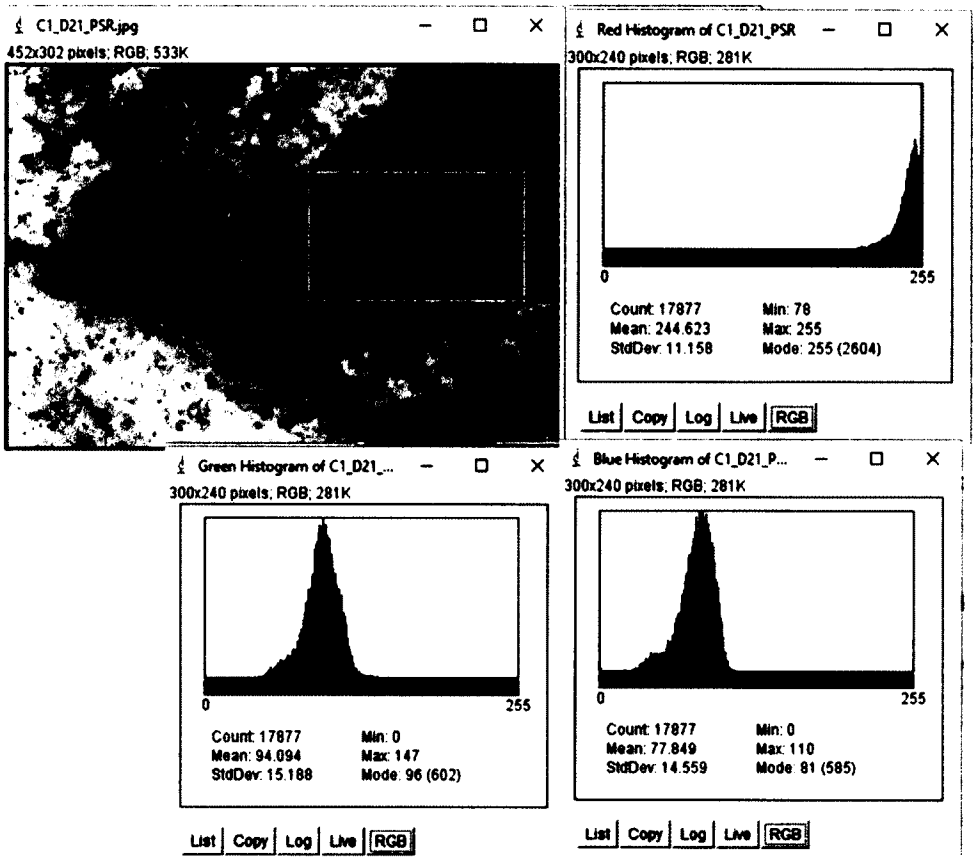

Figure 4-20. Image analysis for Picrosirius Red staining for Control 1 Day 21.

Figure 4-20 shows RGB peaks for Picrosirius Red staining for control 1 on Day 21. The red color has a very low intensity and the colors blue and green are more intense. This suggests that the cellular proliferation is more and collagen production is very less in control 1 on Day 21. This observation is supported by the observations in the previous section suggesting that the collagen production remains low in control 1 on Day 21. Figure 4-21 shows RGB peaks for alginate + HNTs hydrogel control (C2) for day 0.

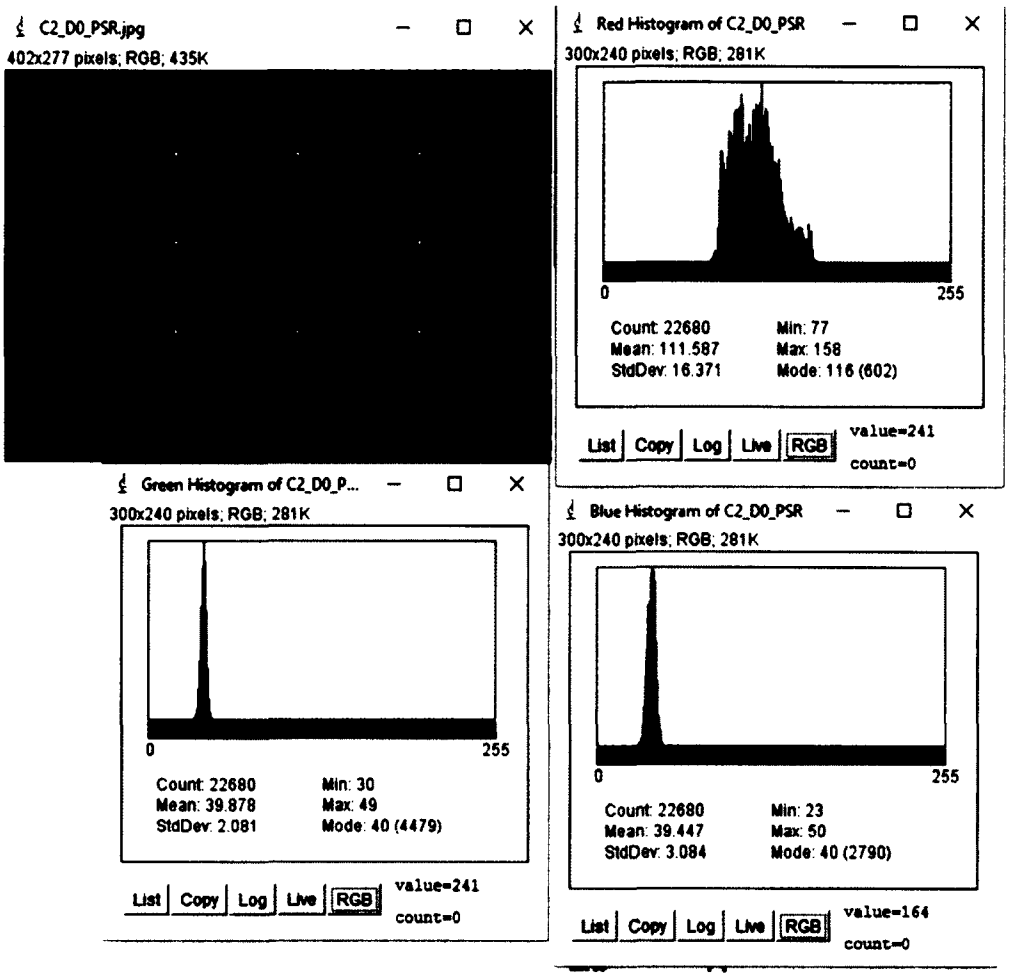

Figure 4-21. Image analysis for Picrosirius Red staining for Control 2 Day 0.

Figure 4-21 shows Picrosirius Red staining for control 2 on day 0. All the three colors show intense staining in the section and this might be due to the section being thick and appearing darker. The high intensity of red in this section does not suggest high collagen production. This inference can be drawn by taking into consideration other constructs and the behavior of control 2 over advancing days. Figure 4-22 shows RGB peaks for alginate + HNTs hydrogel control (C2) for Day 21.

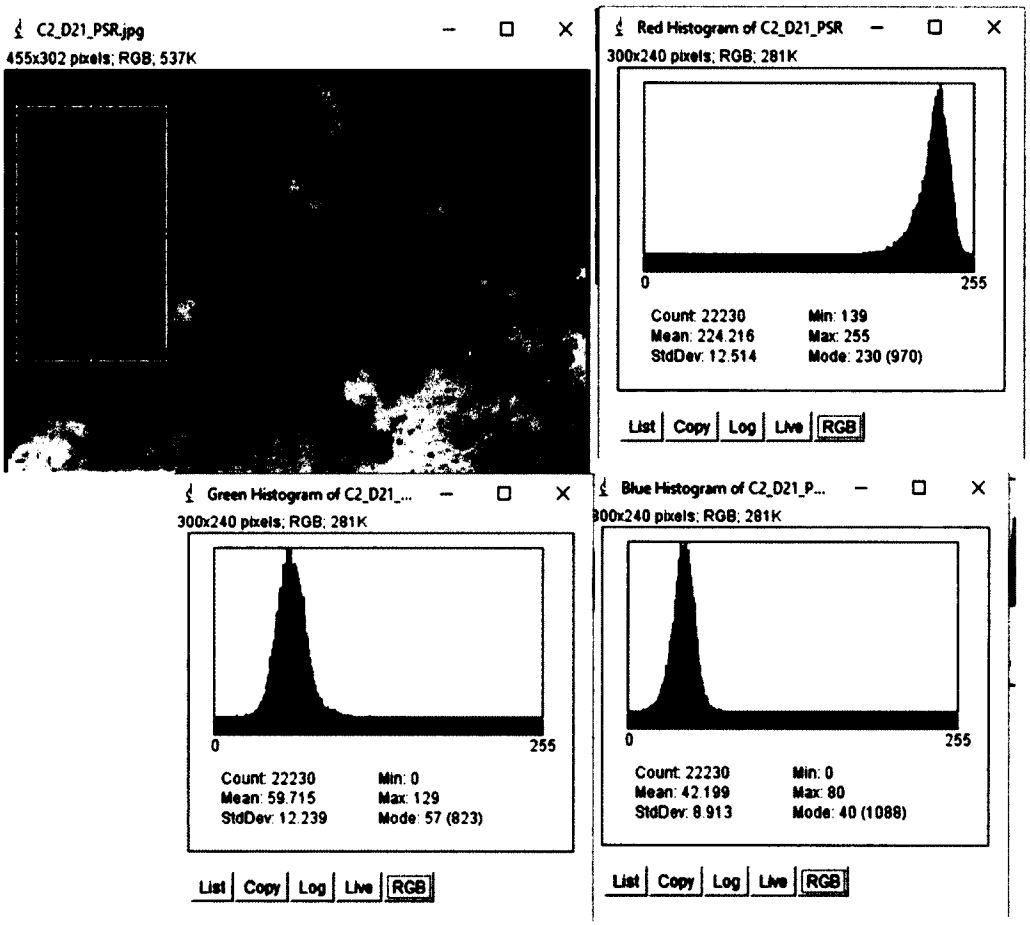

Figure 4-22. Image analysis for Picrosirius Red staining for Control 2 Day 21.

Figure 4-22 shows RGB peaks for Picrosirius Red staining for control 2 on Day 21. The red color shows less intense staining and this suggests less collagen production over a period of 21 days. This observation can also be supported by looking at the previous section images for control 2 for 21 day period. Figure 4-23 shows RGB peaks for alginate + HNTs + BMP 2 experimental (E1) for day 0.

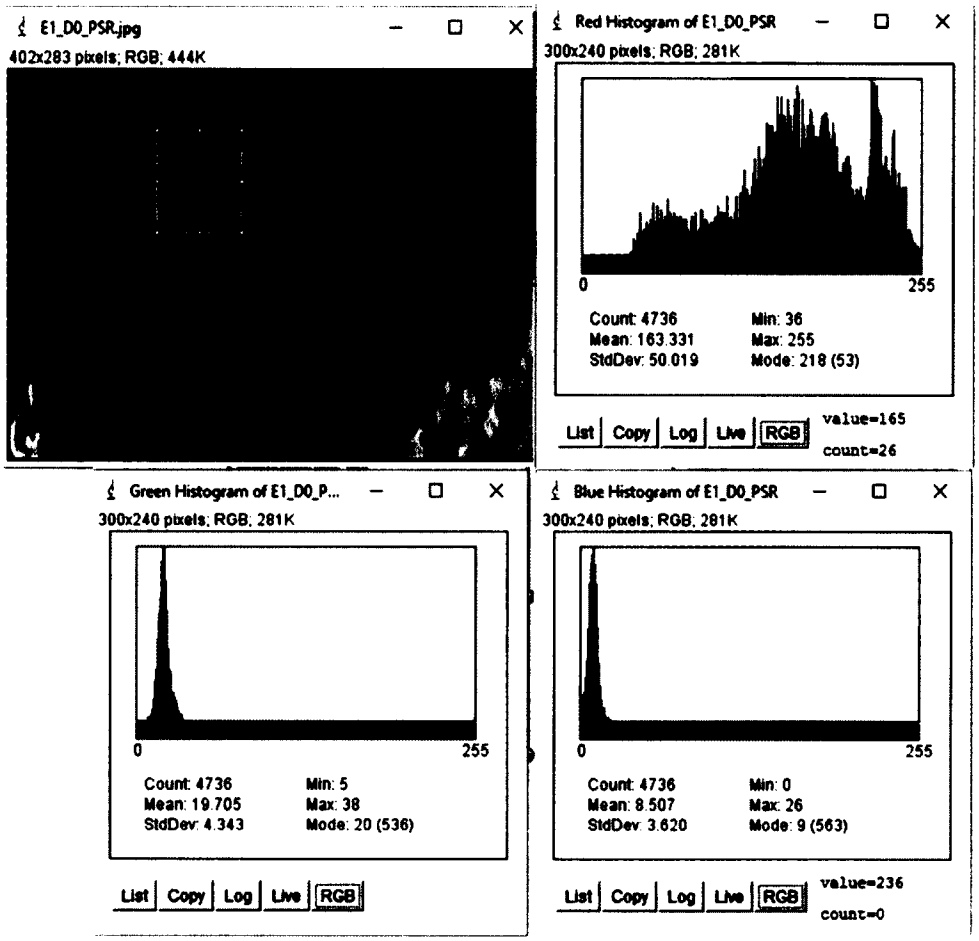

Figure 4-23. Image analysis for Picrosirius Red staining for Experimental 1 Day 0.

Figure 4-23 shows RGB peaks for Picrosirius Red staining for experimental 1 on day 0. The peak for red shows a lot of noise and this might be due to the section being uneven. The intensity for red is still higher than the controls 1 and 2 on day 0. This suggests that the collagen production has already started in the experimental 1 on day 0. This observation supports the inference from the previous section that there is early onset of cellular differentiation in the experimental set 1. Figure 4-24 shows RGB peaks for alginate + HNTs + BMP 2 experimental (E1) for Day 21.

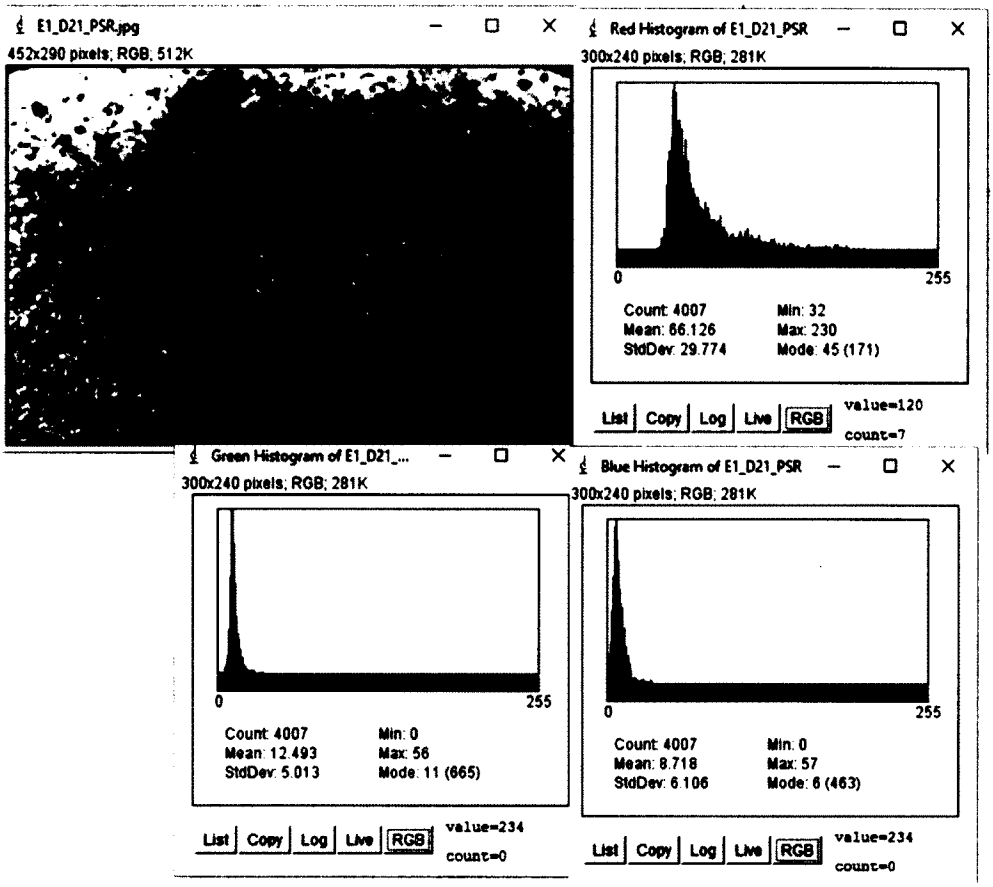

Figure 4-24. Image analysis for Picrosirius Red staining for Experimental 1 Day 21.

Figure 4-24 shows RGB peaks for Picrosirius Red staining for experimental 1 on Day 21. The region of interest here is a dense patch which might be cellular mass secreting collagen. The high red intensity might indicate high collagen secretion. The intensities are also high for green and blue colors and that might be due to the thick mass. The observations are in congruence with the observations from the previous section suggesting high collagen production in experimental 1 for a 21 day period. Figure 4-25 shows RGB peaks for alginate + HNTs + BMP 4 experimental (E3) for day 0.

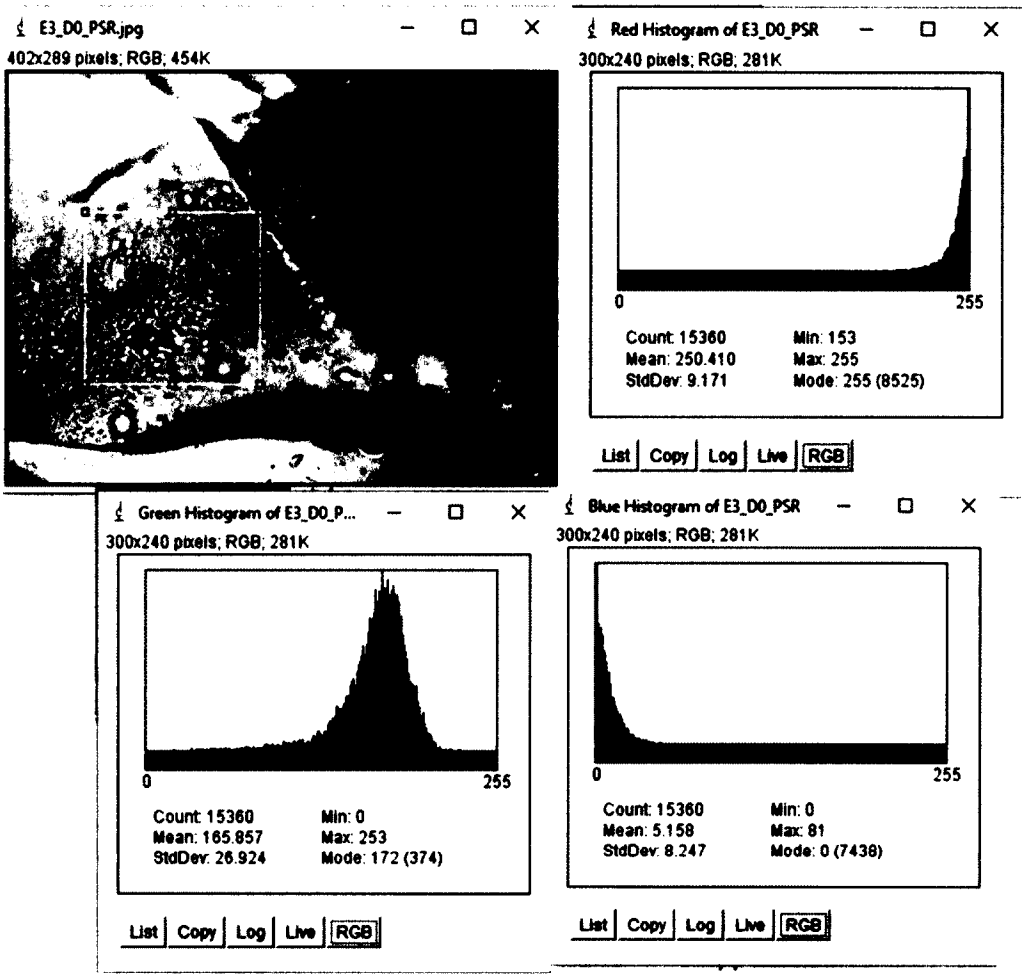

Figure 4-25. Image analysis for Picrosirius Red staining for Experimental 2 Day 0.

Figure 4-25 shows RGB peaks for Picrosirius Red staining for experimental 2 on day 0. There is a high intensity blue color and also a pronounced green color for the region of interest. The red color has the least intensity suggesting that the collagen secretion is low on day 0. The different intensity values for green and blue colors might be due to the uneven sectioning. Figure 4-26 shows RGB peaks for alginate + HNTs + BMP 4 experimental (E3) for Day 21.

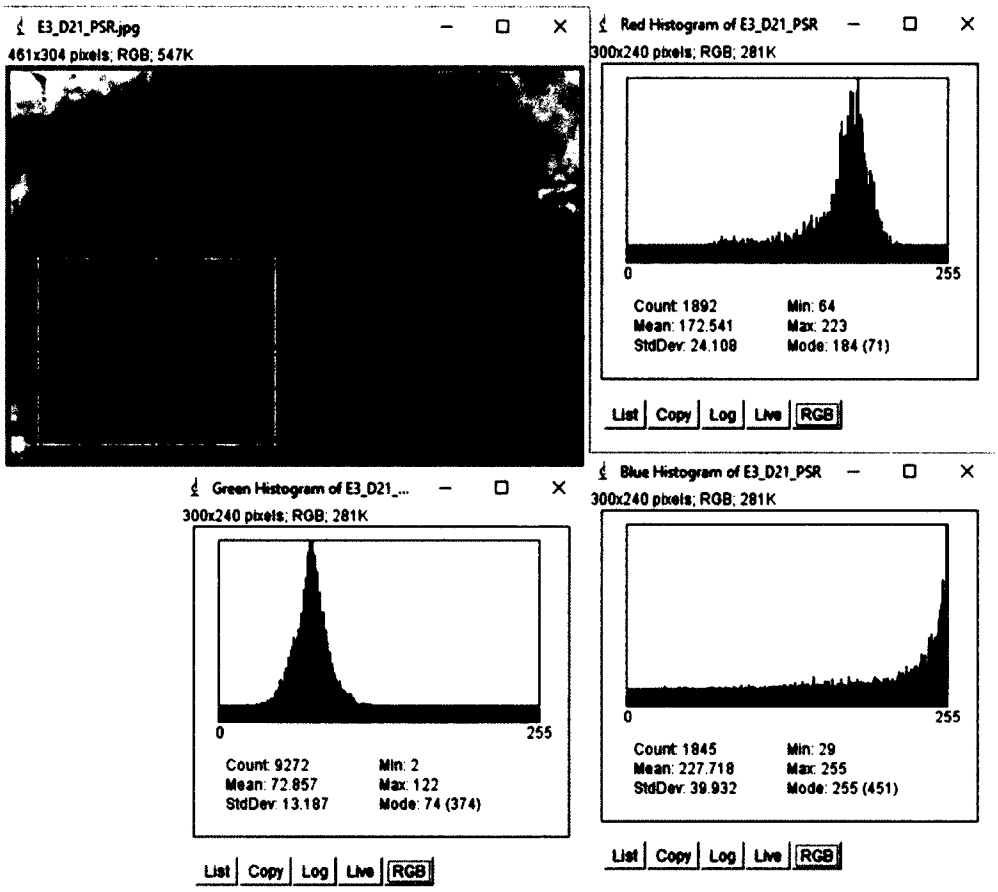

Figure 4-26. Image analysis for Picrosirius Red staining for Experimental 3 Day 21.

Figure 4-26 shows RGB peaks for Picrosirius Red staining for experimental 3 on Day 21. The intensity for green is high and red also has relatively higher intensity suggesting an increased collage production over 21 day period. This observation is supported by the observations in the previous section that the collagen production in experimental 3 increased from day 0 to Day 21. Figure 4-27 shows RGB peaks for alginate + HNTs + BMP 6 experimental (E4) for day 0.

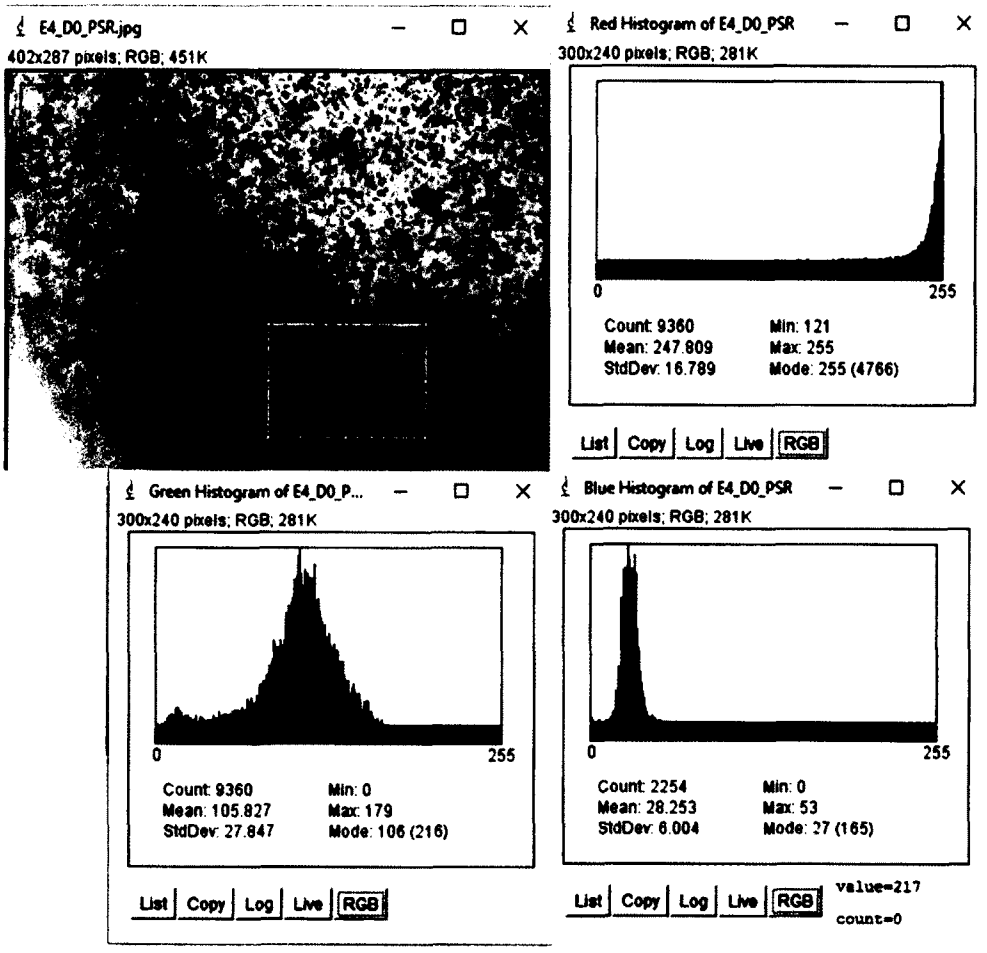

Figure 4-27. Image analysis for Picrosirius Red staining for Experimental 4 Day 0.

Figure 4-27 shows RGB peaks for Picrosirius Red staining for experimental 4 on day 0. The region of interest shows a red colored dense patch however, the red color has low intensity as can be seen in the graph for red. The intensities are high for green and blue suggesting the density of the region being high. This might be due to sectioning or due to collagen deposition. A high intensity green staining for Picrosirius Red is also an indicator for deposition of collagen type III. But it needs further investigation to find out which type of collagen is being deposited in the hydrogel matrix. Figure 4-28 shows RGB peaks for alginate + HNTs + BMP 6 experimental (E4) for Day 21.

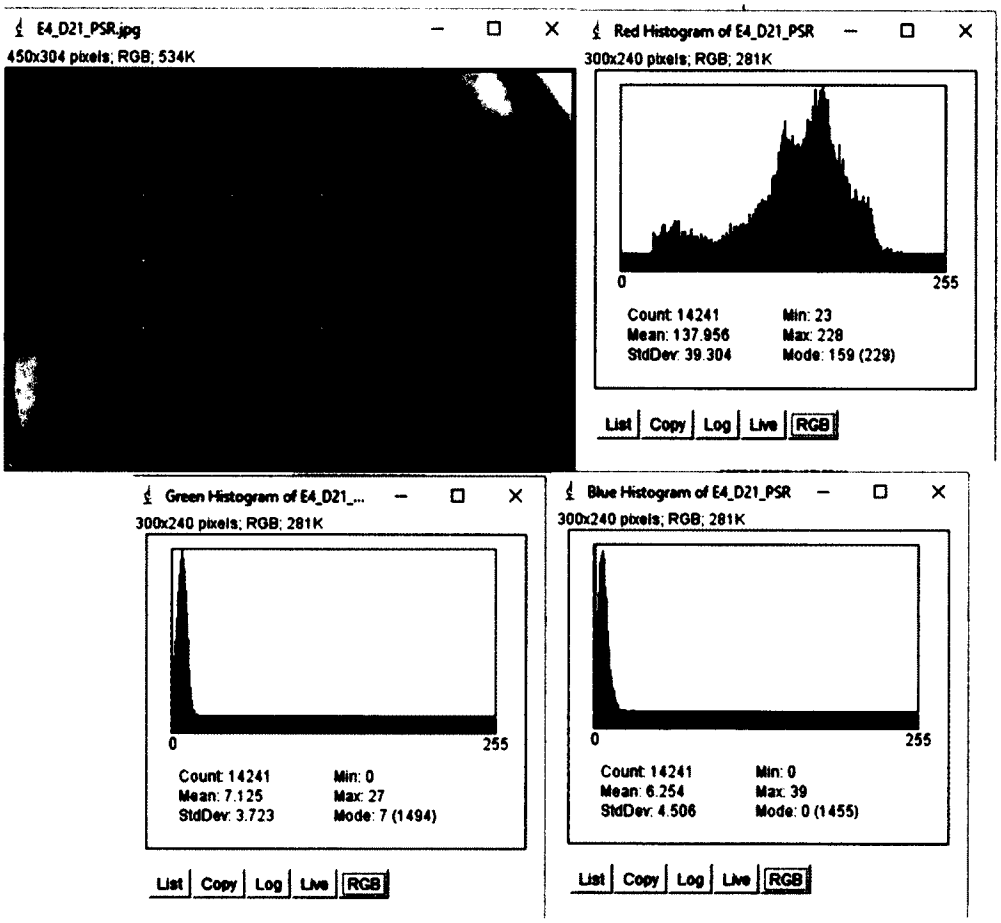

Figure 4-28. Image analysis for Picrosirius Red staining for Experimental 4 Day 21.

Figure 4-28 shows RGB peaks for Picrosirius Red staining for experimental 4 on Day 21. The region of interest shows intensity for red is scattered and it might be due to an uneven section or presence of dense bodies of cellular material. The intensities for green and blue are also high and this might be indication of presence of dense material in the selected area. This observation is supported by the observations in the previous section suggesting high amount of collagen being secreted in the cellular clusters forming dense bodies.

The observations from the image analysis for Picrosirius red stain suggest that the experimentals 1, 3, and 4 performed better with respect to collagen secretion and also there was an increase in the collagen secretion as the days advanced from 0 to 21. It can

be inferred that the addition of HNTs loaded with growth factors like BMP 2, 4, and 6 enhanced cellular differentiation in the hydrogel constructs.

4.3.1.3 *Von Kossa staining.* The Von Kossa stain is 5% v/v silver nitrate which reacts with the phosphate group of calcium phosphate which is the mineral component of bone. Calcium phosphate is secreted by the cells during differentiation. Figures 4-29 to 4-32 (A-F) show Von Kossa staining of the alginate hydrogels for days 0 to 21. Figure 4-29 (A-F) shows the Von Kossa staining for Day 0.

Figure 4-29. Von Kossa staining Day 0 A) Control 1 Alginate-only B) Control 2 Alginate + HNTs C) Experimental 1 Alginate+ HNTs+ BMP 2 D) Experimental 2 Alginate+ HNTs+ BMP 2 with 0.4M Ascorbate E) Experimental 3 Alginate+ HNTs+ BMP 4 F) Experimental 4 Alginate+ HNTs+ BMP 6.

Day 0 shows the staining done after 8 hours of encapsulating the cells in hydrogels. Figure 4-29 (A-F) shows that the cells have not started their differentiation in

any of the control or experimental groups. This is because the initial stage for the cells is to establish anchorage in the matrix and then to produce ECM for cellular communication for differentiation.

Figure 4-30. Von Kossa staining Day 7 A) Control 1 Alginate-only B) Control 2 Alginate + HNTs C) Experimental 1 Alginate+ HNTs+ BMP 2 D) Experimental 2 Alginate+ HNTs+ BMP 2 with 0.4M Ascorbate E) Experimental 3 Alginate+ HNTs+ BMP 4 F) Experimental 4 Alginate+ HNTs+ BMP 6.

In Figure 4-30, the controls 1 and 2 (A and B) show small areas of black-brown coloration which are calcium phosphate deposits stained with Von Kossa. The experimental groups (C-F) show larger brown-black patches of calcium phosphate deposits stained with Von Kossa. Once the osteoblasts have proliferated and established connections with each other they start differentiating and produce substances which lay foundation of new bone such as calcium phosphate. Usually this process starts by Day 7.

The images of the experimental groups (C-F) show the progression of deposition of calcium phosphate by the differentiating cells. Amongst the experimental groups the groups #1 and #3 (C and E) show distinct black depositions of calcium phosphate shown by arrows.

Figure 4-31. Von Kossa staining Day 14 A) Control 1 Alginate-only B) Control 2 Alginate + HNTs C) Experimental 1 Alginate+ HNTs+ BMP 2 D) Experimental 2 Alginate+ HNTs+ BMP 2 with 0.4M Ascorbate E) Experimental 3 Alginate+ HNTs+ BMP 4 F) Experimental 4 Alginate+ HNTs+ BMP 6.

Figure 4-31 (A-F) shows the progression of calcium phosphate deposition by the differentiating osteoblasts on Day 14. The cells have formed distinct deposits of calcium phosphate seen in all the groups (controls and experimental) as brown-black patches. From the images it can be inferred that the deposition of calcium phosphate in the hydrogel matrix is more pronounced on Day 14 than the onset of differentiation (Day 7).

The experimental groups #3 and #4 (C and D) have more depositions than the controls or experimental groups #1 and #2 (seen as deeply stained hydrogel matrix without distinct patches).

Figure 4-32. Von Kossa staining Day 21 A) Control 1 Alginate-only B) Control 2 Alginate + HNTs C) Experimental 1 Alginate+ HNTs+ BMP 2 D) Experimental 2 Alginate+ HNTs+ BMP 2 with 0.4M Ascorbate E) Experimental 3 Alginate+ HNTs+ BMP 4 F) Experimental 4 Alginate+ HNTs+ BMP 6.

Figure 4-32 (A-F) shows the progression of calcium phosphate deposition on Day 21. Compared to the controls 1 and 2 (A and B) the experimental groups (C-F) have more calcium phosphate deposition. Amongst all the experimental groups, experimental groups #3 and #4 (E and F) have the most pronounced deposition seen as deeply stained hydrogel matrix.

Comparing the images of Von Kossa staining, the controls and the experimental groups through the 21-day period show that the deposition of calcium phosphate starts on Day 7 and is more in the experimental groups #3 and #4 (E and F). This suggests that the hydrogels having BMP 4 and 6 loaded HNTs perform better with respect to other groups.

The observations made by visual qualitative analysis of the Von Kossa stained sections of hydrogels can be further ascertained by image analysis done by Image J software. The representative images of Controls 1 & 2 and the experimental groups E1, E 3, and E4 for days 0 and 21 are given in Figure 4-33 to 4-42. Figure 4-33 shows Grayscale intensity for alginate-only hydrogel control (C1) for day 0.

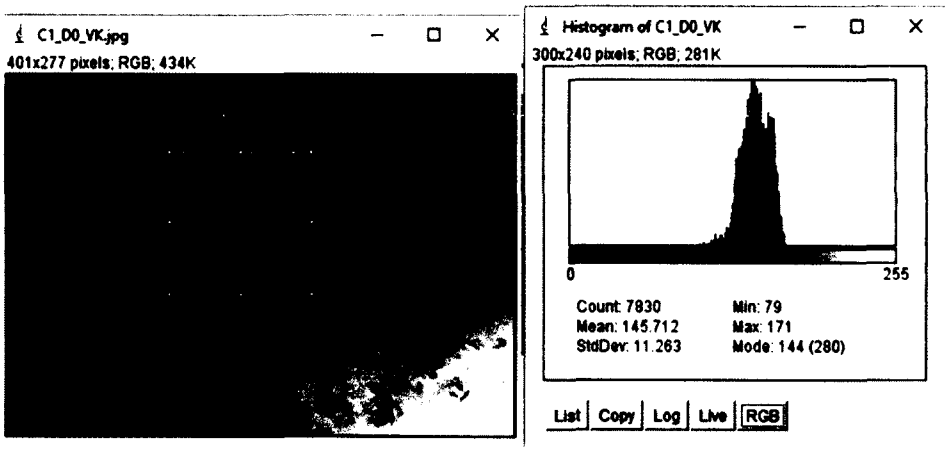

Figure 4-33. Grayscale intensity for Von Kossa staining for Alginate-only hydrogel control 1 (C1) for Day 0.

Figure 4-33 shows grayscale intensity for Von Kossa staining for control 1 on day 0. The grayscale intensity value will show how dark was the staining in the region of interest suggesting increased or slight mineral deposition of hydroxyapatite crystals. The grayscale graph shows less intense staining suggesting that the mineral deposition was not much on day 0 for control 1. Figure 4-34 shows Grayscale peak for alginate-only hydrogel control (C1) for Day 21.

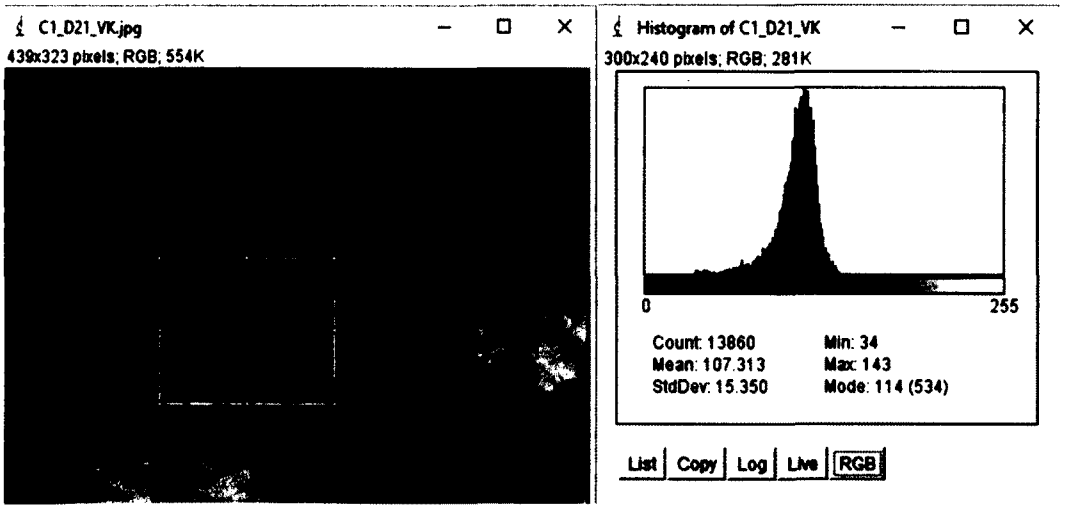

Figure 4-34. Grayscale intensity for Von Kossa staining for Alginate-only hydrogel control 1 (C1) for Day 21.

Figure 4-34 shows grayscale intensity for Von Kossa staining for control 1 on Day 21. The grayscale graph does not show much change in the intensity for the stain suggesting that there was not much mineralization in the control 1 hydrogel matrix after 21 day period. Figure 4-35 shows Grayscale peak for alginate + HNTs hydrogel control (C2) for day 0.

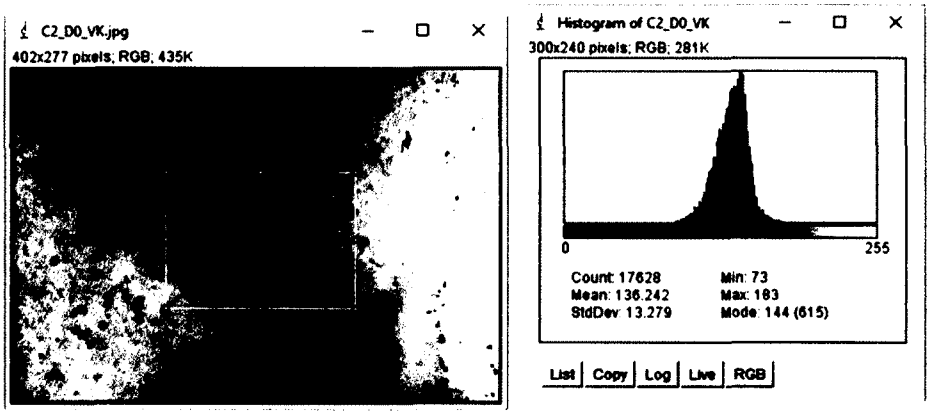

Figure 4-35. Grayscale intensity for Von Kossa staining for Alginate + HNTs hydrogel control 2 (C2) for Day 0.

Figure 4-35 shows grayscale intensity for Von Kossa staining for control 2 on day 0. The intensity of the stain is less on day 0 for control 2 suggesting that the

mineralization has not yet started. Figure 4-36 shows Grayscale peak for alginate + HNTs hydrogel control (C2) for Day 21.

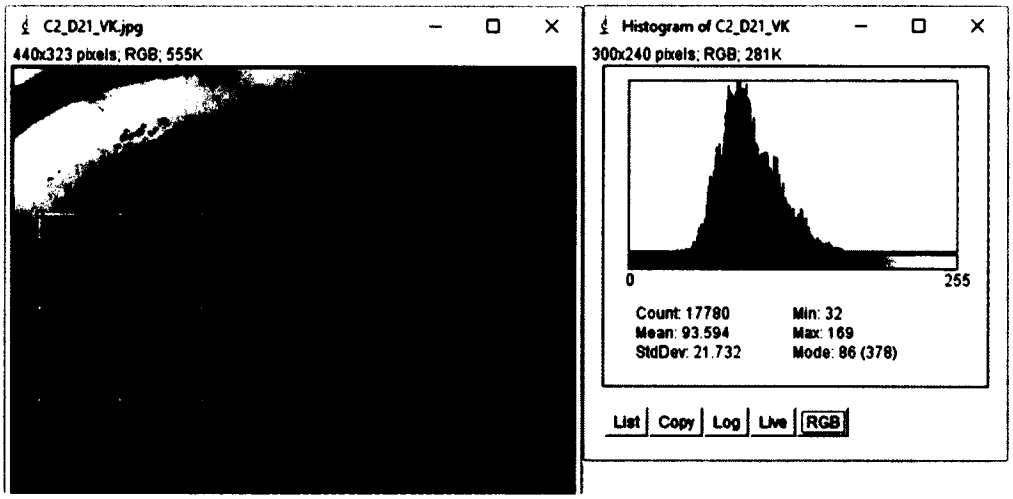

Figure 4-36. Grayscale intensity for Von Kossa staining for Alginate + HNTs hydrogel control 2 (C2) for Day 21.

Figure 4-36 shows grayscale intensity for Von Kossa staining for control 2 on Day 21. The intensity for the staining has increased from day 0 suggesting mineralization and calcium phosphate deposition. This observation is supported by the obsevations in the previous section. Figure 4-37 shows Grayscale peak for alginate + HNTs + BMP 2 experimental (E1) for day 0.

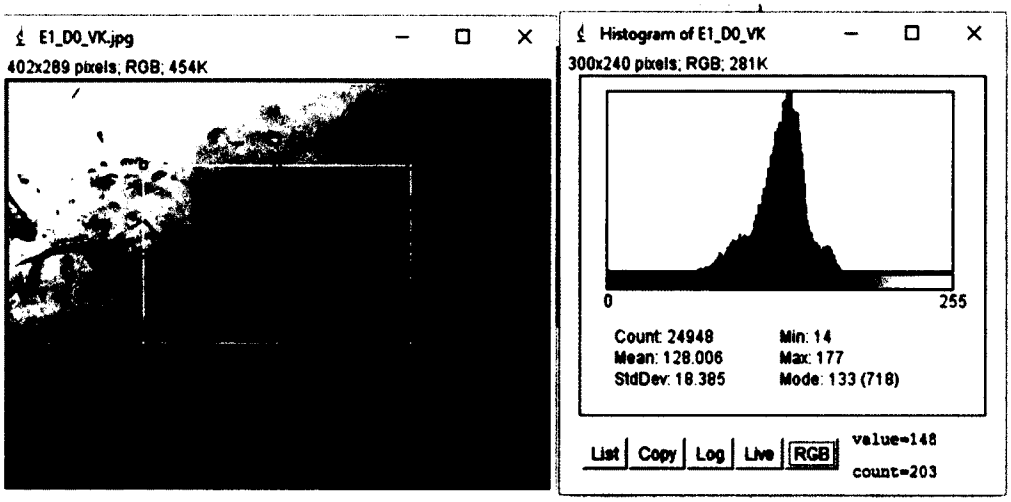

Figure 4-37. Grayscale intensity for Von Kossa staining for Alginate + HNTs + BMP 2 experimental 1 (E1) for Day 0.

Figure 4-37 shows grayscale intensity for Von Kossa staining for experimental 1 on day 0. The intensity for the stain can be compared to the day 0 values of controls 1 and 2. The intensity is low for the staining suggesting that the mineralization has not yet started on day 0. Figure 4-38 shows Grayscale peak for alginate + HNTs + BMP 2 experimental (E1) for Day 21.

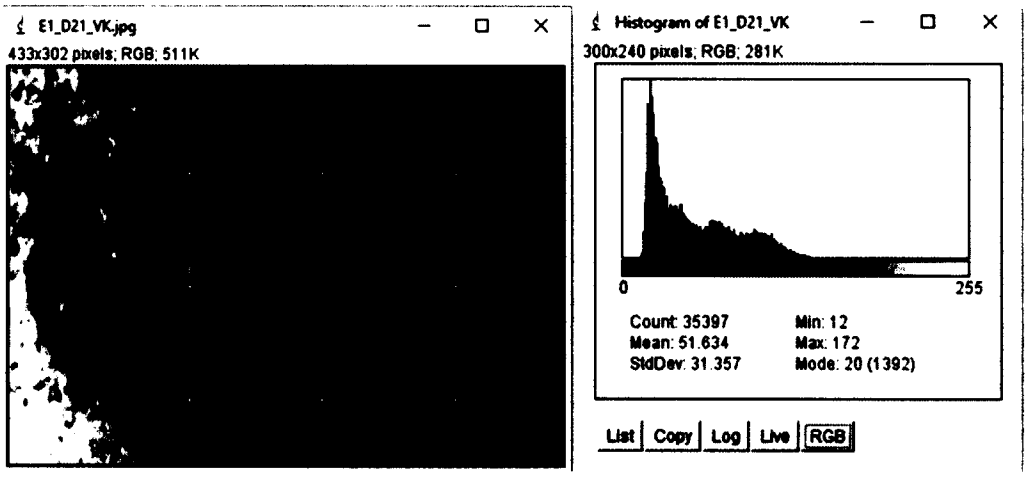

Figure 4-38. Grayscale intensity for Von Kossa staining for Alginate + HNTs + BMP 2 experimental 1 (E1) for Day 21.

Figure 4-38 shows the grayscale intensity for Von Kossa staining for experimental 1 on Day 21. The grayscale intensity for the region of interest shows an increase suggesting that there is mineralization and it is more than that of the controls 1 and 2 on Day 21. Figure 4-39 shows Grayscale peak for alginate + HNTs + BMP 4 experimental (E3) for day 0.

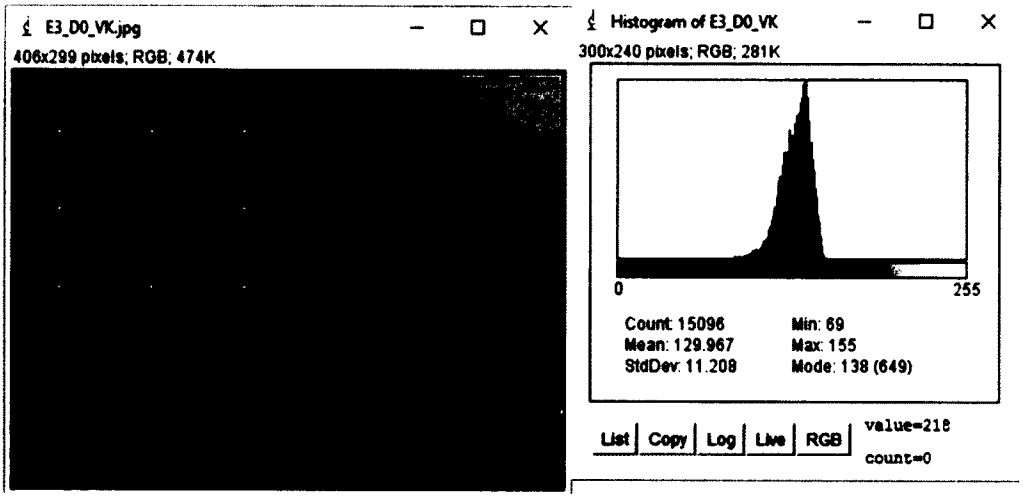

Figure 4-39. Grayscale intensity for Von Kossa staining for Alginate + HNTs + BMP 4 experimental 3 (E3) for Day 0.

Figure 4-39 shows grayscale intensity for Von Kossa for experimental 3 on day 0. The graph for the grayscale shows low intensity of staining suggesting that the mineralization has yet to start. Figure 4-40 shows Grayscale peak for alginate + HNTs + BMP 4 experimental (E3) for Day 21.

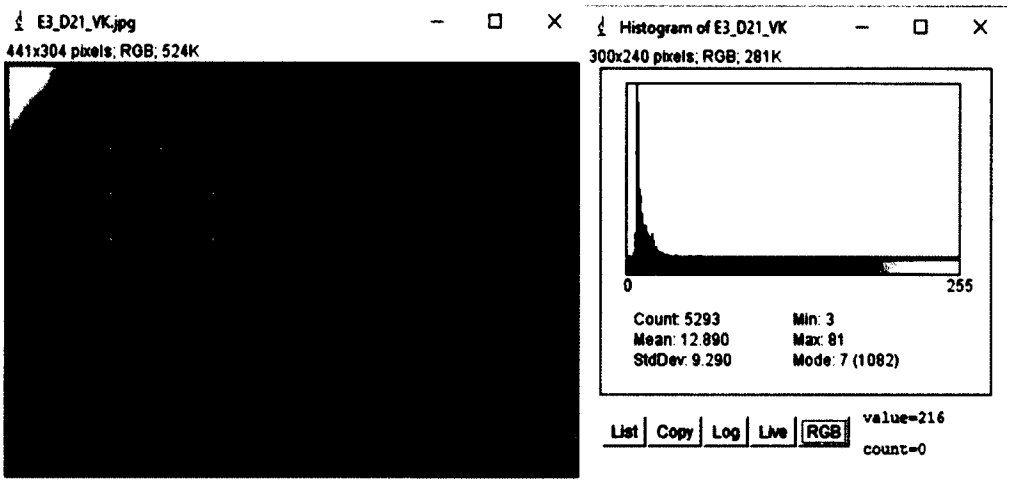

Figure 4-40. Grayscale intensity for Von Kossa staining for Alginate + HNTs + BMP 4 experimental 3 (E3) for Day 21.

Figure 4-40 shows grayscale intensity for Von Kossa for experimental 3 on Day 21. The graph for the grayscale shows a very high intensity value for the region of interest. It suggests that the region of interest has calcium phosphate deposits indicating mineralization. The increase in the mineralization from day 0 to 21 and also a comparable increase in the mineral deposition against controls 1 and 2 is supported by the observations in the previous section. Figure 4-41 shows Grayscale peak for alginate + HNTs + BMP 6 experimental (E4) for day 0.

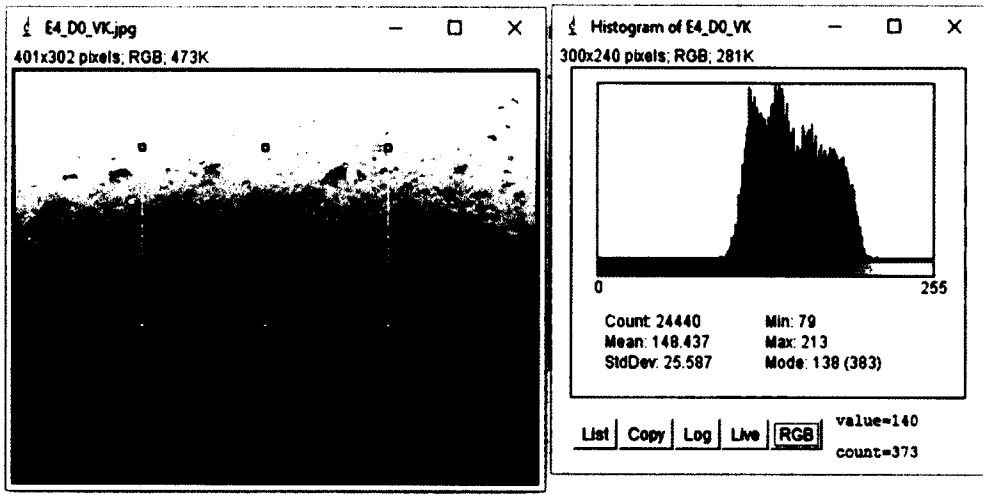

Figure 4-41. Grayscale intensity for Von Kossa staining for Alginate + HNTs + BMP 6 experimental 4 (E4) for Day 0.

Figure 4-41 shows grayscale intensity for Von Kossa for experimental 4 on day 0. There is noise in the grayscale graph which might be due to uneven sectioning but the overall value is comparable to the controls 1 and 2 on day 0. This suggests that the mineralization has not yet started for experimental 4 on day 0. Figure 4-42 shows Grayscale peak for alginate + HNTs + BMP 6 experimental (E4) for Day 21.

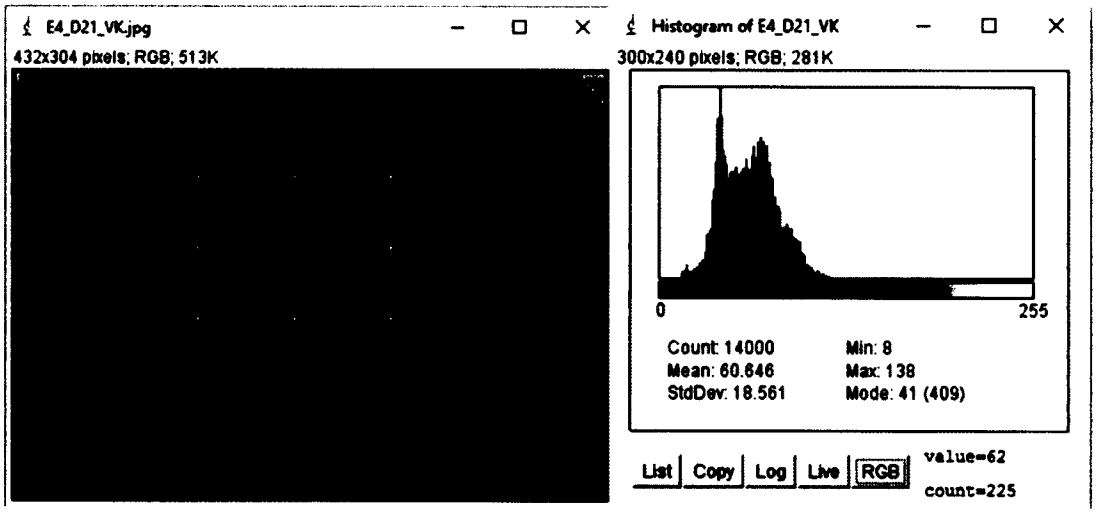

Figure 4-42. Grayscale intensity for Von Kossa staining for Alginate + HNTs + BMP 6 experimental 4 (E4) for Day 21.

Figure 4-41 shows grayscale intensity for Von Kossa for experimental 4 on Day 21. There is noise in the graph which might be due to uneven sectioning or high mineral deposits but the overall intensity for the staining has increased. This indicates high mineral deposition in the experimental 4 matrix on Day 21. It can be inferred taking into consideration the image analysis for Von Kossa that the experimental 1, 3, and 4 performed better with respect to the mineralization. The addition of HNTs and BMPs 2, 4, and 6 enhanced the mineralization promoted cellular differentiation in the respective hydrogel constructs.

Comparing all the three histochemical staining images (Alcian Blue, Picrosirius Red, and Von Kossa, Figures 4-29 to 4-32) a progression of events can be visualized. The ECM production starts early (Day 7) in experimental groups #3 and #4 (hydrogels with BMP 4 and 6 loaded HNTs). The experimental groups #3 and #4 also show early onset of collagen production (Day 0, 8 hours after cell encapsulation). In the case of Von Kossa staining, the experimental groups #3 and #4 have the most calcium phosphate deposition on Day 7 amongst all the four experimental groups.

The observations from all the three histochemical staining analyses suggest that experimental groups #3 and #4 performed better with respect to early onset of differentiation of osteoblasts. The experimental groups #1 and #2 performed better compared to the controls 1 and 2 with respect to differentiation of osteoblasts (production of ECM, collagen and calcium deposition). The results from the histochemical analyses suggest that the hydrogel enhanced with growth factors loaded Halloysite perform better than the control hydrogels of calcium alginate and calcium alginate+ HNTs. This is also substantiated by the image analysis of the histochemical staining images by Image J

software which showed that there was indeed an increase in ECM and collagen production and mineral deposition in experimental sets 1, 3, and 4.

4.3.2 Release Profile Study of BMP 2 from HNTs

The release profile study of BMP 2 from HNTs was measured with custom made sandwich ELISA kits. to estimate the amount of BMP 2 eluted out of the HNTs over a period of 24 hours and 7 days. This measurement was done to investigate if the amount of growth factor eluted from the HNTs was similar to the amount secreted in the body and to mimic the natural internal environment. Figure 4-43 is the calibration curve for the ELISA kit with known standards.

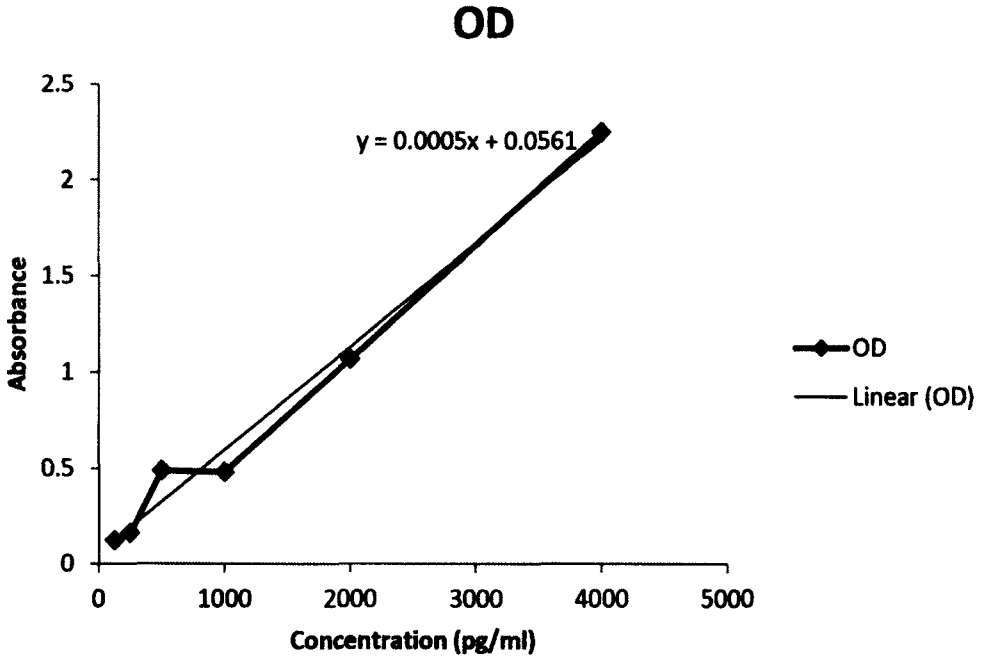

Figure 4-43. Calibration curve for BMP 2 standards.

Absorbance is on the Y-axis and concentrations of the standard is on X-axis. Figure 4-44 shows the conversion plot for absorbance to log concentrations used to calculate BMP 2 release, $y = 0.0005x + 0.0561$.

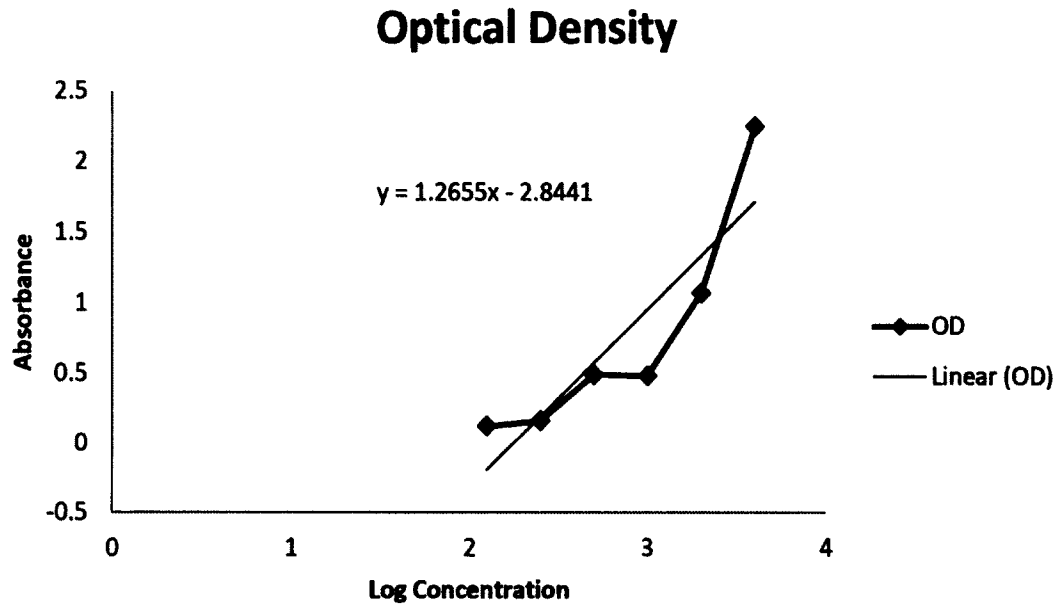

Figure 4-44. Graph showing conversion of absorbance to log concentrations.

Figure 4-45 shows the trend of BMP 2 release from HNTs for a period of 24 hours. The release was achieved by the vacuum loaded HNTs in HBSS at room temperature. The amount of BMP 2 release was estimated by sandwich ELISA and reading the plate on absorbance plate reader. The experiment was repeated thrice to reduce error and to check for the reproducibility of results. The values are the means of the readings of BMP 2 from HNTs at the respective time points recorded from the three repetitions of the experiment. The error bars reflect the standard deviation at each data point calculated by standard deviation and the average of the triplicate samples (detailed process of calculation of the standard deviation described in Appendix B). [59]

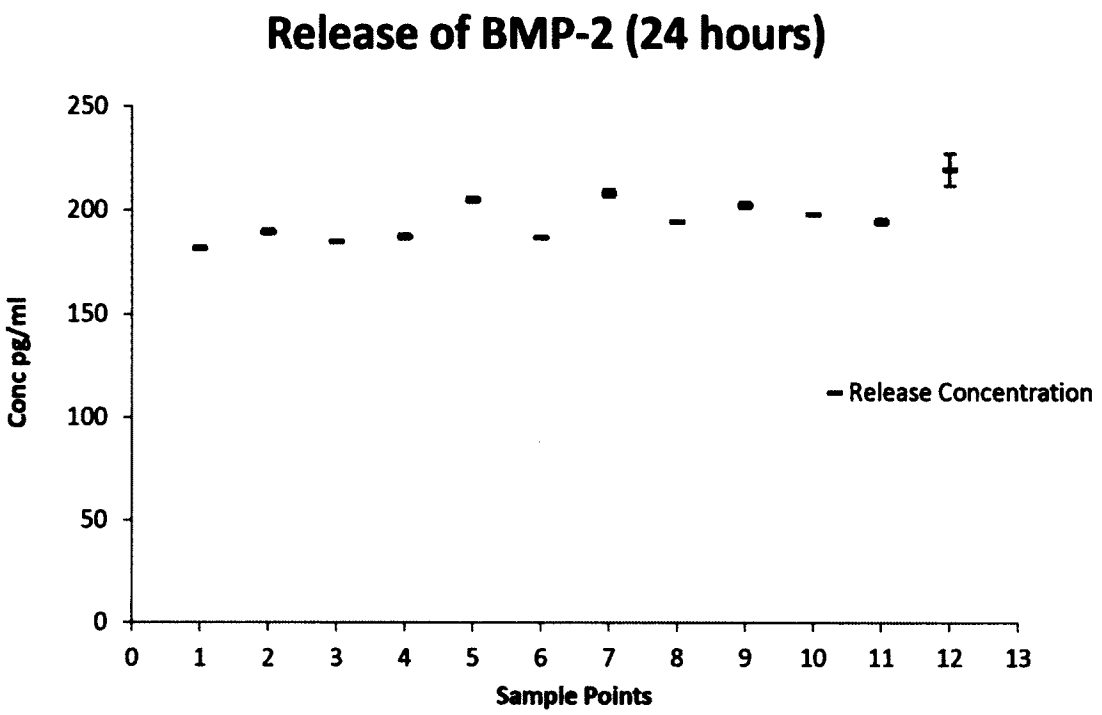

Figure 4-45. Release profile of BMP 2 from HNTs for 24 hours.

The graph shows a sustained release of the growth factor for 24 hours in the range of picograms per ml which is comparable to the range the growth factors are secreted in the body. [54] HNTs are cylindrical in shape with the inner lumen comprising of concentric layers of aluminosilicate. When any drug or bioactive agent is vacuum-loaded into the HNTs, the molecules become trapped in both the lumen and the outer surface. Before starting the release study of BMP 2 we washed the sample of loaded HNTs with distilled water twice to remove the BMP 2 coated on the outer surfaces of the HNTs. It cannot be guaranteed that all the molecules are removed during the washing step as can be seen in the initial burst release of BMP 2 within first one hour of the study. The trend seen here is not of the cumulative release but that of individual data points. The concentration seen in the graph cannot be regarded as accurate estimate as the standards provided by the manufacturer showed resolution problems. The data should be viewed

cautiously and regarded as a qualitative estimate of the protein released from the HNTs. The raw data tables and supplementary tables are provided in Appendix B.

The graph of the release profile study for BMP 2 from HNTs for 7 days is given in the Figure 4-46. The calibration curves in Figures 4-43 and 44 were used to the calculations in the plotting of graph in Figure 4-46.

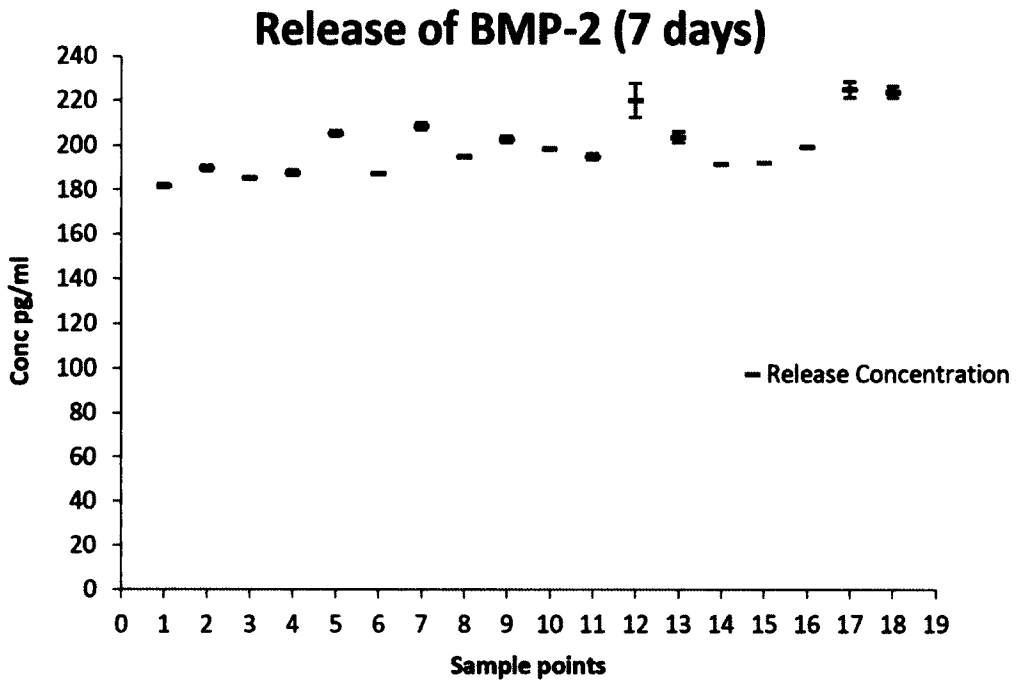

Figure 4-46. The graph of the release profile study for BMP 2 from HNTs for 7 days.

The release profile study of BMP 2 from HNTs was extended for a period of 7 days. The experiment was repeated three times to reduce error and check for reproducibility of the results. The values are the means of the readings of BMP 2 from HNTs at the respective time points recorded from the three repetitions of the experiment. The error bars reflect the standard deviation at each data point calculated by standard deviation and the average of the triplicate samples (detailed process of calculation of the standard deviation described in Appendix B). [59]

The release of BMP 2 from HNTs was extended and sustained for a period of 7 days. The initial release was in picograms per ml range and after 24 hours was in nanograms per ml range. This range of released BMP 2 is comparable to the range BMP 2 is effective in the body. The graph for BMP 2 release from the HNTs for a period of 7 days shows a release profile which is characterized by an initial high burst of BMP 2 release within initial 24 hours and later steady release for the period of 7 days. As described earlier, the release profile of BMP 2 for 24 hours was estimated by the use of custom made sandwich ELISA kits. The trend seen here is not of the cumulative release but that of individual data points. The concentration seen in the graph cannot be regarded as accurate estimate as the standards provided by the manufacturer showed resolution problems. The data should be viewed cautiously and regarded as a qualitative estimate of the protei released from the HNTs. The raw data tables and supplementary tables are provided in Appendix B.

The release profile of BMP 2 from the HNTs suggests that an extended and sustained release can be obtained from HNTs for a period of 7 days. The release is in pico and nanograms range which is the effective range for BMP 2 in natural tissue environment. Even though the concentrations cannot be regarded as accurate due to the resolution error in the kit, especially below the concentration of 50 pg/ml, the qualitative trend shows that the range in which the BMP 2 is released is comparable to the effective range in natural tissues. The results obtained for 7-day release are encouraging as the cellular differentiation process peaks at Day 7. Hence, a sustained release of BMP 2 for a period of 7 days from HNTs is beneficial for early onset of cellular differentiation which might lead to accelerated regeneration of the damaged bone tissue.

The study of release of BMP 2 from HNTs could not be extended beyond 7-day period as the growth factor degrades structurally at room temperature if kept beyond a week. A comparison of release profiles of BMPs 4 and 6 from HNTs with BMP 2 would have been ideal but could not be conducted as no ELISA kits were commercially available to detect these molecules at picogram or nanogram range.

4.3.3 FE-SEM imaging and material testing with BET pore size and surface area analyses

4.3.3.1 *FE-SEM imaging.* Lyophilized calcium alginate hydrogel beads with and without HNTs were FE-SEM imaged to visualize and compare the surface morphologies of the beads. The study of the surface morphology is important as it reveals changes that addition of HNTs brings about in calcium alginate hydrogels. A modified surface might be more desirable with respect to the biological properties of the hydrogel and might suggest other differences in the mechanical properties of the HNT-calcium alginate hydrogels. Figure 4-47 compares the general morphologies of lyophilized alginate-only and alginate+ HNTs hydrogel beads at 500 μm and 1 mm magnification, respectively.

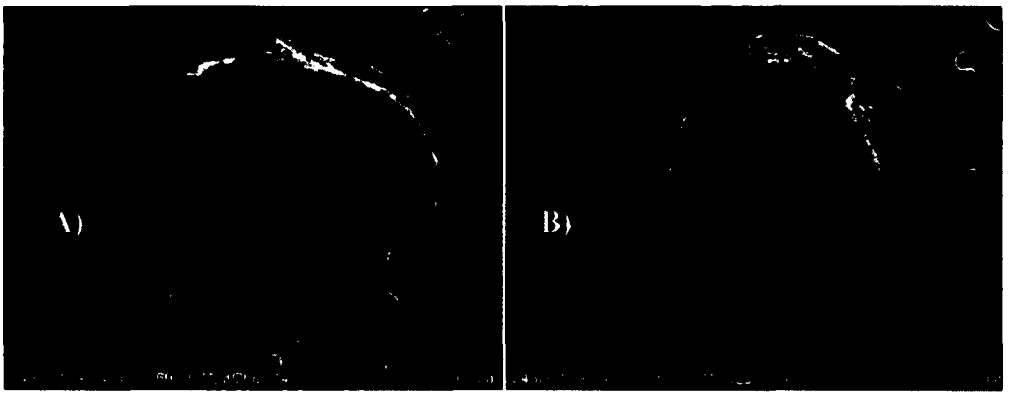

Figure 4-47. FE-SEM images showing A) Alginate-only bead and B) Alginate+ HNTs bead.

Figure 4-47 (A) shows the general morphology of lyophilized alginate-only beads at 500 μm. The surface of the bead appears to have ridges and folds. Figure 4-47 (B) shows the general morphology of lyophilized alginate+ HNTs beads at 1 mm. The surface of the bead appears to have less ridges and folds than alginate-only bead (A). The surface also appears rougher than the alginate-only bead (A). The beads were imaged at different magnifications (500 μm for alginate-only bead and 1 mm for alginate+ HNT bead) as the alginate-only bead shrunk in size and surface features were not clearly visible at 1 mm magnification. Figure 4-48 (A-D) shows surface morphologies of alginate-only and alginate+ HNTs hydrogel beads at higher magnification.

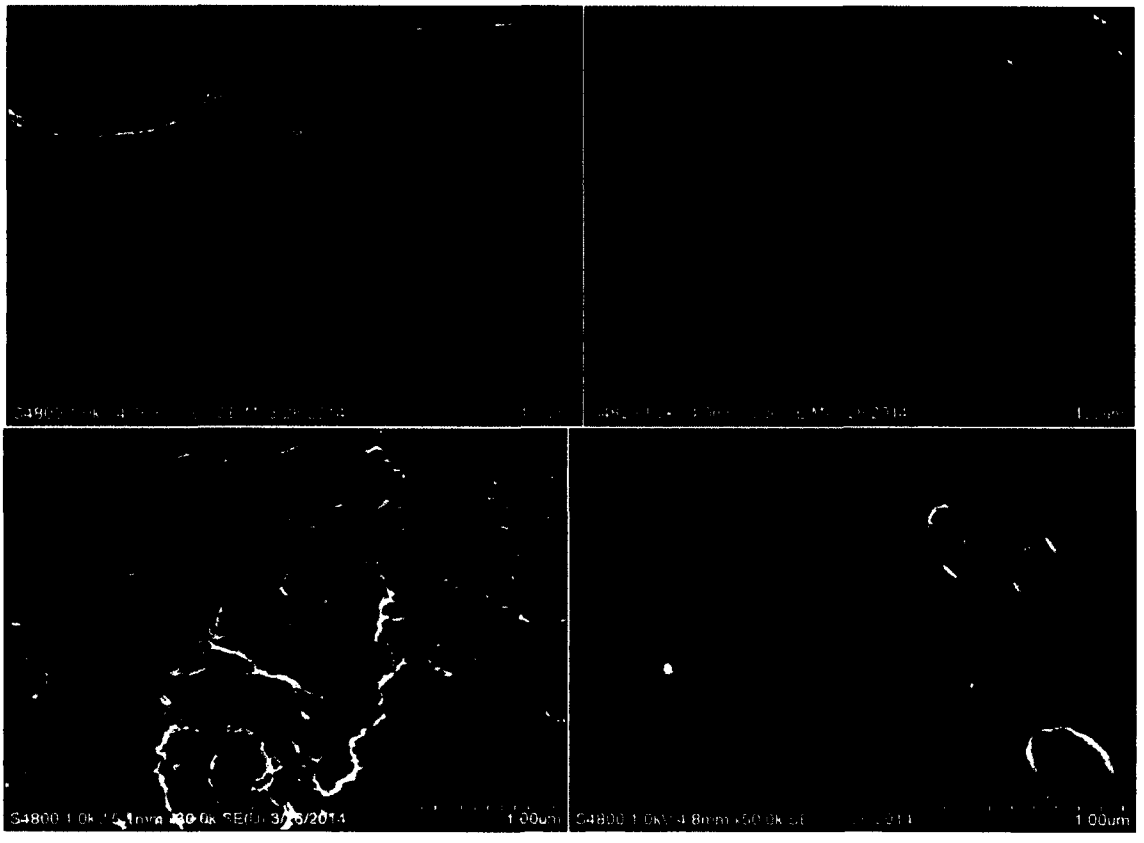

Figure 4-48. FE-SEM images showing the surface morphology of A) Alginate-only bead 100 μm magnification B) Alginate+ HNTs bead 100 μm magnification C) Alginate-only bead 1 μm magnification D) Alginate+ HNTs bead with HNT protruding out of the surface at 1 μm magnification.

Figures 4-48 (A and B) show the surfaces of alginate-only bead and alginate+ HNTs bead, respectively, at 100 μm magnification. The surfaces of both the beads look different with the image B showing a relatively rougher surface of alginate+ HNTs hydrogel bead. At 1 μm magnification the surface of alginate-only bead (C) looks rough and has finer creases and cracks. The image D shows the surface of alginate+ HNTs hydrogel bead with halloysite sticking out of the bead's surface. The surface of the bead in image D also shows fold and minute surface elevations which might be due to halloysite bunches trapped in the hydrogel matrix.

A comparison of images in Figures 4-47 (A and B) and 4-48 (A-D) shows that the addition of HNTs modifies the surface of the hydrogels by making it rough and the bead more rigid. The rigidity of the bead with HNTs was more as it did not shrink after lyophilization and retained it surface integrity without cracking.

4.3.3.2 *BET pore size and surface area analysis of hydrogels*. BET pore size and surface area analysis was done with helium adsorption-desorption method to analyze the material properties of the alginate-only and alginate+ HNTs hydrogels. This analysis would help to assess the differences in the material properties of the hydrogels with the addition of HNTs. The curve used to plot the adsorption-desorption curve of helium for both the types of hydrogels is Langmuir curve. Figure 4-49 shows BET Langmuir isotherm showing the adsorption-desorption of helium for alginate-only hydrogel.

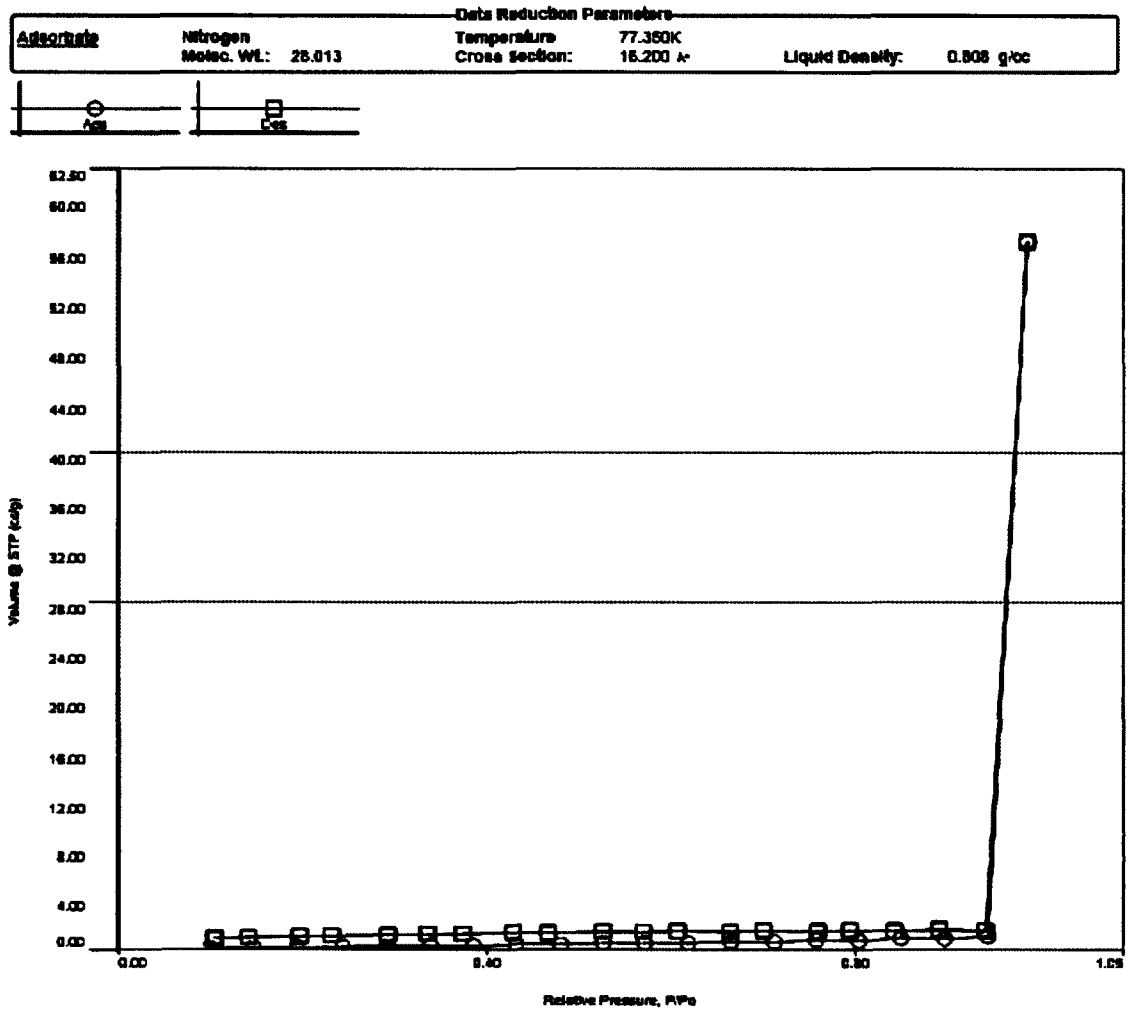

Figure 4-49. BET Langmuir isotherm showing the adsorption-desorption of helium for alginate-only hydrogel.

Figure 4-49 shows Langmuir isotherm of adsorption-desorption of helium for alginate-only hydrogel. The red isotherm line is for adsorption of helium and blue line is for desorption. Both the lines (adsorption and desorption) have values that coincide for volume of gas at the respective values of relative pressure. The summary of analysis showed that the cumulative surface area for the alginate-only hydrogel was 2.264 m2 /g, cumulative pore volume was 3.054 cc /g, and pore radius was 1.385 Å. Figure 4-50

shows BET Langmuir isotherm showing the adsorption-desorption of helium for alginate+ HNTs hydrogel.

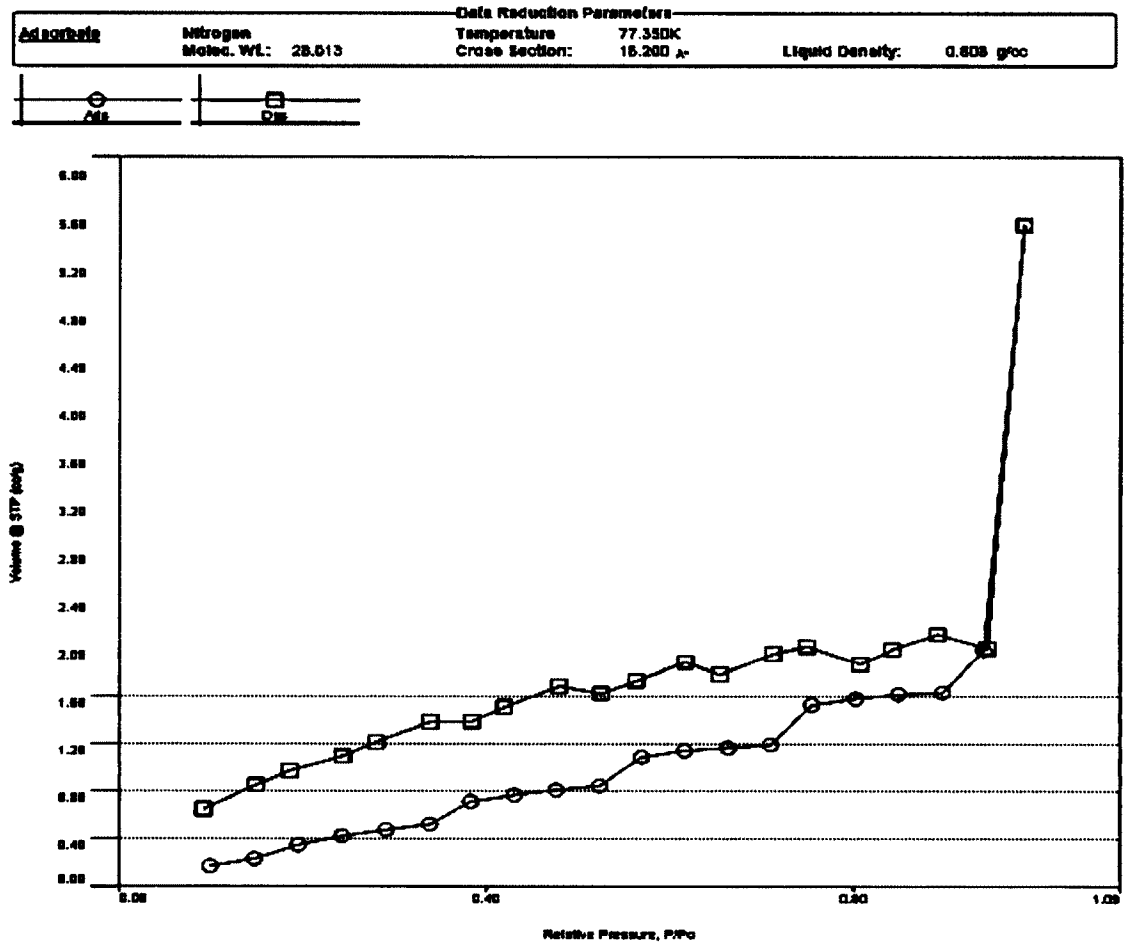

Figure 4-50. BET Langmuir isotherm showing the adsorption-desorption of helium for alginate+ HNTs hydrogel.

Figure 4-50 shows BET Langmuir isotherm of adsorption-desorption of helium for alginate+ HNTs hydrogel. The red isotherm line is for adsorption of helium, and the blue line is for desorption. Both the lines, unlike the isotherm curve for alginate-only hydrogel, show that the values for volumes of adsorbed and desorbed helium differ at the respective values of relative pressure. The results are summarized in Table 2.

Table 2: BET results summary

Hydrogels	**Alginate**	**Alginate + HNTs**
Surface Area	8.485 m^2/g	6.955 m^2/g
Pore Volume (Cumulative)	3.054 cc /g	2.325 cc /g
Pore Radius	1.385 Å	1.010 Å

A comparison of both the isotherms in Figures 4-49 and 4-50 shows that adsorption and desorption profiles of helium are different for both the types of hydrogels. The summary of analysis shows that the hydrogels also differ in their cumulative pore sizes and pore volumes significantly as can be seen in Table 2. Cumulative surface area of the hydrogels also differs slightly for both the types of hydrogels. The alginate-only hydrogels have slightly larger cumulative surface area (2.264 m^2/g) than the alginate+ HNT hydrogels (2.099 m^2/g). The alginate-only hydrogels have cumulative pore volume of 3.054 cc /g which is larger than the cumulative pore volume of alginate+ HNTs hydrogels (cumulative pore volume = 2.325 cc /g). The pore size of alginate-only hydrogels is larger (pore radius = 1.385 Å) than alginate+ HNT hydrogels (pore radius = 1.01 Å).

The summary of the BET pore size and surface area analysis suggests that addition of HNTs make the alginate hydrogels more rigid by reducing the pore size and volume. This alteration of material properties by the addition of HNTs might make the Halloysite enhanced hydrogels better candidates than alginate-only hydrogels for implant materials.

Looking at the results from the FE-SEM surface morphology analysis (Figure 4-47 and 4-48) and BET pore size and surface area analysis (Table 2, Figure 4-49 and 4-50) suggests that alginate+ HNTs have more rough surface and rigid structure making them structurally better suited as implant materials.

CHAPTER 5

NANOSEEDS

5.1 Introduction

In the previous chapter, the concept of nanoenhanced bioactive hydrogels was discussed in detail. The results suggest that hydrogels can be enhanced with HNTs to improve their material and biological properties. Another potential application is the use of nanoenhanced hydrogels as a chemoattractive delivery system designed to recruit the body's own cells to populate and regenerate damaged bone tissue.

In Chapter 4, the base material for the hydrogels was calcium alginate. In the current chapter, calcium alginate is combined with similar materials such as calcium phosphate cement (CPC), chitosan lactate, and HNTs. The hydrogel composites comprised of calcium alginate, CPC, and chitosan were enhanced with HNTs loaded with BMP 2. The objective of the addition of the mentioned materials was to develop scaffold materials that can be used as chemoattractant beacons to attract progenitor cells to the site of injury.

CPCs, individually and in combination with chitosan lactate, has material properties which make them suitable materials to be used as bone cement. [25] Unlike PMMA, they do not produce toxic monomers or require high setting temperatures. [25, 27] Apart from their desired material properties they also provoke a histogenic response from osteoblasts and mesenchymal stem cells. [25]

The hypothesis of this project was that the combination of calcium alginate, CPC, and chitosan with BMP 2-loaded HNTs would enhance the material properties of the scaffolds and would act as chemoattractants for the osteoprogenitor cells.

5.2 Materials and Methods

All plasticware was obtained from Mid Scientific, St. Louis, MO. The chemicals met the ACS standards and purchased from Sigma Aldrich. Preosteoblasts were obtained from ATCC, Manassas, VA. The cell culture growth and maintenance medium were obtained from GIBCO, Life Technologies. The growth factor, BMP 2, was purchased from ProSpec Militany, Tel Aviv, Israel. The collagen type I, used for coating the seeding 12 well plates, was obtained from GIBCO, Life Technologies (Grand Island, NY). The NucBlue Live Ready Probes, fluorescent vital stain was obtained from Thermo Fisher Scientific (Grand Island, NY). Histochemical stain kits: Von Kossa, Alcian Blue, and Picrosirius Red, were purchased from Polysciences Inc. (Warrington, PA).

5.2.1 Cell Migration Study

The cell migration study needed a matrix to hold the nanoseed constructs in place. The matrix also created a space where the cells could be seeded and held until they attached and began active migration. The matrix was made of collagen type I as it would mimic the body's internal conditions and is an often used material in bioengineering. Collagen type I is the most abundant component of connective tissues in the body, in the scar tissue and also makes up the organic component of bones. [45]

5.2.1.1 *Coating cell culture well plates and seeding.* The coating procedure is described in Section 3.2.4. After coating the wells, the plates were kept in 37 °C incubator for the collagen gels to form. The gels were lightly washed with HBSS buffer

to remove the traces of chemicals. Hydrogel nanoseed constructs were prepared as per the procedure described in Section 3.2.1 and enhanced with HNTs vacuum loaded with BMP 2 as per the process described in Section 3.2.2.1. The nanoseeds were placed at a corner of the coated well and cell suspension was injected in the collagen matrix at the opposite corner. The growth medium was added after 30 minutes to avoid eluting out the seeded cells. The cells in the suspension were treated with NucBlue fluorescent stain as per the procedure described in Section 3.2.5.2.

5.2.1.2 *Fixing the gel matrices and histochemical staining.* The gel matrices with the nanoseeds and the cells were fixed on Days 0, 3, and 7. The cells were imaged on the respective days to visualize their migration in response to the eluted BMP 2 from the nanoseeds. The differentiation response of the cells was visualized by staining with histochemical stains (Alcian Blue and Von Kossa). The histochemical staining procedures for Alcian Blue and Von Kossa are described in details in Sections 3.2.5.3, 3.2.5.4, and 3.2.5.5 Picrosirius Red staining was not suitable for this study as the cells were seeded on collagen gel matrix and Picrosirius Red stains for collagen.

5.2.2 Release profile study of BMP 2 from HNTs and various hydrogel composites

The release profile for BMP 2 was studied in the previous project with the alginate hydrogels. This release profile study focused only on the elution of BMP 2 from the HNTs. For the nanoseed hydrogels to be chemoattractant, the BMP 2 needs to be eluted out of the hydrogels. In this project, the release profile of BMP 2, both from HNTs and hydrogels enhanced with HNTs loaded with BMP 2, was studied. The detailed procedure for release profile study is given in Section 3.2.6.

5.2.3 FE-SEM imaging and comparison of surface morphologies of different hydrogel composites

The hydrogel composites consisting of calcium alginate as the base material were enhanced with materials like CPC, chitosan lactate, and HNTs. This was done to improve the mechanical properties and also the osteogenic response of the bone progenitor cells. [25]

To compare and contrast the different surface morphologies of the hydrogel composites, the hydrogel constructs were lyophilized and imaged under FE-SEM. The detailed process is described in Section 3.2.3.

5.2.4 Preosteoblast pilot study using the composite hydrogels

The cells after migration should be able to proliferate and differentiate on the hydrogel composites to achieve the purpose of tissue regeneration. A pilot study was conducted to test if the hydrogels provide the cells a favorable surface for differentiation.

The cells were seeded onto the hydrogel composite films directly. The study was conducted for a period of 3, 7, and 14 days. The hydrogel composite films were fixed with the cells on them on Day 3, 7, and 14. As the films were too thick for the light to pass through, microscopic imaging could not be performed. Instead, the films were subjected to an indirect stain elution study to quantify the differentiation markers.

The films were stained as per the protocols for Alcian Blue and Picrosirius Red stains. The stained films were then washed with 7% v/v acetic acid and the stains were eluted with the samples stored at 4 °C. The UV/VIS mode of NANODROP 2000 spectrophotometer was used to determine the absorbance of the samples and the values were plotted to estimate the amount of mucopolysaccharides, in case of Alcian Blue stain, and collagen, in case of Picrosirius Red stain.

5.3 Results and Discussion

This section discusses the results from experiments detailed in Section 5.2 of the current chapter.

5.3.1 Histochemical Analysis

The histochemical analysis of the gel matrices seeded with preosteoblasts and hydrogel composite constructs was done to assess if the cells migrated and differentiated in response to the secreted BMP 2. If the cells were found to have moved from the location of injection or seeding (cell reservoir), it would suggest the chemoattractant potential of the HNT-BMP 2 enhanced hydrogel composites.

5.3.1.1 *Alcian Blue staining.* Alcian Blue staining, in this project, was done to analyze the response of the cells to the secreted BMP 2 during or after their migration towards the hydrogels or nanoseeds. Alcian Blue stains the acidic mucopolysaccharides of the ECM formed after the cellular differentiation. Figures 5-1 to 5-3 show the Alcian Blue staining for Days 1, 3, and 7. Figure 5-1 (A-F) shows the Alcian Blue staining for Day 1.

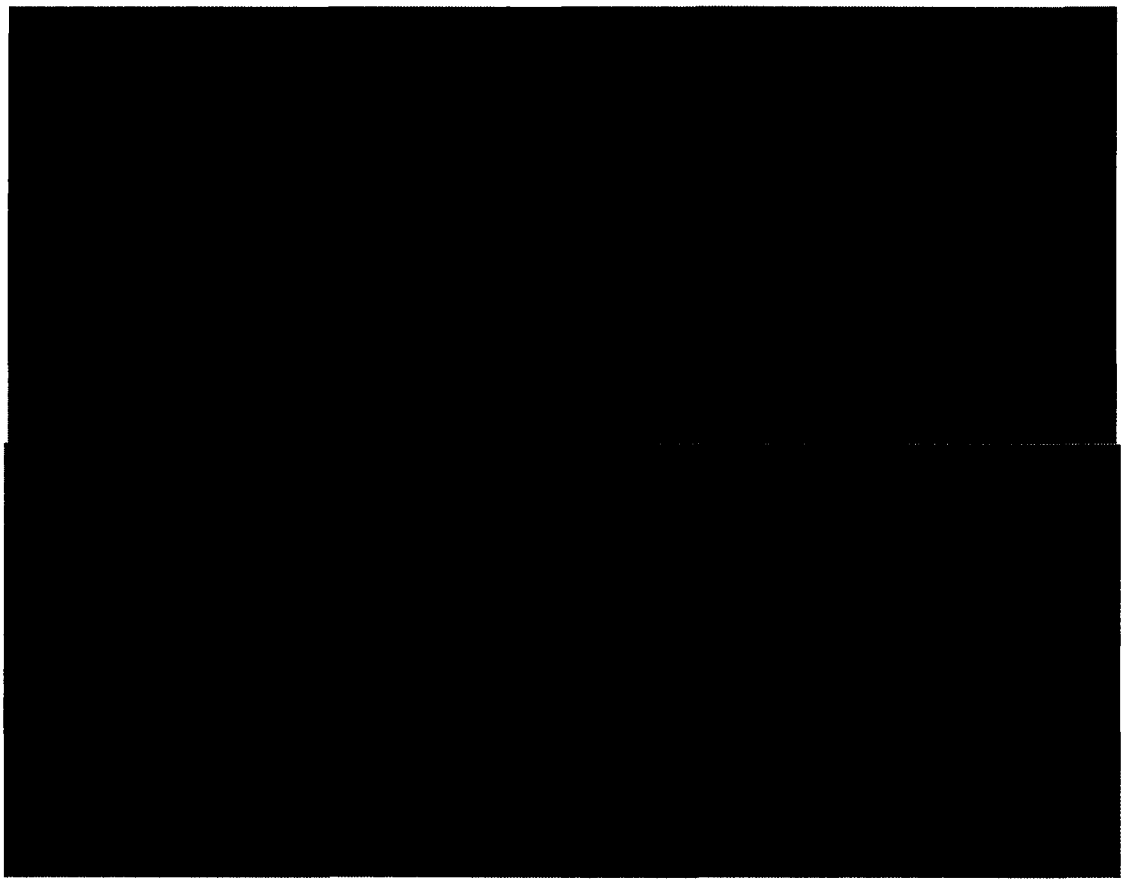

Figure 5-1. Day 1 Alcian Blue Staining of the preosteoblast cells on collagen matrices with hydrogel nanoseed constructs. A) Well 1 with alginate-only hydrogels B) Well 2 with alginate+ HNT+ BMP 2 C) Well 3 alginate+ CPC + HNT D) Well 4 alginate + CPC+ HNT+ BMP 2 E) Well 5 alginate+ CPC+ Chitosan lactate + HNT F) Well 6 alginate+ CPC+ Chitosan lactate + HNT+ BMP 2.

Figure 5-1 (A-F) shows Day 1 Alcian Blue staining for the cells in response to different hydrogel composite constructs with or without BMP 2. These images only show the cell reservoir that is the site of initial cell seeding. The cells have attached themselves and are proliferating in the collagen I matrix after seeding. Figure 5-1 (A) shows the control with alginate-only hydrogel construct and cells seeded in cell reservoir at the opposite pole. Figures 5-1 (B-F) are all experimental groups showing alginate hydrogel composite constructs. In all the groups (control and experimental) the cells are attached to the collagen matrix and are proliferating. This state suggests that the matrices have

retained their cellular properties and the cells are growing normally in the matrix. Figure 5-2 shows Day 3 Alcian Blue staining.

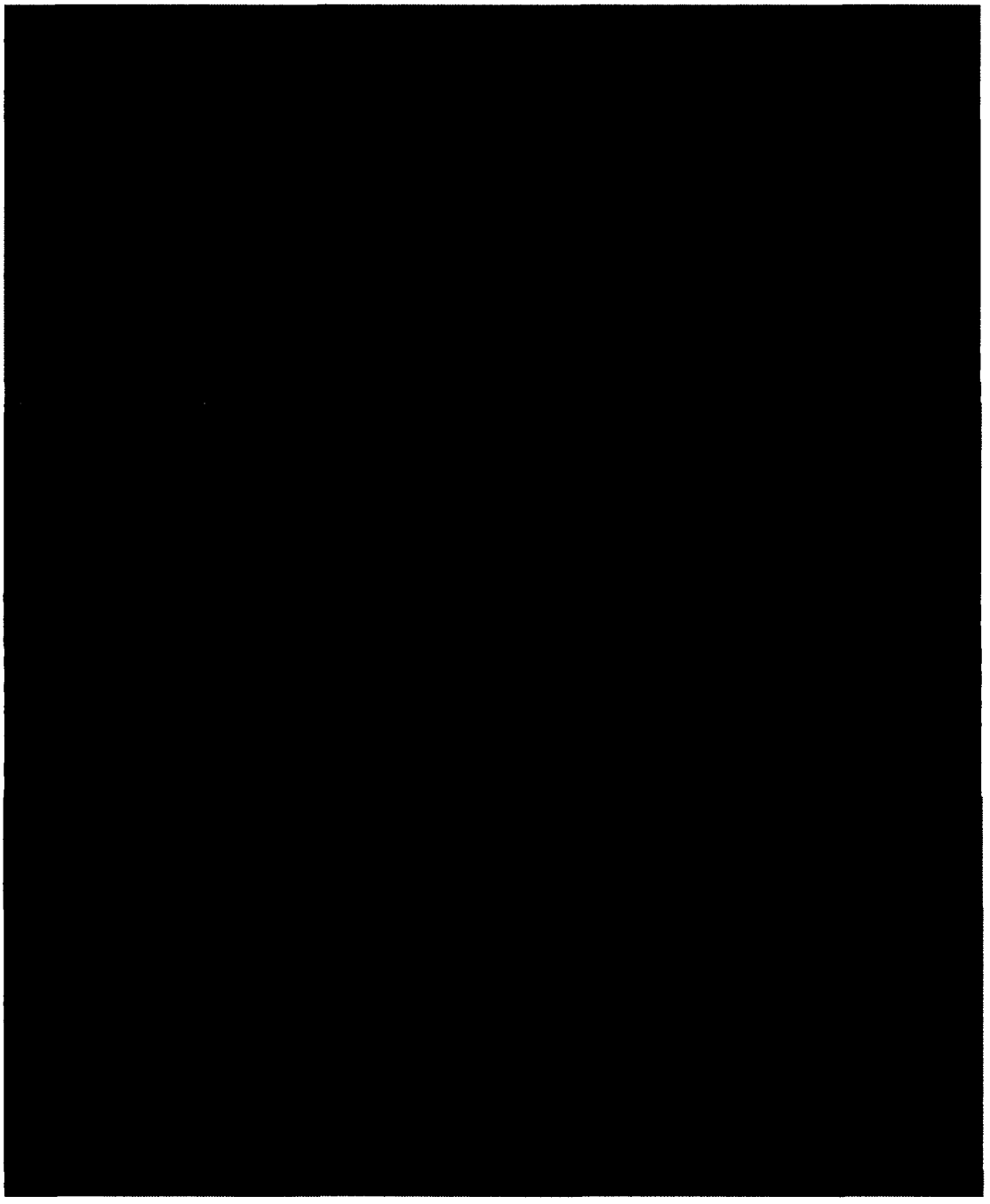

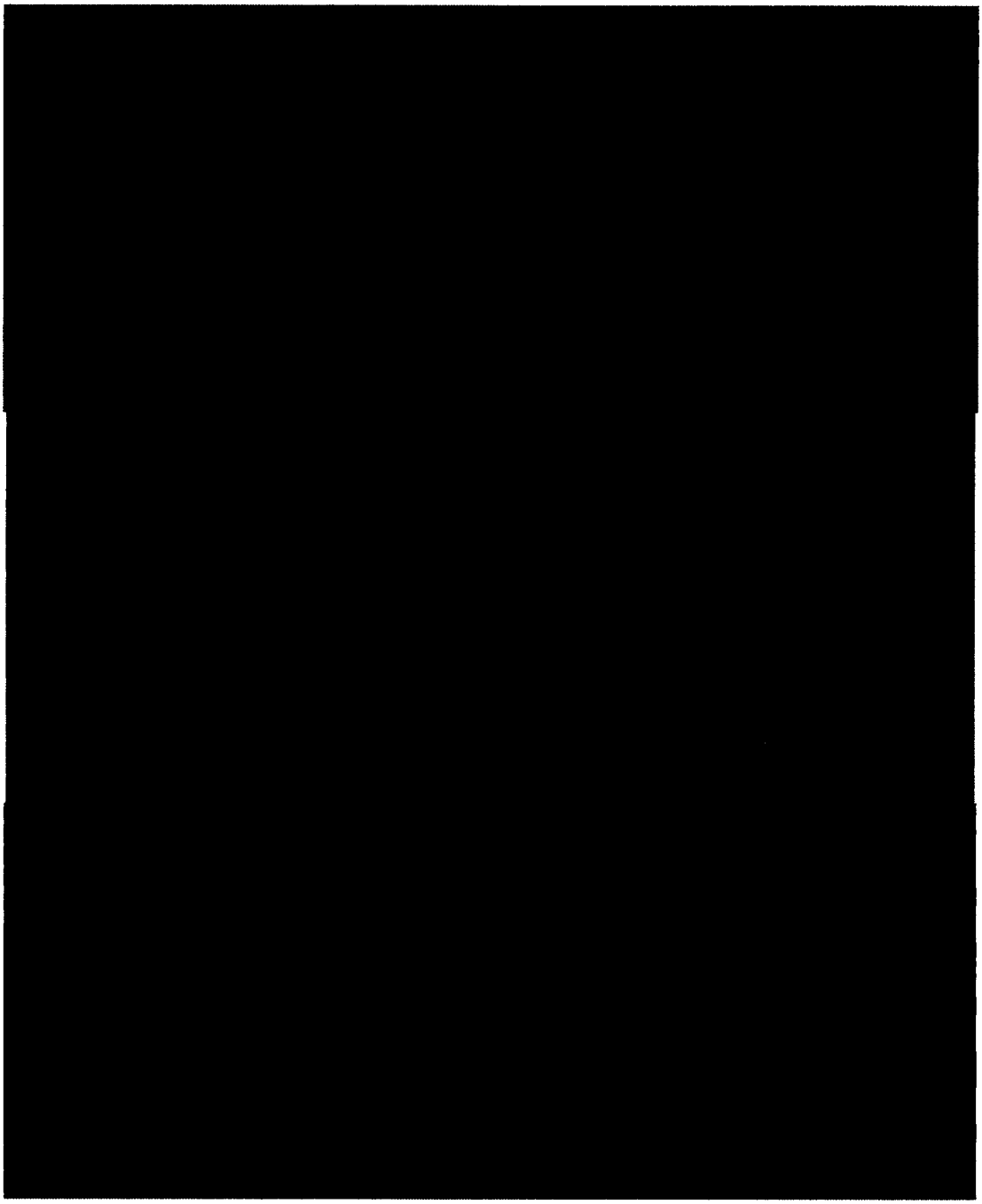

Figure 5-2. Day 3 Alcian Blue staining of the preosteoblast cells on collagen matrices with hydrogel nanoseed constructs. A) Well 1 with alginate-only hydrogels, site of initial seeding B) Well 1 with alginate-only hydrogels, center C) Well 2 with alginate+ HNT+ BMP 2, site of initial seeding D) Well 2 with alginate+ HNT+ BMP 2, center E) Well 3 alginate+ CPC+ HNT, site of initial seeding F) Well 3 alginate+ CPC+ HNT, center G) Well 4 alginate + CPC+ HNT+ BMP 2, site of initial seeding H) Well 4 alginate + CPC+ HNT+ BMP 2, center I) Well 5 alginate+ CPC+ Chitosan lactate + HNT, site of initial seeding J) Well 5 alginate+ CPC+ Chitosan lactate + HNT, center K) Well 6 alginate+ CPC+ Chitosan lactate + HNT+ BMP 2, site of initial seeding L) Well 6 alginate+ CPC+ Chitosan lactate + HNT+ BMP 2, center.

Figure 5-2 (A-L) shows Day 3 staining of the cells in response to the hydrogel composites or nanoseeds. Figure 5-1 (A and B) shows cells at the site of injection and center, respectively, for alginate-only hydrogels (control). The images show that the cells have proliferated and have started producing ECM at the site of injection or seeding but there is no migration towards the hydrogel bead. This suggests that the alginate itself does not have chemoattractant properties. Figure 5-2 (C and D) shows cells at the site of injection and center, respectively, for alginate+ HNTs+ BMP 2 (experimental group). The images show the cells attached and producing ECM. Some of the cells have migrated towards the bead in response to BMP 2 as seen in the image D.

Figure 5-2 (E and F) shows cells at the site of injection and center, respectively, for alginate+ CPC+ HNTs. The images show the cells attached and producing ECM. There is no migration towards the bead suggesting the composite (alginate+ CPC+ HNTs) is not chemoattractant in itself. Figure 5-2 (G and H) shows cells at the site of injection and center, respectively, for alginate+ CPC+ HNTs+ BMP 2. The images show the cells have attached and are producing ECM. Some of the cells have also migrated towards the hydrogel composite bead in response to BMP 2.

Figure 5-2 (I and J) shows cells at the site of injection and center, respectively, for alginate+ CPC+ Chitosan lactate+ HNTs. The images show that the cells have attached and are producing ECM but there is no migration towards the hydrogel composite bead suggesting that the composite bead is not chemoattractant. Figure 5-2 (K and L) shows cells at the site of injection and center, respectively, for alginate+ CPC+ Chitosan lactate+ HNTs+ BMP 2. The images show that the cells have attached and are producing ECM. The image showing the center (L) of the gel matrix shows that some of the cells

have migrated towards the bead in response to the BMP 2. Figure 5-3 (A-L) shows Alcian Blue staining for Day 3.

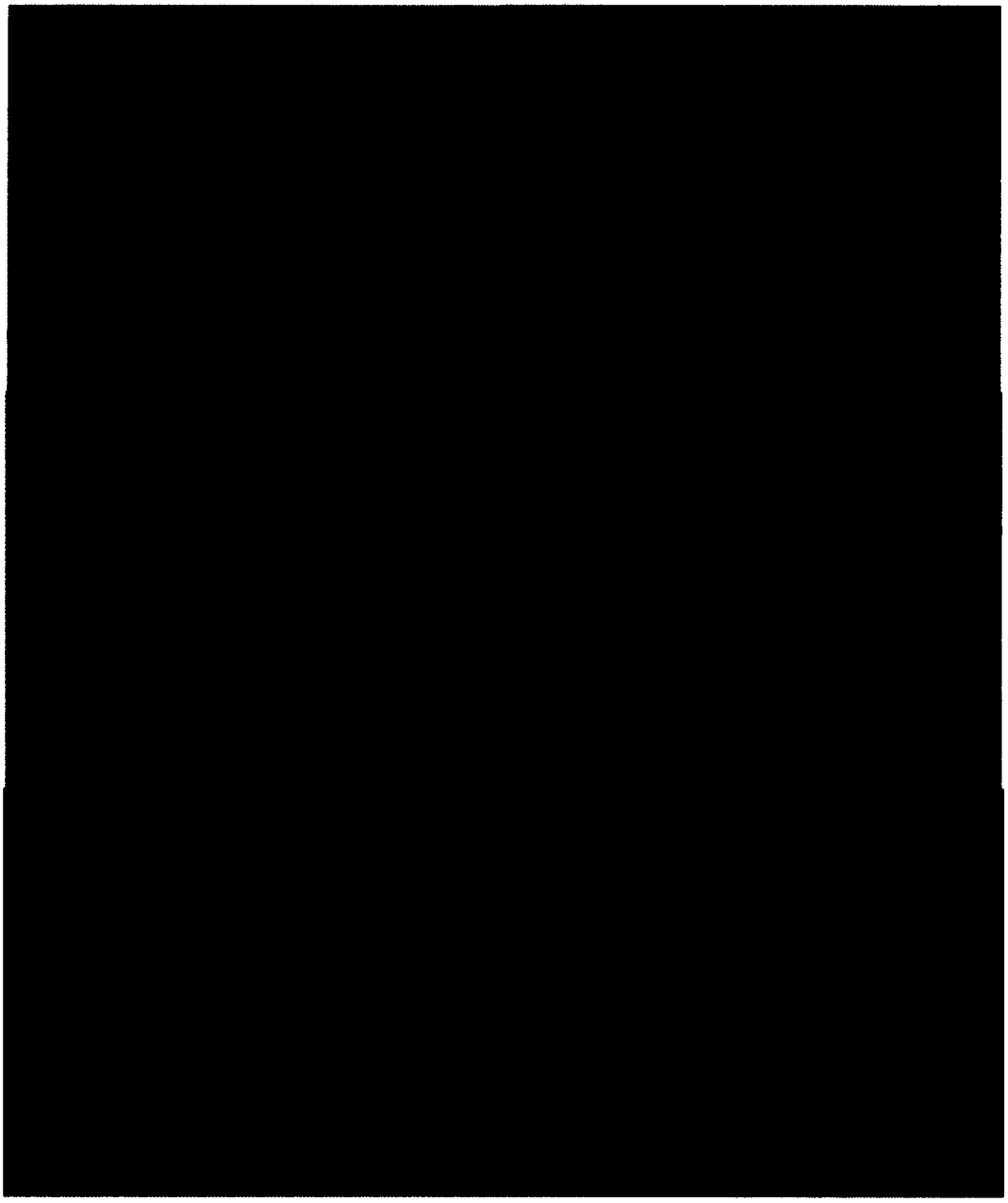

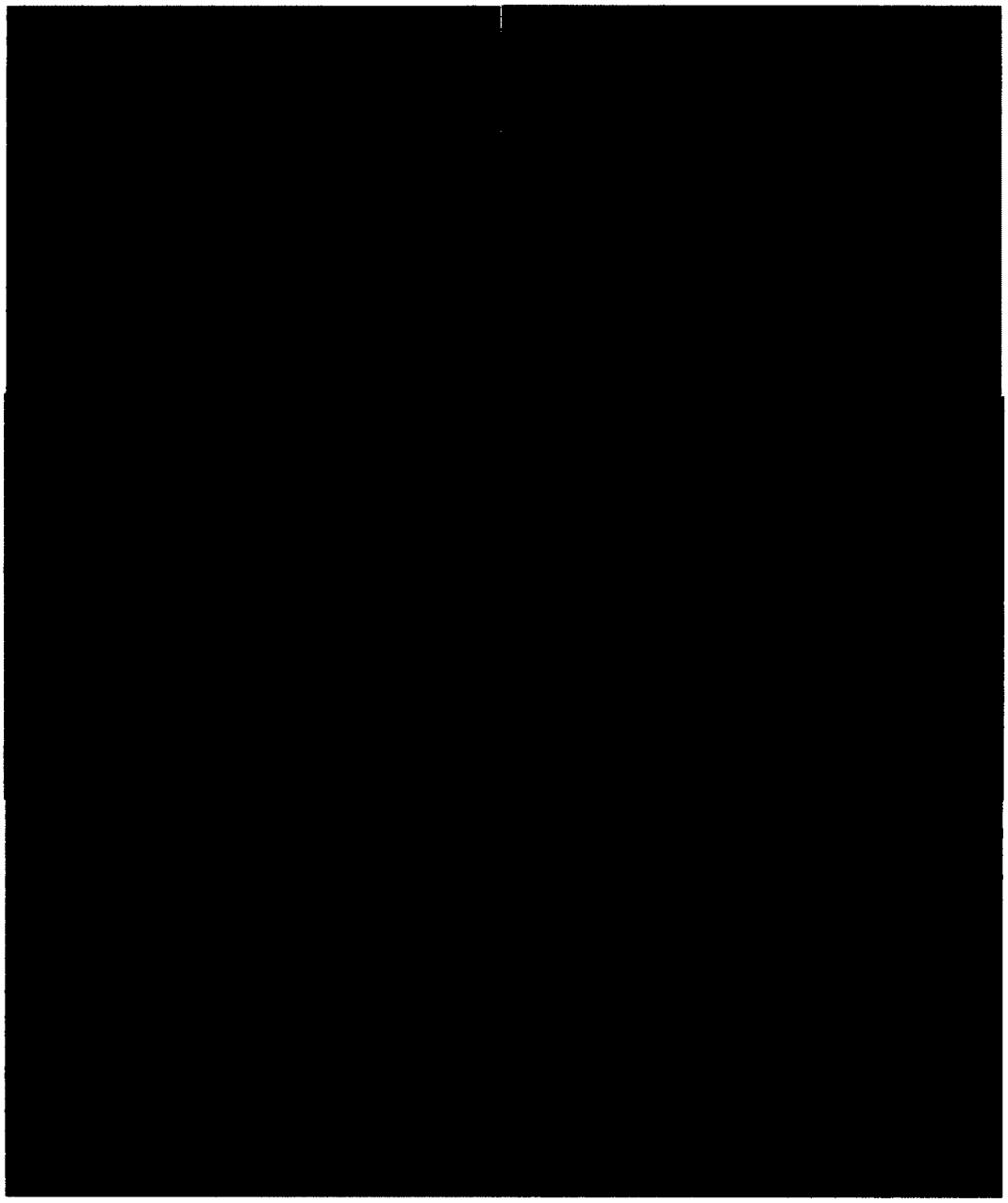

Figure 5-3. Day 7 Alcian Blue staining of the preosteoblast cells on collagen matrices with hydrogel nanoseed constructs. A) Well 1 with alginate-only hydrogels, site of initial seeding B) Well 1 with alginate-only hydrogels, center C) Well 2 with alginate+ HNT+ BMP 2, site of initial seeding D) Well 2 with alginate+ HNT+ BMP 2, center and near bead (insert) E) Well 3 alginate+ CPC + HNT, site of initial seeding F) Well 3 alginate+ CPC + HNT, center G) Well 4 alginate+ CPC+ HNT+ BMP 2, site of initial seeding H) Well 4 alginate + CPC+ HNT+ BMP 2, center and near bead (insert) I) Well 5 alginate+ CPC+ Chitosan lactate + HNT, site of initial seeding J) Well 5 alginate+ CPC+ Chitosan lactate + HNT, center K) Well 6 alginate+ CPC+ Chitosan lactate+ HNT+ BMP 2, site of initial seeding L) Well 6 alginate+ CPC+ Chitosan lactate+ HNT+ BMP 2, center and near bead (insert).

Figure 5-3 (A-L) shows Day 7 Alcian Blue staining for the cells in response to different hydrogel composite constructs with or without BMP 2. Figure 5-3 (A and B) shows cells that have produced deep blue stained ECM at the site of injection (A) and no migration towards the control bead (B). Figure 5-3 (C and D) shows deeply stained ECM producing cells at the site of injection (C), migrating cells at the center and also to the end where the alginate+ HNTs+ BMP 2 hydrogel bead is located (D, and the insert). The migrating cells are also more as compared to the Day 3 images (Figure 5-2, D).

Figure 5-3 (E and F) shows cells producing deep blue stained ECM (E) and no migration towards the alginate+ CPC+ HNTs bead (F). Figure 5-3 (G and H) shows the cells that are producing deep blue stained ECM (G) and there is migration towards the alginate+ CPC+ HNTs+ BMP 2 bead shown by the image H and the insert. The cells at the center of the collagen gel matrix show that they have started differentiating and some of the cells have migrated near the bead.

Figure 5-3 (I and J) shows the cells producing deep blue stained ECM matrix and no migration towards alginate+ CPC+ Chitosan lactate+ HNTs bead. Figure 5-3 (K and L) shows a dense ECM matrix produced by the cells and no individual cells can be seen in the matrix. The site of injection shows a continuous ECM produced by the differentiating cells (K) and the cells that have migrated towards the bead have produced ECM as well as can be seen in image L and insert.

As can be seen in Figure 5-3 (K and L), the migration is complete and the cells produce ECM in response to the BMP 2. This is the construct that has the most cells migrating and producing ECM uniformly as compared to other constructs. The images with constructs or nanoseeds with BMP 2 in the HNTs show that cells are attracted

towards them and differentiate. The alginate composites without the growth factor, BMP 2, are not chemoattractants.

5.3.1.2 *Von Kossa staining.* Von Kossa stains the phosphate group, in calcium phosphate, brown-black. Calcium phosphate is also known as hydroxyapatite and is the inorganic component of bone. The Von Kossa staining, in this project, would help in visualizing the calcium phosphate secreted by the cells in response to the BMP 2 released from the hydrogel constructs. Figures 5-4, 5-5, and 5-6 show the Von Kossa staining for alginate hydrogel composites or nanoseeds. Figure 5-4 (A-F) shows the Von Kossa staining of the cells for different alginate hydrogel composites or nanoseeds on Day 1.

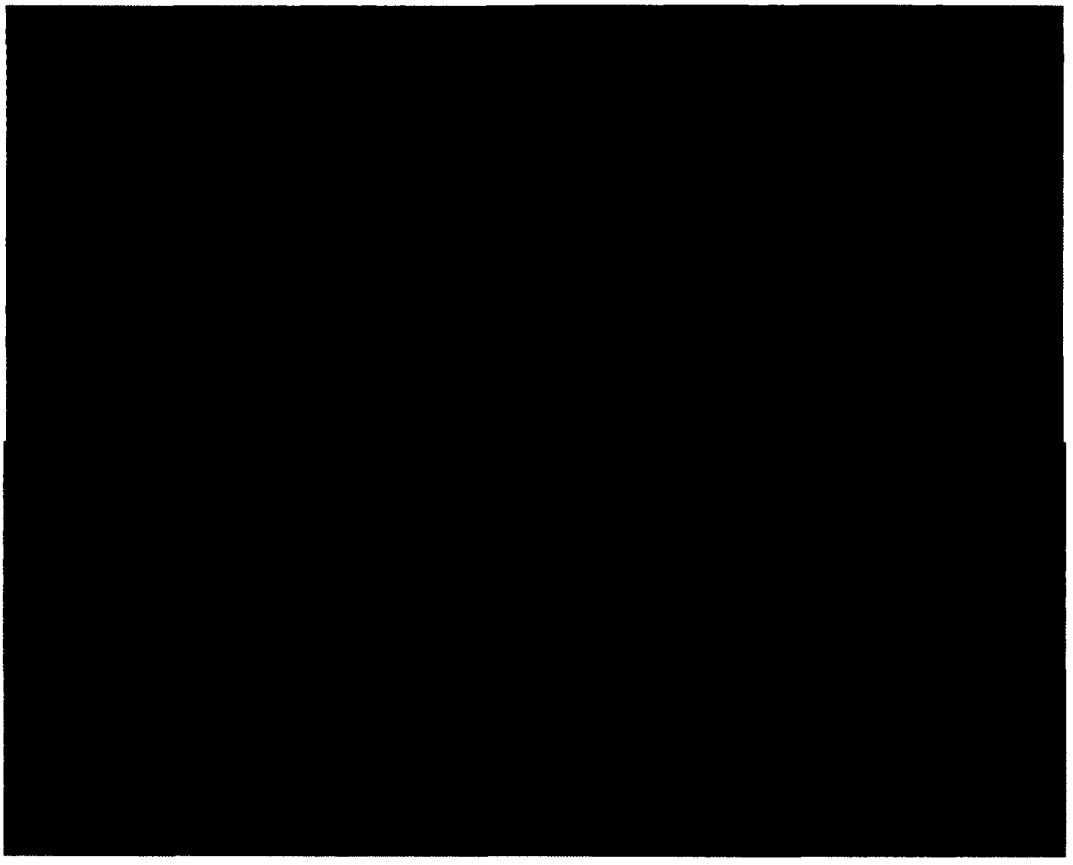

Figure 5-4. Day 1 Von Kossa Staining of preosteoblast cells on collagen matrices with hydrogel nanoseed constructs. A) Well 1 with alginate-only hydrogels B) Well 2 with alginate+ HNT+ BMP 2 C) Well 3 alginate+ CPC + HNT D) Well 4 alginate + CPC+ HNT+ BMP 2 E) Well 5 alginate+ CPC+ Chitosan lactate + HNT F) Well 6 alginate+ CPC+ Chitosan lactate + HNT+ BMP 2.

Image A shows cells that have attached and are proliferating on the collagen gel matrix in the well containing the alginate-only hydrogel control bead. The experimental groups are shown in images B-F. The cells in these images are also well attached and are proliferating, suggesting that the collagen gel matrices provide a conducive environment for cellular growth and that no inhibitory effect is seen on Day 1.

Figures 5-5 (A-L) show the Von Kossa staining for Day 3 for the alginate hydrogel composite constructs.

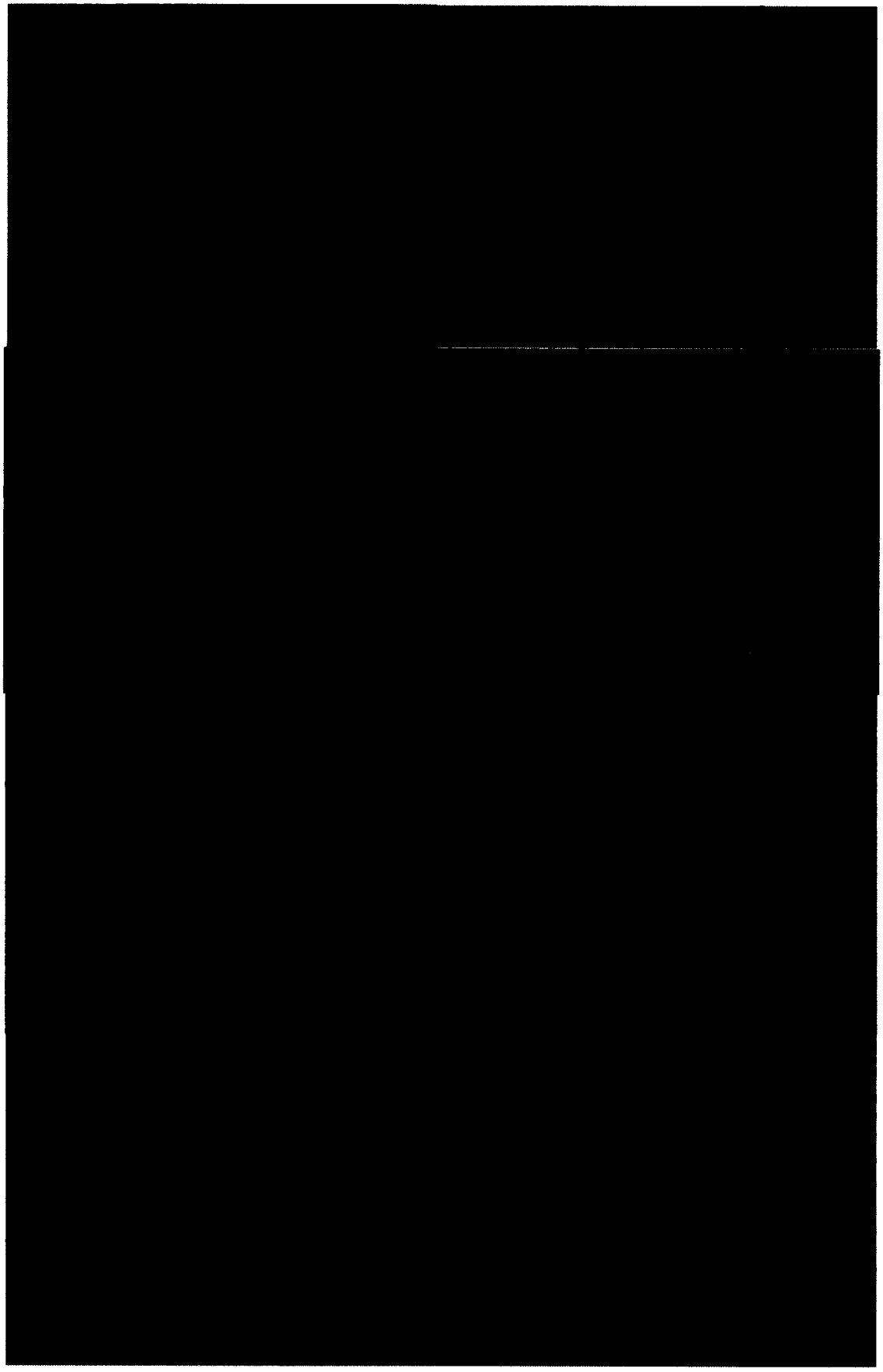

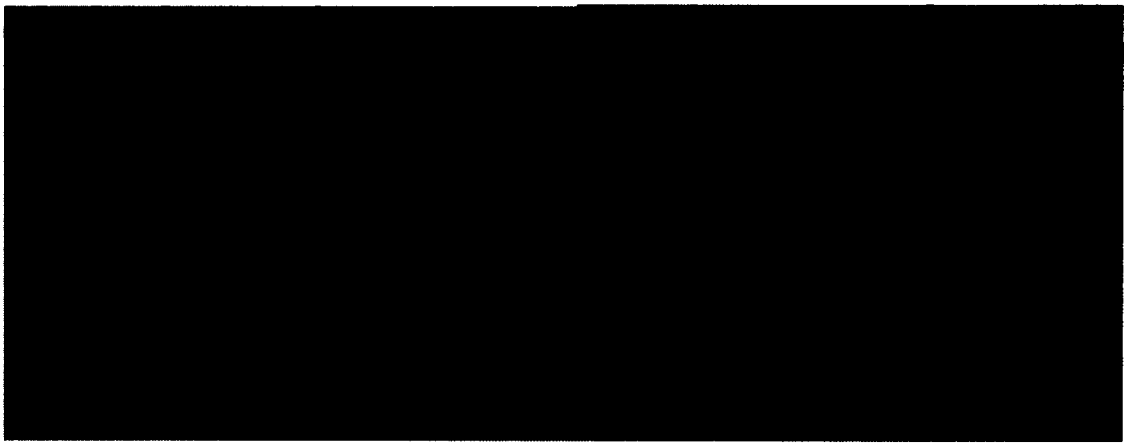

Figure 5-5. Day 3 Von Kossa staining of the preosteoblast cells on collagen matrices with hydrogel nanoseed constructs. A) Well 1 with alginate-only hydrogels, site of initial seeding B) Well 1 with alginate-only hydrogels, center C) Well 2 with alginate+ HNT+ BMP 2, site of initial seeding D) Well 2 with alginate+ HNT+ BMP 2, center E) Well 3 alginate+ CPC+ HNT, site of initial seeding F) Well 3 alginate+ CPC + HNT, center G) Well 4 alginate + CPC+ HNT+ BMP 2, site of initial seeding H) Well 4 alginate + CPC+ HNT+ BMP 2, center I) Well 5 alginate+ CPC+ Chitosan lactate + HNT, site of initial seeding J) Well 5 alginate+ CPC+ Chitosan lactate + HNT, center K) Well 6 alginate+ CPC+ Chitosan lactate + HNT+ BMP 2, site of initial seeding L) Well 6 alginate+ CPC+ Chitosan lactate + HNT+ BMP 2, center.

Figure 5-5 (A and B) show the cells in the control group. The cells have started to differentiate and are producing calcium phosphate deposits at the site of injection seen as small brown-black spots in image A. There is no migration towards the bead, as seen in image B. Figure 5-5 (C and D) show the cells in well with alginate+ HNTs+ BMP 2. Image C shows larger brown-black spots at the site of injection suggesting differentiating cells. Image D shows the center of the matrix with differentiating cells and brown patches.

Figures 5-5 (E and F) show the differentiating cells in well with alginate+ CPC+ HNTs producing calcium phosphate (brown spots) at the site of injection (E) and no migration of the cells (F). Figure 5-5 (G and H) shows the differentiating cells in well with alginate+ CPC+ HNTs+ BMP 2. Image G shows the differentiating cells producing

calcium phosphate as brown patches at the site of injection. Image H shows the migrating cells which are differentiating at the center of the collagen gel matrix producing calcium phosphate deposits as brown patches.

Figures 5-5 (I and J) show the differentiating cells in the well with alginate+ CPC+ Chitosan lactate+ HNTs. Image I shows differentiating cells producing calcium phosphate deposits as brown patches and no migration towards the bead as seen in image J. Figures 5-5 (K and L) show the differentiating cells in the well with alginate+ CPC+ Chitosan lactate+ HNTs+ BMP 2. Image K shows the differentiating cells producing calcium phosphate seen as brown spots and image L shows the migrating and differentiating cells producing the calcium phosphate deposits. Overall, Figure 5-5 shows that most calcium phosphate production takes place in the well with the differentiating cells in the well with alginate+ CPC+ Chitosan lactate+ HNTs+ BMP 2 (K and L).

Figure 5-6 (A-L) shows the Von Kossa staining for Day 7 for alginate hydrogel composites or nanoseeds.

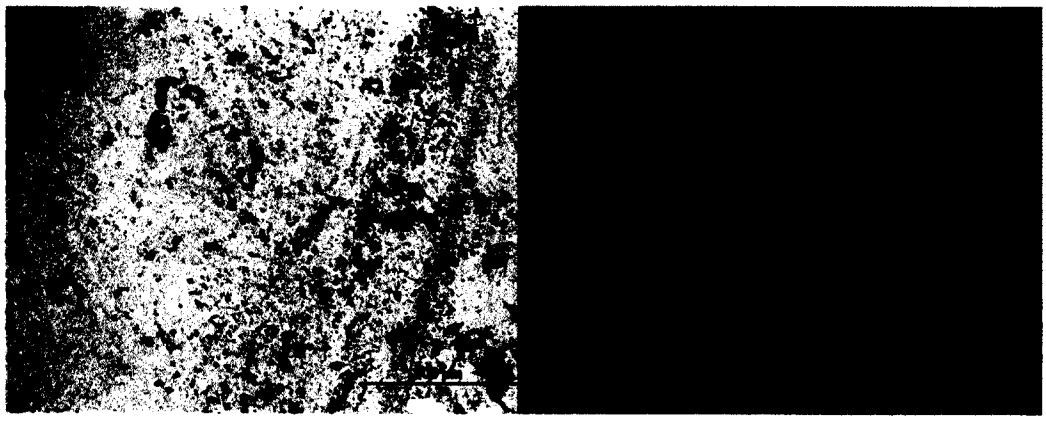

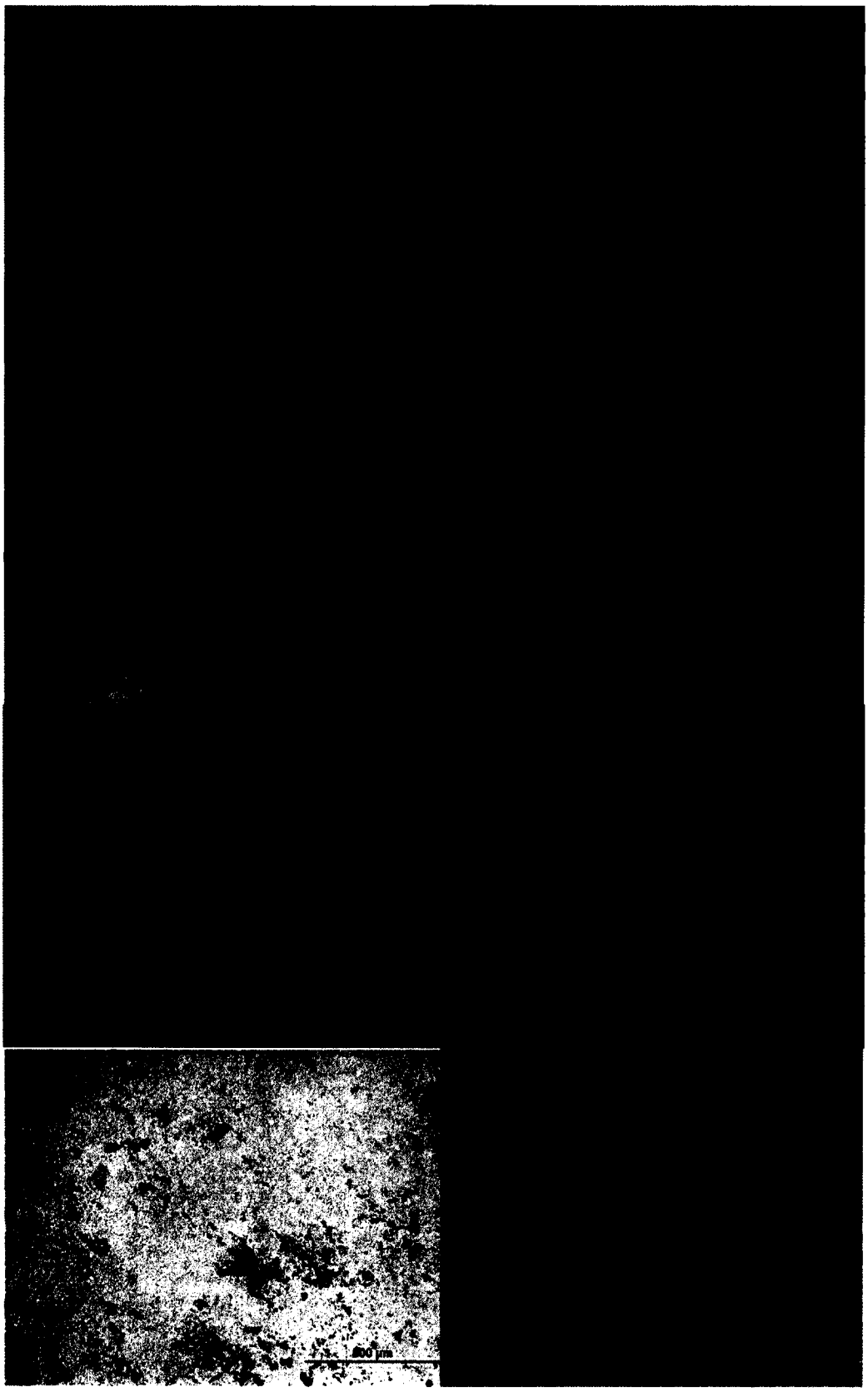
500 µm

Figure 5-6. Day 7 Von Kossa staining of the preosteoblast cells on collagen matrices with hydrogel nanoseed constructs. A) Well 1 with alginate-only hydrogels, site of initial seeding B) Well 1 with alginate-only hydrogels, center C) Well 2 with alginate+ HNT+ BMP 2, site of initial seeding D) Well 2 with alginate+ HNT+ BMP 2, center E) Well 3 alginate+ CPC + HNT, site of initial seeding F) Well 3 alginate+ CPC + HNT, center G) Well 4 alginate + CPC+ HNT+ BMP 2, site of initial seeding H) Well 4 alginate + CPC+ HNT+ BMP 2, center and near bead (insert) I) Well 5 alginate+ CPC+ Chitosan lactate + HNT, site of initial seeding J) Well 5 alginate+ CPC+ Chitosan lactate + HNT, center K) Well 6 alginate+ CPC+ Chitosan lactate + HNT+ BMP 2, site of initial seeding L) Well 6 alginate+ CPC+ Chitosan lactate + HNT+ BMP 2, center and near bead (insert).

Figure 5-6 (A and B) show the differentiating cells in the control well. The cells have produced calcium phosphate deposits at the site of injection (A) and cells have not migrated towards the control bead (B). Figure 5-6 (C and D) shows the differentiating cells in the well with alginate+ HNTs+ BMP 2. The cells have produced calcium phosphate seen as brown spots at the site of injection (C) and at the center of the collagen gel matrix by the cells that have migrated towards the bead (D).

Figure 5-6 (E and F) shows the differentiating cells in the well with alginate+ CPC+ HNTs. The cells at the site of injection have produced calcium phosphate deposits that are seen as dark brown or black patches (E) and no migration seen towards the bead (F). Figure (G and H) shows the differentiating cells in the well with alginate+ CPC+ HNTs+ BMP 2. The cells at the site of injection have produced calcium phosphate

deposits (G) the cells have migrated and differentiated towards the bead in response to the BMP 2 (H and the insert).

Figure 5-6 (I and J) shows the differentiating cells in the well with alginate+ CPC+ Chitosan lactate+ HNTs. The cells produce dark brown stained calcium phosphate deposits at the site of injection (I) and the cells have not migrated towards the bead as can be seen in image J. Figure 5-6 (K and L) shows the differentiating cells in the well with alginate+ CPC+ Chitosan lactate+ HNTs+ BMP 2. The cells at the site of injection (K) and the migrating cells (L and insert) show calcium phosphate production seen as dark brown patches.

As seen in all of the figures above, cells differentiate after Day 3 in all the wells at the site of injection but migrate and differentiate towards the hydrogel beads or nanoseeds with BMP 2 in the HNTs. This suggests that the alginate hydrogel composites without BMP 2 are not chemoattractants.

The observations from both the histochemical staining experiments (Alcian Blue and Von Kossa) suggest that alginate hydrogel composites enhanced with HNTs with BMP 2 can act as chemoattractants and induce cellular migration and differentiation *in vitro*. The observations from the histochemical staining experiments suggest that the nanoseeds have potential to be used as implant material for bone regeneration. The following subsections will further illustrate if the alginate hydrogel constructs (nanoseeds) have the potential to function as implant materials.

5.3.1.3 *Preosteoblast pilot study on the composite hydrogels.* A pilot study of seeding preosteoblasts directly on composite hydrogel films with HNTs but without any growth factors was done to see if the alginate hydrogels enhanced with CPC, chitosan

lactate, and HNTs have any effect on the cellular differentiation. The study was done for a 14 day period and the samples were taken for histochemical staining on Days 3, 7, and 14. The hydrogel composite films with the preosteoblasts were stained with histochemical stains Alcian Blue and Picrosirius Red and then these films were destained as described in the methods section. Figure 5-7 shows the Alcian Blue staining and quantitative analysis by Nanodrop 2000 spectrophotometry.

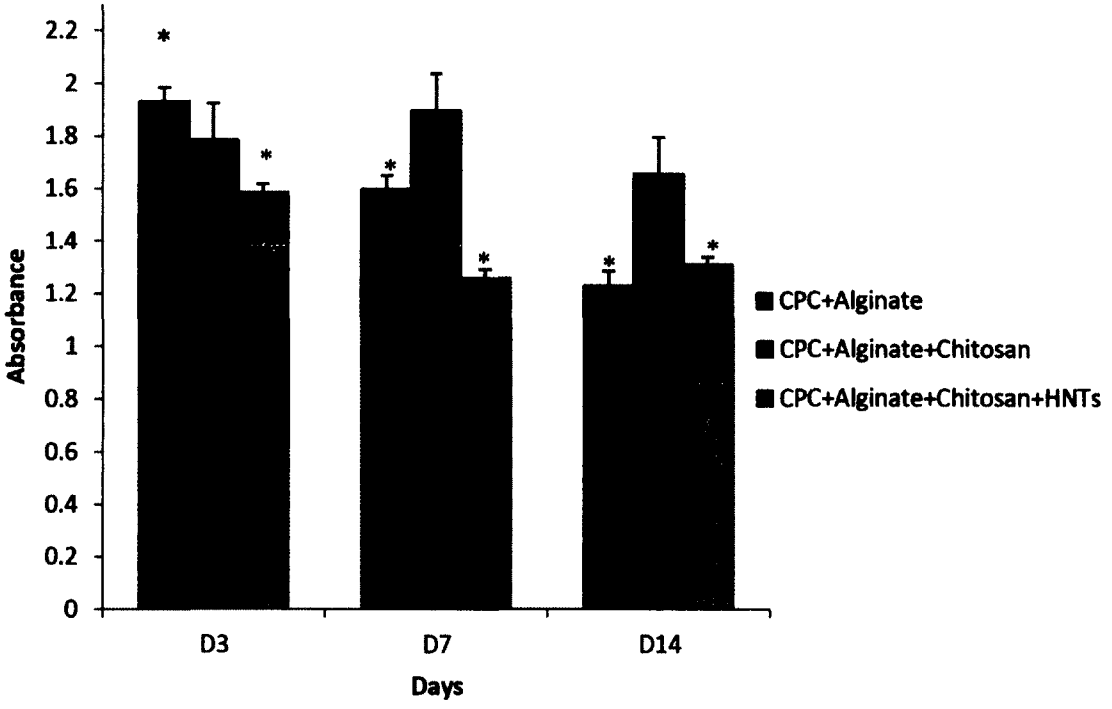

Figure 5-7. Graph showing the absorbance (at 450-495 nm) of the eluted Alcian Blue stain against the number of days and different hydrogel composition. (n=6), $p<0.05$. Error bars show standard deviation.

The graph in Figure 5-7 shows the absorbance of the eluted Alcian Blue stain against the number of days for different hydrogel composites. Alcian Blue staining results shows that the CPC + alginate films had synthesized a greater

amount of proteoglycan Day 3 (Mean: 1.93158) but there was a drop by Day 14 (Mean: 1.22901). The CPC + alginate films also had comparatively more ECM than the rest of the films as shown in Figure 8 on Day 3. The CPC+ alginate+ Chitosan films maintained ECM levels relatively equal on Days 3 (Mean: 1.7848), 7 (Mean: 1.89605) and 14 (Mean: 1.6552). The CPC+ alginate+ Chitosan+ HNTs films had the least ECM polysaccharides on Day 3 (Mean: 1.586) when compared against the other scaffolds. The levels of ECM polysaccharides decreased on Day 7 (Mean: 1.25685) but remained relatively similar on Day 14 (Mean: 1.3081).

Picrosirius Red staining was done for estimating the amount of collagen produced by the cells on the hydrogel composite films. Figure 5-8 shows the Alcian Blue staining and quantitative analysis by Nanodrop 2000 spectrophotometry.

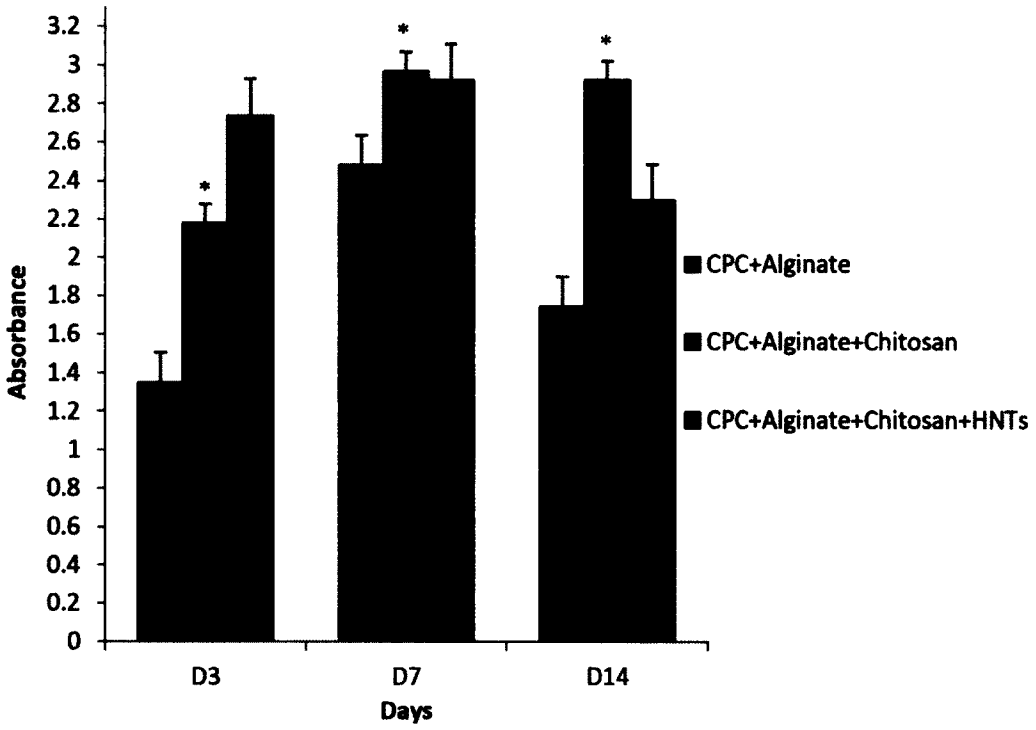

Figure 5-8. Graph showing the absorbance (at 620-750 nm) of the eluted Picrosirius Red stain against the number of days. (n=6), $p<0.05$. Error bars show standard deviation.

Figure 5-8 shows the graph of absorbance of the eluted Picrosirius Red stain against the number of days for different hydrogel composites. Picrosirius Red staining data showed that the CPC+ alginate films had accumulated the less amount of collagen on Day 3 (Mean: 1.35) but increased by Day 7 (Mean: 2.46) with a decrease noted on Day 14 (Mean: 1.74). The CPC+ alginate films also had produced a lesser amount of collagen when compared with the other two coatings (Figure 9). In contrast, CPC+ alginate+ chitosan films produced an initial higher amount of collagen (Mean: 2.1781), which increased on Day 7 (Mean: 2.97) and remained somewhat similar through Day 14 (Mean: 2.9198). CPC+ alginate+ chitosan+ HNT films produced the most collagen by Day 3 (Mean: 2.74) when compared against the other scaffolds. The levels of collagen increased slightly on Day 7 (Mean: 2.9196) and decreased in amount by Day 14 (Mean: 2.30). The cumulative supports the observation that cells on all substrates produced a base organic extracellular matrix.

A two ANOVA with replacement was used to check for the significance of the results at α=0.05 for both the experiments (Alcian Blue and Picrosirius Red assays). The statistical analysis was conducted by using MS Excel 2013 Toolpak©. The statistical analyses showed that there was significance across the days and across the groups with CPC+ alginate and CPC+ alginate+ Chitosan + HNTs for Alcian Blue staining as suggested by the higher F-stat values against F-critical values. There was also a significant interaction within the groups across days suggesting that the trend seen in the graph is significant. For Picrosirius Red staining there was significance observed for the group CPC+ alginate+ Chitosan for all the three days as suggested by the higher F-stat

values against F-critical values. There was also a significant interaction within the groups across days suggesting that the trend seen in the graph is significant.

The cumulative observation of both the stain elution studies suggests that all the hydrogel composites support the ECM and collagen production on all days. A relationship was observed between the two graphs of stain elution studies for ECM mucopolysaccharides and collagen production throughout the 14 day period. While the cells on CPC/alginate produced more ECM mucopolysaccharides on Day 3 the cells on other groups namely, CPC/alginate+ Chitosan and CPC/alginate+ Chitosan+ HNTs, synthesized more collagen. The production of ECM mucopolysaccharides and collagen, both are important for the differentiating cells as this is the organic template for the formation of new bone.

Looking at both the graphs (Figures 5-7 and 5-8), CPC/alginate+ Chitosan was the composition that produced both ECM mucopolysaccharides and collagen in relatively stable amounts throughout all the days. The next composition to follow is CPC/alginate+ Chitosan+ HNTs which produced comparable amounts of ECM mucopolysaccharides and collagen on Days 7 and 14.

5.3.2 Release Study of BMP 2 from HNTs and Various Hydrogel Composites

In the previous project, the release profile of BMP 2 from HNTs was studied. In the current project, the objective of studying the release profile of BMP 2 was to determine if it is released out of the hydrogel matrix and the concentration of the released BMP 2. This would suggest that the BMP 2 is indeed, released out of the hydrogels and not just out of the HNTs and would suggest the hydrogel constructs have chemoattractant potential.

5.3.2.1 *Release profile of BMP 2 from HNTs.* The release profile study of BMP 2 from HNTs was repeated to check the reproducibility of the release profile experiment observations from the previous nanoenhanced bioactive hydrogels project. The experiments were repeated for a period of 24 hours and 7 days. Figure 5-9 shows the calibration curve for BMP 2 standards.

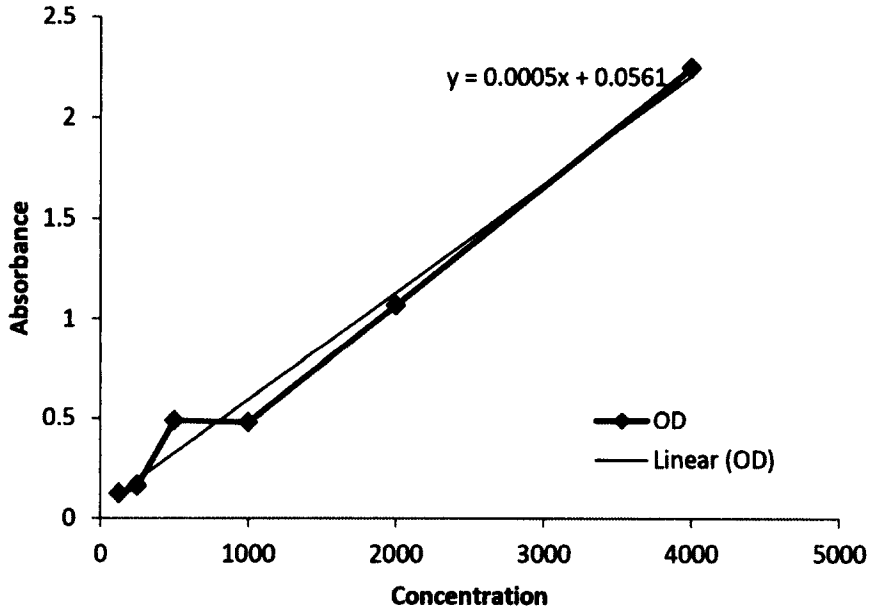

Figure 5-9. Calibration curve for BMP 2 standards with absorbance (OD) and the corresponding concentrations.

Figure 5-9 shows the calibration curve for BMP 2 standards that were used to calculate the concentration of BMP 2 released from the HNTs and hydrogels. Figure 5-10 shows the conversion for the absorbance values and the corresponding concentrations.

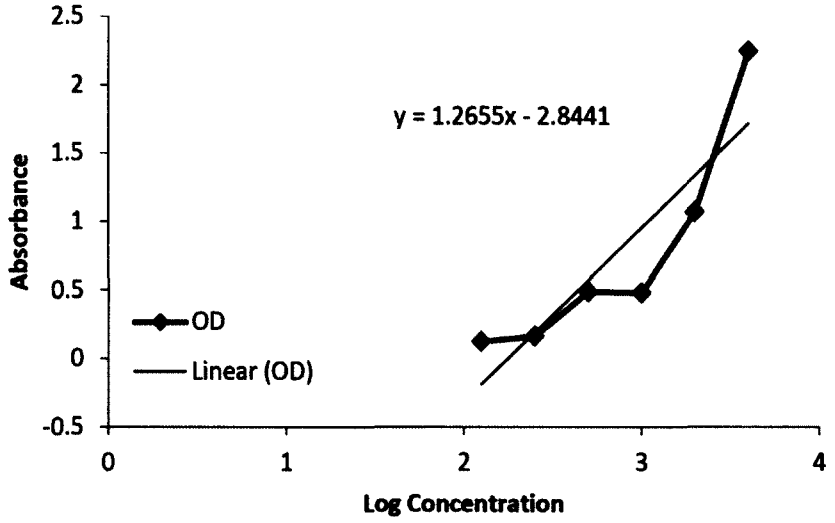

Figure 5-10. Graph for conversion for the absorbance OD values to corresponding concentrations.

Figure 5-10 shows the graph with the conversion for the absorbance to concentration. Figure 5-11 shows the BMP 2 release from HNTs for 24 hours.

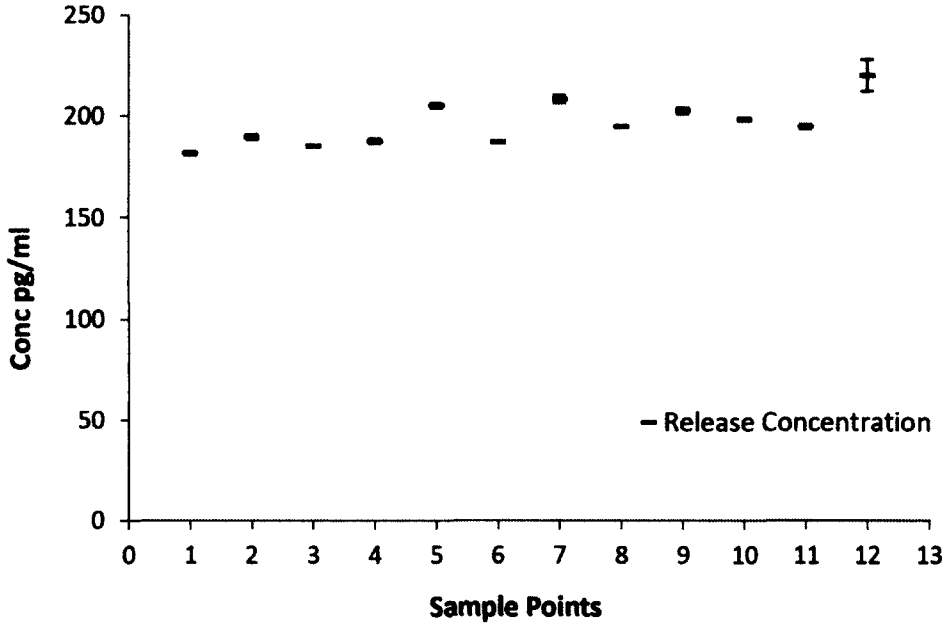

Figure 5-11. Graph showing release of BMP 2 from the HNTs for 24 hours.

The graph in Figure 5-11 shows that the results of the release profile of BMP 2 from the previous study are reproducible as they are comparable. The release of BMP 2 from HNTs is sustained for a period of 24 hours. The objective of this study was to confirm that the growth factor is released into the hydrogel matrix and the graph shows the release for a period of 24 hours. The error bars represent the standard deviation calculated by the standard deviation of the data point and the average of the triplicate samples (detailed process of calculation of the standard deviation described in Appendix B). [59]

As described earlier, the release profile of BMP 2 for 24 hours was estimated by the use of custom made sandwich ELISA kits. The trend seen here is not of the cumulative release but that of individual data points. The concentration seen in the graph cannot be regarded as accurate estimate as the standards provided by the manufacturer showed resolution problems. The data should be viewed cautiously and regarded as a qualitative estimate of the protein released from the HNTs. The raw data tables and supplementary tables are provided in Appendix B.

The study was extended to a period of 7 days to check if the growth factor is released for extended periods form the HNTs. Figure 5-12 shows the graph of release profile of BMP 2 from HNTs for 7 days.

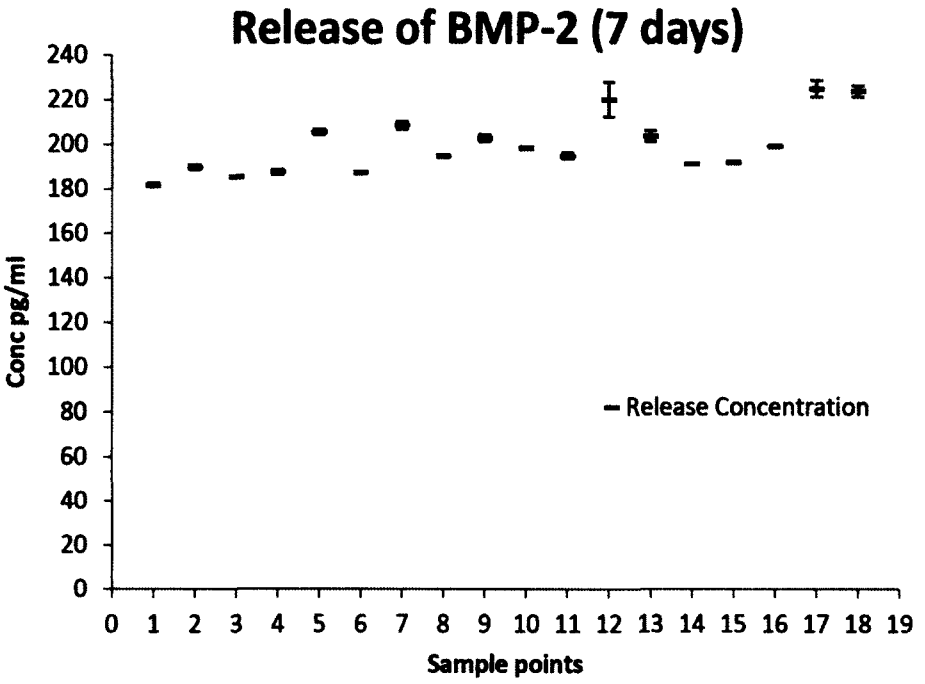

Figure 5-12. Graph showing the release profile of BMP 2 from HNTs for 7 days.

Figure 5-12 shows the graph for BMP 2 release profile from HNTs for a 7 day period. This graph validates that the results obtained in previous study are reproducible and also confirms that the HNTs release the growth factor in the hydrogel matrix for an extended period of 7 days. The calibration curves used for the calculation of the values are the same given in Figure 5-9 and 5-10. The release of the growth factor is in nanograms per ml range. The error bars represent the standard deviation calculated by the standard deviation of the data point and the average of the triplicate samples (detailed process of calculation of the standard error described in Appendix B). [59]

The release profile of BMP 2 from the HNTs suggests that an extended and sustained release can be obtained from HNTs for a period of 7 days. The release is in pico and nanograms range which is the effective range for BMP 2 in natural tissue environment. Even though the concentrations cannot be regarded as accurate due to the

resolution error in the kit, especially below the concentration of 50 pg/ml, the qualitative trend shows that the range in which the BMP 2 is released is comparable to the effective range in natural tissues. The results obtained for 7-day release are encouraging as the cellular differentiation process peaks at Day 7. Hence, a sustained release of BMP 2 for a period of 7 days from HNTs is beneficial for early onset of cellular differentiation which might lead to accelerated regeneration of the damaged bone tissue.

5.3.2.2 *Release profile of BMP 2 from HNT enhanced hydrogels.* The release profile study of BMP 2 from hydrogels enhanced with HNTs was carried out to investigate if the BMP 2 was released from the hydrogels into the surrounding medium. The study was conducted for a period of 36 hours.

Figure 5-13 shows the release profile graph of BMP 2 from hydrogels enhanced with growth factor loaded HNTs.

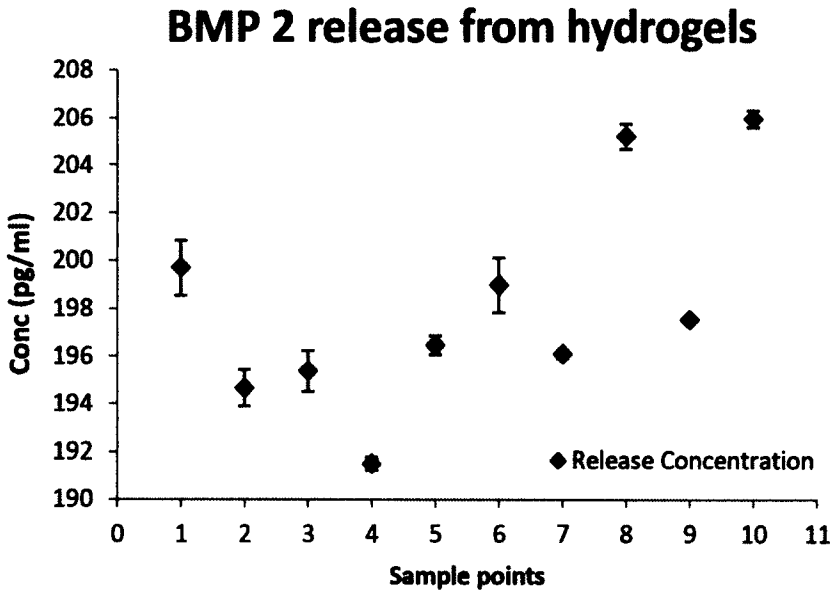

Figure 5-13. Graph of release profile of BMP 2 from hydrogels enhanced with HNTs.

Figure 5-13 shows the release profile of BMP 2 from the HNTs in hydrogel matrix. The calibration curves used are the same used in Figure 5-9 and 5-10. The graph shows a qualitative trend and the concentrations are not accurate as mentioned earlier due to the resolution problem and noise in the standards of the kit.

The trend shows an extended and sustained release can be observed for a period of 36 hours in the above graph. This result supports the observation that the cells migrated towards the nanoseeds (Nanoenhanced hydrogels with BMP 2 loaded HNTs) placed at one end of the collagen gel matrix in Section 5.3.1. The growth factor is released out of the gel matrix serving as the chemoattractant signal.

It would have been ideal to have a release profile for 7 days. The experiment could be performed only for a period of 36 hours or three days as the hydrogels broke in the HBSS solution due to continuous rocking of the platform. The error bars represent the standard deviation calculated by the standard deviation of the data point and the average of the triplicate samples (detailed process of calculation of the standard deviation is described in Appendix B). [59]

5.3.3 FE-SEM Imaging and Comparison of the Hydrogel Composites Surface Morphologies

FE-SEM imaging was done to understand the differences between the surfaces of the alginate hydrogels when enhanced with CPC, Chitosan lactate, and HNTs. It is important to understand how the surfaces are modified by the addition of the composite materials as this will shed light on the material interactions and some of the material properties that are altered. Figure 5-14 shows a general comparison of the surfaces and overall morphology of the hydrogel beads with addition of the composite materials at lower and higher magnification.

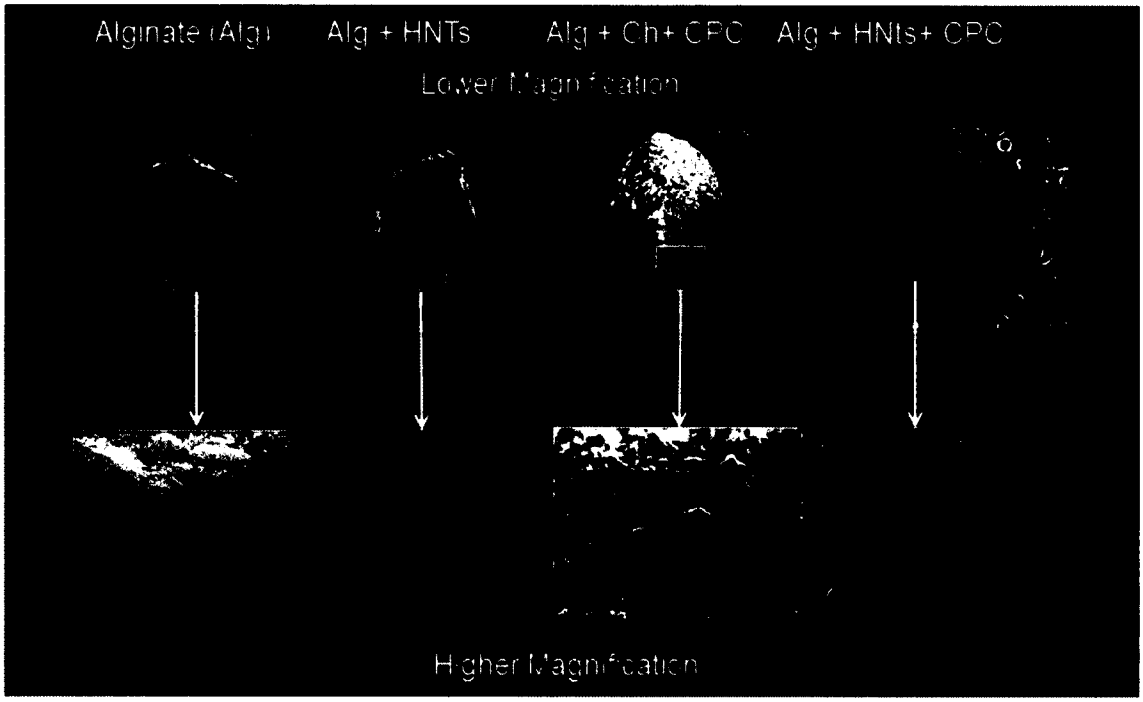

Figure 5-14. A comparison of different hydrogel constructs surface morphologies at higher magnification.

Figure 5-14 shows a general overview of the surface morphologies of the alginate hydrogel composite beads. The lower magnification images show the overall morphologies of the hydrogel beads. The alginate-only bead has smooth surface and looks shriveled compared to the rest of the hydrogel composites. The hydrogel beads with HNTs, CPC, and chitosan lactate have retained their size and shape even after lyophilization and have rough surfaces. The bead with alginate+ CPC+ chitosan lactate has the most rigid and well retained structure after lyophilization. The ridges and surface features are uniform and well defined in this composition of the hydrogel composite.

The higher magnification images in Figure 5-14 show the corresponding surfaces in details for the respective alginate hydrogel composite compositions. alginate-only hydrogel shows a relatively smooth surface devoid of any surface features. The alginate+ HNTs and alginate+ CPC hydrogels have relatively rough surface. The most well defined

surface features can be seen in the higher magnification image of alginate+ CPC+ chitosan lactate bead with well-defined ridges and grooves. These images provide a general understanding of how the surfaces get modified by the addition of composite materials. Figure 5-15 (A-D) shows the surface topography of the alginate composites in greater details at higher magnifications.

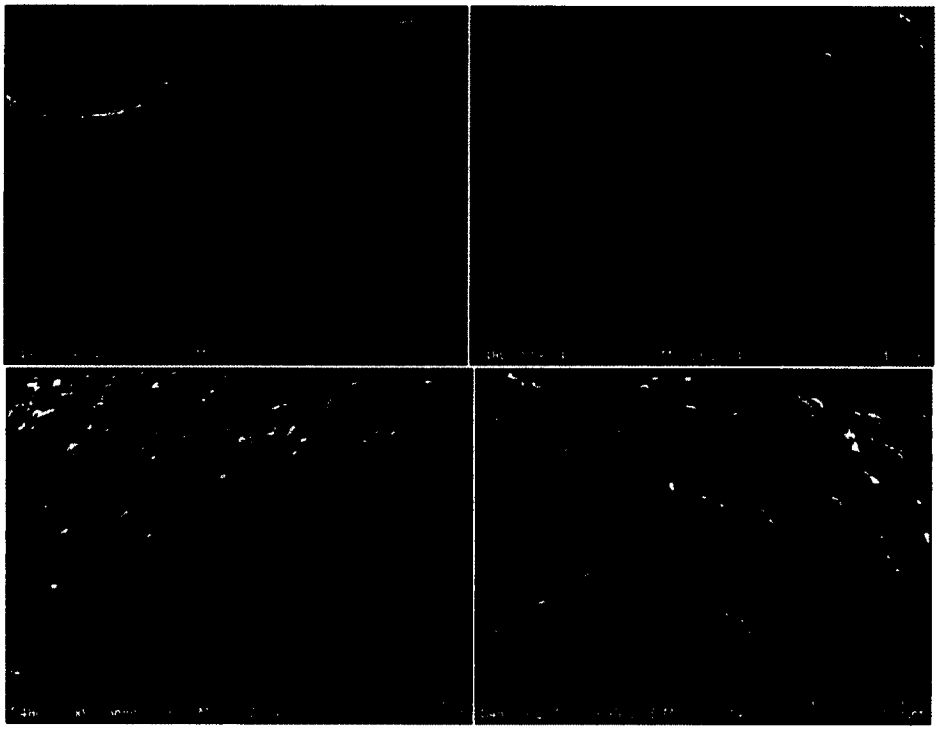

Figure 5-15. FE-SEM images of A) alginate-only B) alginate+ HNTs C) alginate+ CPC and D) alginate+ CPC+ Chitosan showing the surface morphology at 100 μm magnification.

Figure 5-15 (A and B) show the FE-SEM images of alginate-only and alginate+ HNTs hydrogel beads at 100 μm scale. The surface of alginate-only hydrogel (control) looks smooth and there are no ridges or grooves on the surface. There are only slight elevations with few pores visible in the image. The surface of the hydrogel with HNTs shows a relatively rough surface with small and sharp mound like elevations protruding out of the surface. No pores or ridges and grooves are visible in the image.

Figure 5-15 (C and D) show the FE-SEM images of alginate hydrogels enhanced with CPC (C) and CPC+ Chitosan lactate (D). The surface alginate+ CPC hydrogel shows distinct ridges and grooves and some pores sunken in the surface. The elevations protruding out of the surface look uniform giving a well-defined appearance to the surface of the bead (C). The surface of the alginate+ CPC+ chitosan lactate bead shows longer elevations as compared with alginate+ CPC hydrogel bead. Ridges and grooves are not visible at this magnification but pores can be seen on the mound shaped elevations (D). The surface also appears to be rougher when compared to surfaces of alginate-only and alginate+ HNTs hydrogel beads (A and B). Figure 5-16 shows the surface topography of the alginate hydrogel composites at higher magnification (10 μm)

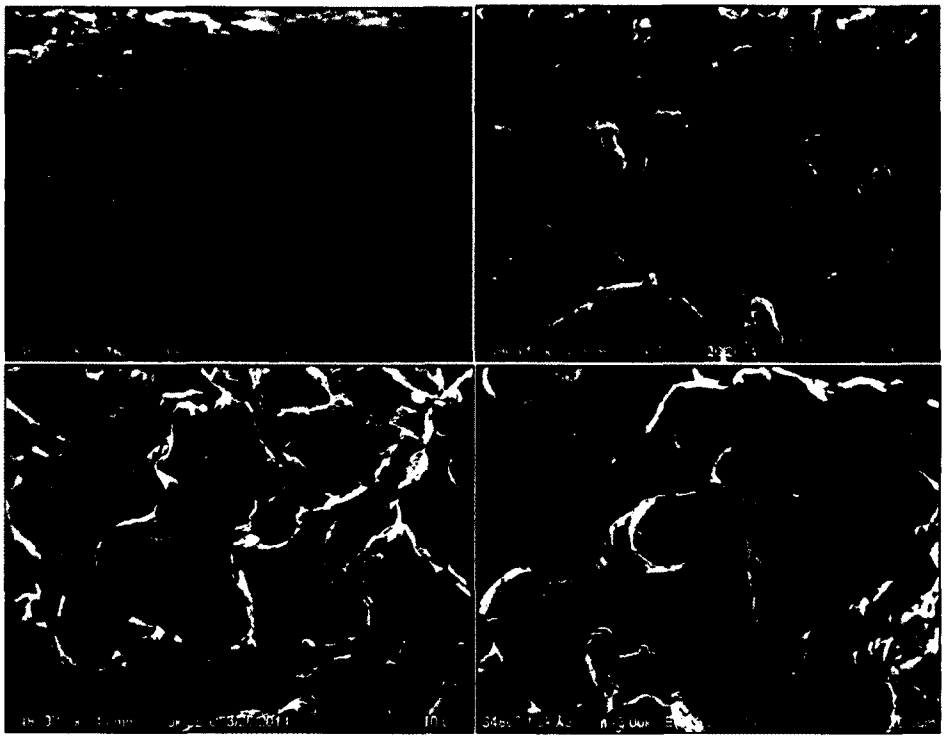

Figure 5-16. FE-SEM images of A) alginate-only B) alginate+ HNTs C) alginate+ CPC and D) alginate+ CPC+ Chitosan showing the surface morphology at 10 μm magnification.

Figure 5-16 (A-D) shows FE-SEM images of the alginate hydrogel composite surfaces at higher magnification (10 μm scale). The surface of the alginate-only hydrogel (A) shows an area of rough surface surrounded by smooth surface. This rough surface looks sunken into the bead and might have resulted out of scratch during handling of the bead. alginate+ HNTs hydrogel (B) shows relatively smaller elevations and HNTs sticking out of the surface. The alginate+ CPC hydrogel (C) surface looks crumpled and has sharp ridge like elevations. The alginate+ CPC+ Chitosan lactate (D) surface shows similar elevations as seen in image C but the elevations are larger.

Comparing all the images from Figures 5-14, 5-15, and 5-16, the observations suggest that addition of composite materials like HNTs, CPC, and chitosan lactate modifies the surface of alginate hydrogels and makes it rougher with surface features like elevations, ridges, and grooves. The modification of surface might be beneficial for cellular attachment as cells will find a favorable surface to anchor themselves on to the hydrogels. The enhancement of alginate hydrogels with the composite materials will make the hydrogels more suitable as implant materials.

CHAPTER 6

HYDROGEL COATINGS FOR TITANIUM IMPLANTS

6.1 Introduction

Severe bone injuries have been secured by orthopedic implants for over fifty years. [48] Stainless steel was replaced by titanium because of its excellent biocompatibility. [48] Titanium and its alloys do not corrode as seen in stainless steel and other metal alloys. [48] It is relatively inert and has suitable material properties that make useful for stabilizing broken bone fragments. [48] Despite of its virtues, titanium faces certain drawbacks such as it failure to osteointegrate with surrounding bone tissue and it is prone to post-surgical infections. [20, 26, 37]

Post-surgical infections are one of main causes of the titanium implant failure. [20, 26, 37] In worst case, the implant needs to be completely removed from the body, the surrounding tissue debrided and cleaned, and a new implant be inserted at the site of injury. [35] This procedure can lead to complications due to patient's physiological state, health status, age, and clinical condition.

In the previous chapters (Chapters 4 and 5), the applications of calcium alginate and composite hydrogels have been discussed in detail. In the current chapter, the application of bioactive hydrogels enhanced with CPC, chitosan lactate and HNTs loaded with anti-infective drug, gentamicin sulfate, is discussed. Gentamicin sulfate (henceforth

referred to as GS) is widely used in the field of orthopedic medicine to treat infections from gram-negative strains of bacterium. [38]

The primary hypothesis of this project was to develop anti-infective hydrogel coatings for titanium implants that will inhibit the growth of gram negative bacterium, *E. coli*, in this study. The secondary hypothesis was to investigate if anodization of the surface retains or enhances the osteogenic properties of titanium by laying hydroxyapatite foundation to make it favorable to the osteogenic cells and enhancing its osteointegration. The graphical representation in Figure 6-1 below shows the objectives and the construct with anodized titanium and anti-infective hydrogel.

Figure 6-1. Graphical representation of the anti-microbial hydrogel (H) coating applied to anodized titanium (AT). From left to right, bacteria (B) encounter the anti-microbial hydrogel and released gentamicin (G) altering their metabolism leading to cell death. T = titanium.

6.2 Materials and Methods

Plasticware was obtained from Mid Scientific, St. Louis, MO. All chemicals for synthesis, physical, and chemical analysis were purchased from Sigma Aldrich, St. Louis, MO. Gentamicin disks were obtained from Thermo Scientific, Waltham, MA. Titanium sheets (foils of thickness 0.1 mm) were obtained from Sigma-Aldrich, St. Louis, MO.

6.2.1 Anodization of Titanium

The anodization apparatus was set up in CTH 316. The details of the procedure for anodization are described in Section 3.1.7. Anodization for the titanium sheets was for 1, 2, 3, and 4 minutes. The difference in the surface of the sheet for the different time durations was analyzed by FE-SEM.

6.2.1.1 *SBF study on the osteogenic properties of anodized titanium.* To ascertain whether titanium retains its osteogenic potential after anodization, the sheets anodized for different time duration were kept immersed in simulated body fluid (SBF) for seven days. The SBF was replaced every day for the duration of the experiment. After seven days the sheets kept in SBF were gently washed and air dried for imaging under FE-SEM. EDX analysis was performed for elemental analysis.

6.2.2 Bacterial Inhibition Study on the GS-HNT Enhanced Hydrogel Constructs

The hydrogels enhanced with GS loaded HNTs were tested for their bactericidal properties on Muller-Hinton agar plates. The bacterial studies were carried out for 24 hours. If the bacteria fail to grow within the immediate 24 hours, the chances of post-surgical infection due to the implant are reduced. [26, 38, 39, 52] The details of the bacterial inhibition studies are given in Section 3.2.7.

6.2.3 Release Profile Study of GS from HNTs and Hydrogels Enhanced with HNTs

A release profile study was conducted for both the hydrogels and HNTs to estimate the amount of GS released from them. The release profile procedure is explained in details in Section 3.2.6.

6.3 Results and Discussion

This section discusses the results from the experiments from the previous section from the current chapter.

6.3.1 FE-SEM Imaging of the Anodized Titanium

The anodized and non-anodized titanium were imaged by FE-SEM to analyze the difference between their surfaces. Figure 6-2 shows the anodized titanium surfaces after 1 minute, 2 minutes, 3 minutes, and 4 minutes and non-anodized titanium (control) for comparison.

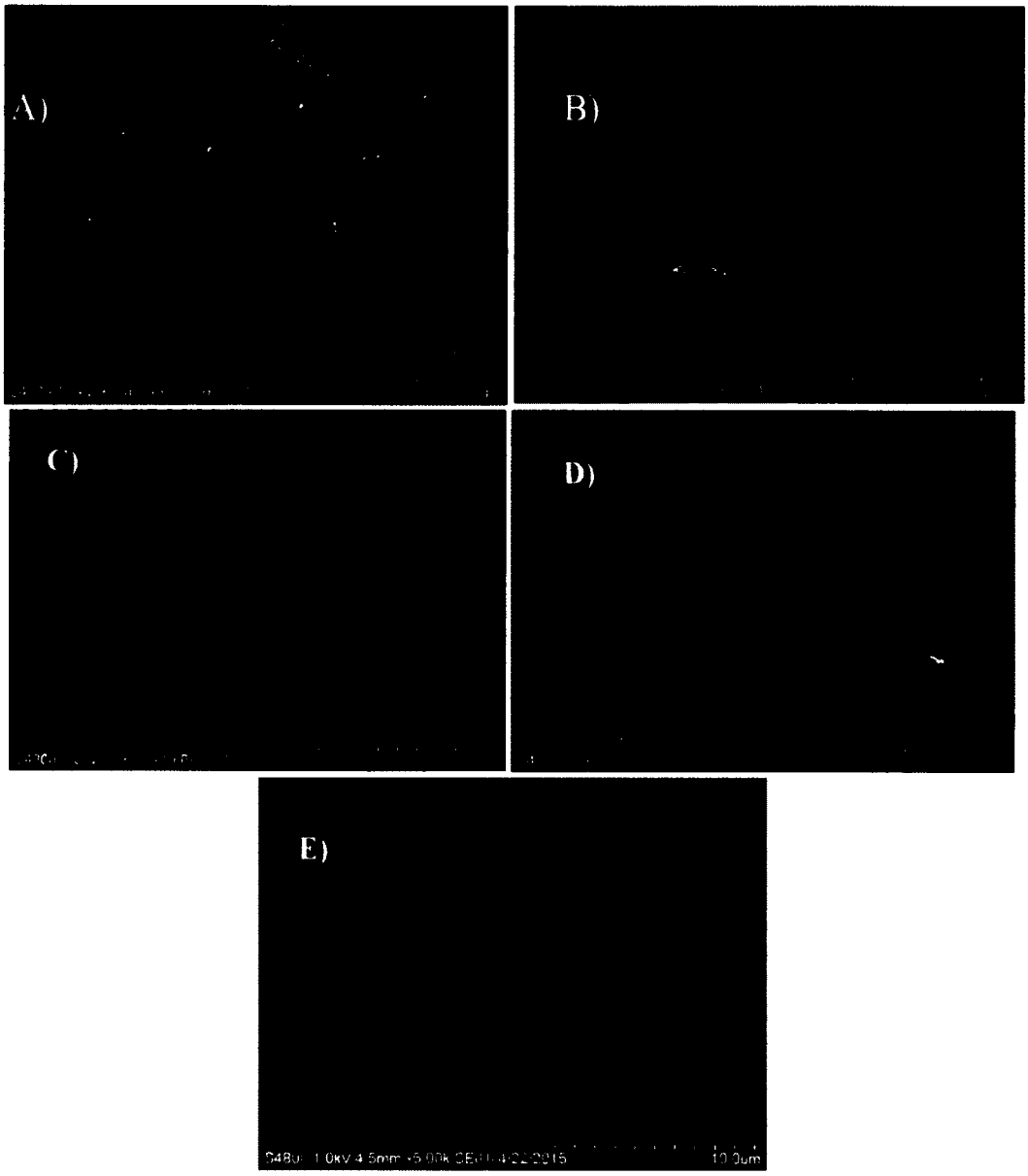

Figure 6-2. Titanium surfaces after anodization at 5μm magnification A) 1 minute B) 2 minutes C) 3 minutes D) 4 minutes and E) Non-anodized titanium (control) at 10 μm magnification.

Figure 6-2 (A) shows titanium after 1 minute of anodization. The surface is not visibly modified and looks similar to the control in Figure 6-2 (E). The surface modification by anodization visibly shows after 2 minutes (B-D) and is significantly different in titanium anodized for 4 minutes (D). The observations from the images in Figure 6-2 (A-E) suggest that the titanium surface gets etched and modified after 2

minutes of anodization. Further analysis of properties of the anodized titanium was done by immersing the anodized titanium in SBF for 7 days as described in the following section.

6.3.1.1 *FE-SEM imaging and EDX of the SBF- titanium study.* The SBF-titanium study was done to investigate if the osteogenic properties of titanium were retained even after anodization. This study is important to assess how anodization of titanium affects its osteogenic properties. If the osteogenic properties get enhanced, as suggested by larger and more deposits of hydroxyapatite crystals on the anodized titanium surface, then this would suggest that anodization would improve the biological properties of titanium and help in better integration of the implant in the host tissue.

Figures 6-3 and 6-4 show the results of EDX analysis for the titanium sheets kept immersed in SBF for 7 days. Figure 6-3 shows the EDX analysis report for control sheet (Non- anodized titanium).

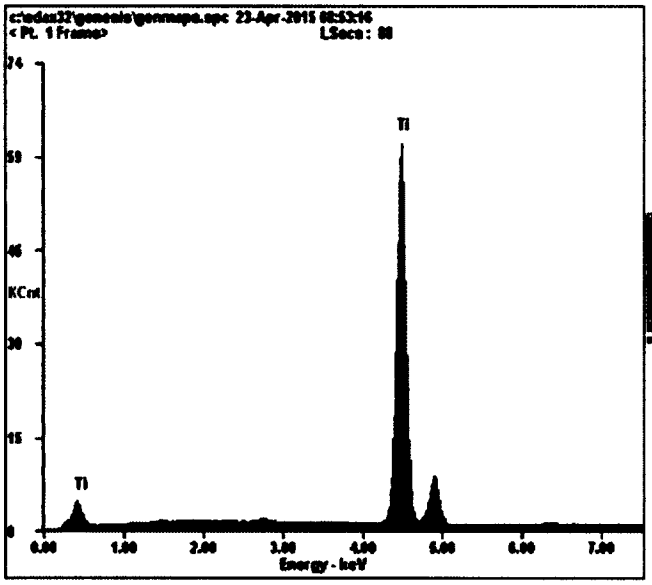

Element	Wt%	At%
TiK	100.00	100.00
Matrix	Correction	ZAF

Figure 6-3. EDX analysis of control titanium sheet in SBF for 7 days.

Figure 6-3 shows the graph and analysis report of the EDX analysis for the non-anodized titanium sheet after immersion in SBF for 7 days. Although visual inspection showed a thin powdery layer on the titanium sheet, the EDX could not detect any other element such as calcium, phosphorous, or oxygen on the surface of the sheet. The elemental analysis shows only titanium which is the component of the sheet. This analysis suggests that the deposition of hydroxyapatite on the sheet was negligible or was too low for the EDX to detect. Figure 6-3 shows the EDX analysis report for titanium anodized for 4 minutes and immersed in SBF for 7 days.

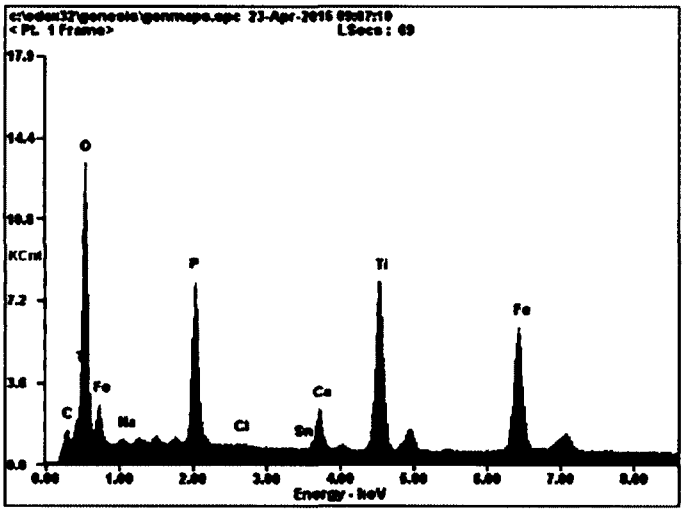

Element	Wt%	At%
CK	09.82	18.50
OK	40.31	56.99
NaK	00.47	00.47
PK	08.05	05.88
ClK	00.00	00.00
SnL	00.00	00.00
CaK	02.28	01.28
TiK	15.63	07.38
FeK	23.44	09.49
Matrix	Correction	ZAF

Figure 6-4. EDX analysis of 4 minutes anodized titanium in SBF for 7 days.

Figure 6-4 shows the EDX elemental analysis of the 4-minute anodized titanium, showing the peaks for calcium, phosphorous, oxygen, and other elements. The significant deposition of calcium, phosphorous, and oxygen suggest that hydroxyapatite crystals were formed on the surface after 7 days. Only 4-minute anodized titanium sheet was used for the EDX analysis as the cost for running one sample was high and the observations from Section 6.3.1, suggested that 4 minute anodized sheets had significantly modified

surface, compared to other anodized surfaces and the control. A visual comparison can be done in Figures 6-3 and 6-4 for other anodized titanium sheets and the control sheet (non-anodized titanium) immersed in SBF for 7 days.

Figure 6-5 shows the FE-SEM images for the surface morphology and hydroxyapatite crystal depositions on non-anodized titanium (control) and 4-minute anodized titanium.

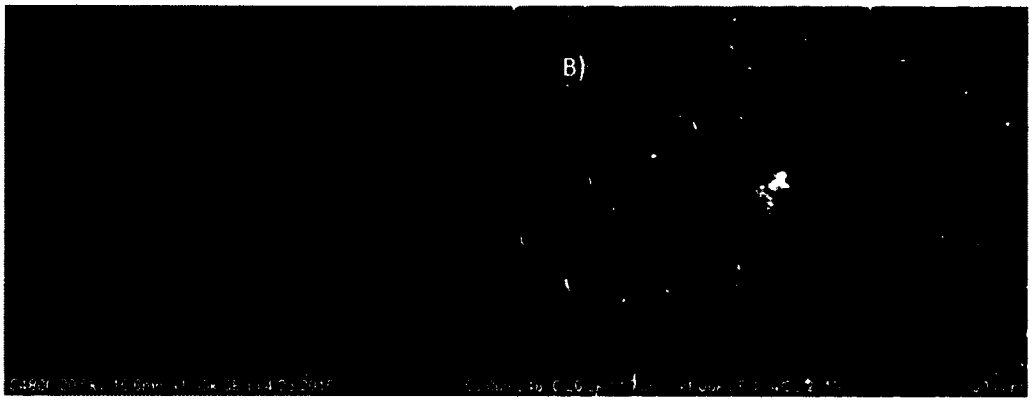

Figure 6-5. FE-SEM images of A) non-anodized and B) 4 minute anodized titanium after 7 days in SBF with the marked area showing hydroxyapatite crystal at 50 μm.

Figure 6-5 shows the smooth surface of non-anodized titanium (A) with small deposits of hydroxyapatite crystals shown by arrows. The surface of 4 minute anodized titanium shows a rough and porous surface with a big chunk of hydroxyapatite crystal marked by the circle. Figure 6-6 shows FE-SEM images of the 1-minuut through 4-minute anodized titanium immersed in SBF for 7 days at higher magnification.

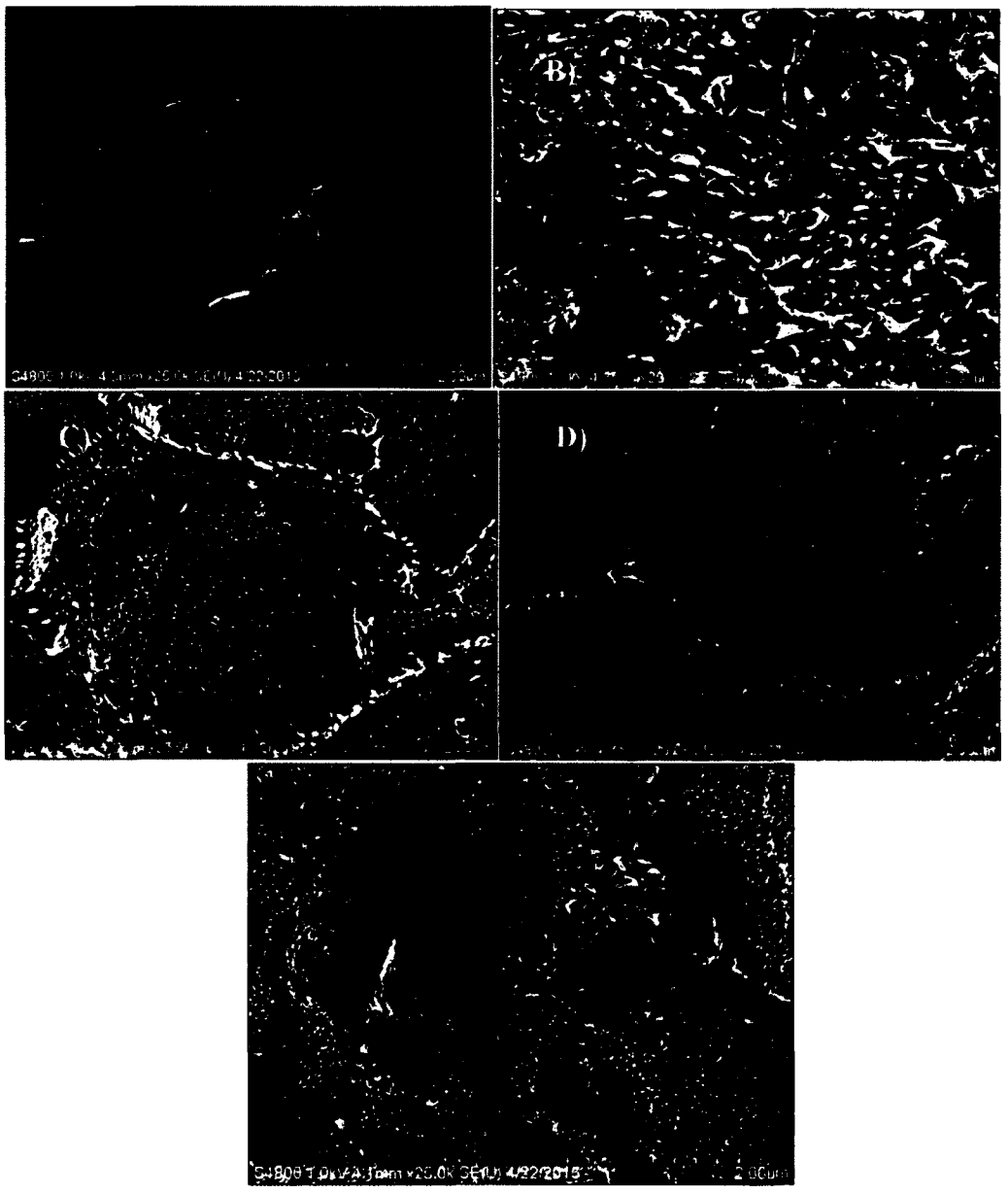

Figure 6-6. FE-SEM images showing the different surfaces of titanium and the hydroxyapatite crystals after immersing in SBF for 7 days at 2 μm A) Control- Non-anodized titanium B) 1 minute anodized titanium C) 2 minutes anodized titanium D) 3 minutes anodized titanium E) 4 minutes anodized titanium.

Figure 6-6 (A-E) shows the surfaces of the anodized and non-anodized titanium immersed in SBF after 7 days. All the anodized titanium sheets show deposition of white powdery spikes which are calcium phosphate or hydroxyapatite crystals (B-E). Non-

anodized control (A) shows a thin layer of white powdery mass on its surface but it is not as prominent as the crystals seen on the surfaces on the anodized titanium sheets (B-E).

The 1-minute anodized sheet (B) shows larger spikes or hydroxyapatite crystals and the 2, 3, and 4 minute anodized sheets (C-E) show numerous small crystals on their surfaces. The visual comparison suggests that anodization carried for different durations modify the surfaces by producing different degrees of roughness and pores. This renders different surface properties to the titanium sheets leading to the formation of hydroxyapatite crystal deposits that are of different sizes and shapes. These crystals may be deposited in varying densities as seen in 1-minute anodized titanium sheet (B) and in 4-minute anodized titanium sheet (E). The increased deposition of calcium phosphate (hydroxyapatite) on the surfaces of the anodized titanium suggests that anodization might improve the osteogenic and osteointegrative properties of titanium making it a better implant material.

6.3.2 Bacterial Inhibition Study on the GS-HNT Enhanced Hydrogel Constructs

Bacterial inhibition study was done with the GS-HNT enhanced hydrogel constructs to investigate if the anti-infective properties of GS are retained after loading in the HNTs and encapsulation within the hydrogels. This study would also investigate the anti-infective capabilities of GS-HNT enhanced hydrogels. Figure 6-7 shows the image of negative control, LB agar plate with no bacterial colonies and no anti-infective agent GS on it after 24 hours. Sterile conditions were maintained throughout the duration of the study and plate was incubated at 37 °C.

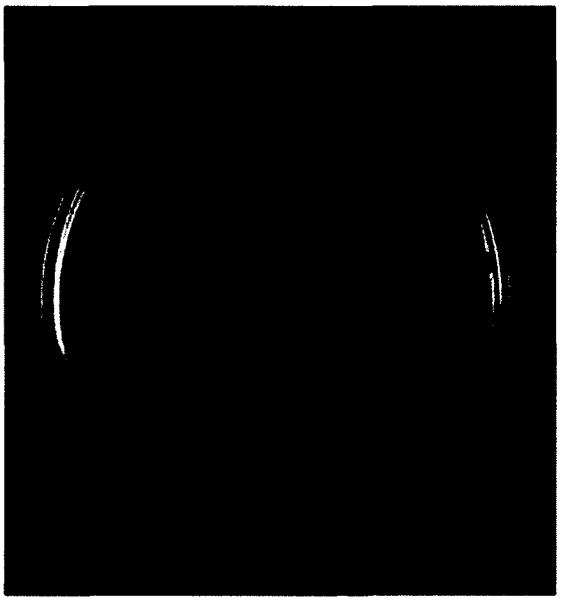

Figure 6-7. Negative control plate with no bacteria and/ or anti-infective agent GS.

Figure 6-8 shows the image of positive LB agar plate with bacterial colonies or lawn and without the anti-infective GS after 24 hours of inoculation.

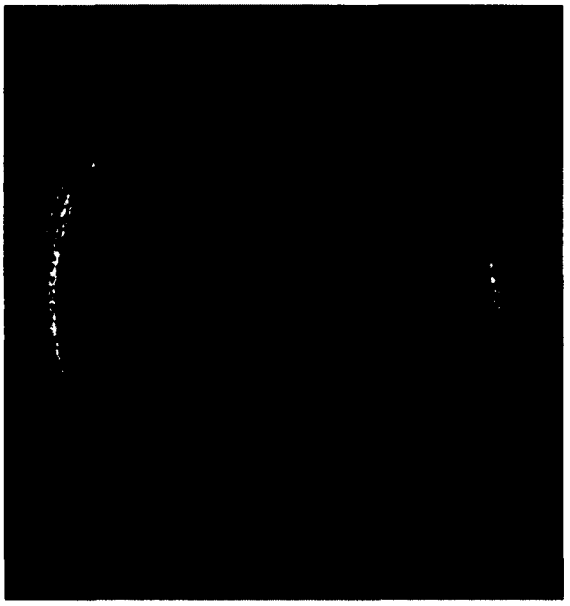

Figure 6-8. Positive control plate with bacterial lawn and no anti-infective agent GS.

Sterile conditions were maintained for the duration of the study and the plate after inoculation was incubated at 37 °C. The bacterial lawn is continuous without any breaks

or irregular empty patches. This continuity suggests that the bacteria used in the study were healthy and could readily form colonies on the nutrient plates after inoculation. Figure 6-9 (A-D) shows the images of the plates for bacterial inhibition study for anti-infective hydrogel constructs.

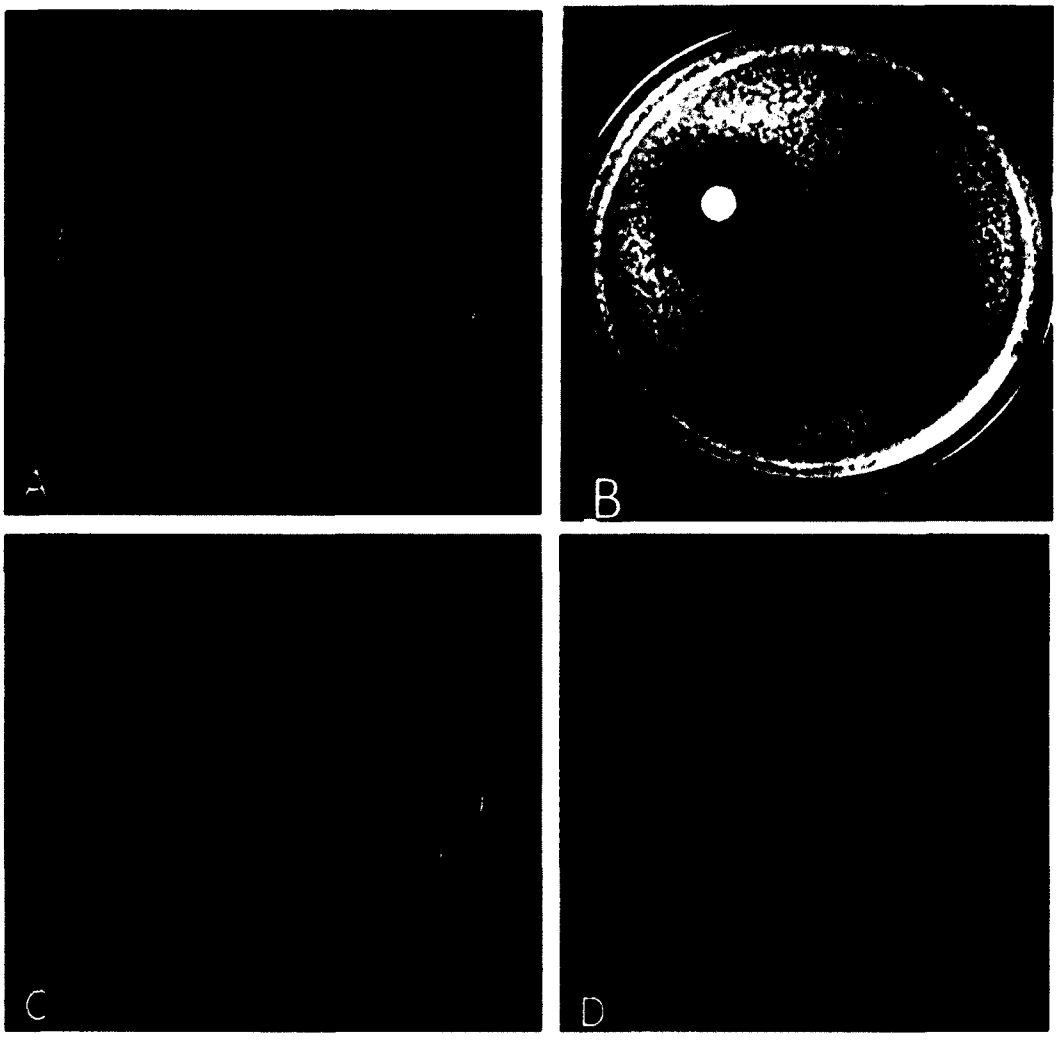

Figure 6-9. Bacterial growth inhibition studies (A) Alginate+ HNTs+ CPC+ chitosan, alginate+ HNTs+ CPC, alginate-only, and alginate+ HNTs on LB agar plate. (B) Gentamicin control disk (60 mg gentamicin) shows a large zone of inhibition. (b) *E. coli* growing as a continuous lawn.(C) Mueller-Hinton plate with hydrogels with gentamicin sulfate showing zones of inhibition (top) alginate+ HNTs+ CPC+ chitosan+ gentamicin, (bottom) alginate+ HNTs+ CPC+ gentamicin, (D) alginate+ HNTs+ gentamicin, (n=6).

Figure 6-9 (A) shows the different compositions of the alginate hydrogels without anti-infective GS in the individual quadrants on a lawn of bacteria after 24 hours of inoculation. The hydrogels without GS do not form zones of inhibition on the bacterial lawn, as they do not possess anti-infective properties themselves. Figure 6-9 (B) shows GS standard disk (60 mg gentamicin) in first half area of the plate serving as positive control. The disk produces a distinct zone of inhibition on the bacterial lawn which is about 2 cm in diameter (measured form the center of the disk) after 24 hours of inoculation. The other half area of the plate shows a continuous lawn of bacteria growing without any irregular empty patches after 24 hours of inoculation that served as the negative control. Images in Figure 6-9 (C and D) show the hydrogels with gentamicin sulfate after 24 hours of inoculation. The images show zones of inhibition (top) alginate+ HNTs+ CPC+ chitosan+ GS, (bottom) alginate+ HNTs+ CPC+ GS in image C, and alginate+ HNTs+ GS in image D. The zones of inhibition in both the images are about 2 cm in diameter suggesting that the GS released from the HNTs in the hydrogels inhibited the growth of the bacteria on the LB agar plate and have diameter comparable to the GS standard disk in the positive control. The results from the images of the bacterial inhibition study suggest that GS can inhibit the growth of the bacteria and retains its anti-infective properties after it is loaded into HNTs and encapsulatied into hydrogels.

To further quantify the bacterial colony-forming units (CFUs) on the control and experimental plates, we used an image analysis software called OpenCFU© to count the CFUs. The results are summarized in Table 3.

Table 3. Results of image analysis of the bacterial plates

Plate	No. of CFUs	
Negative control	NA	
Positive control	765	
	Outside zone of inhibition	Near the beads
Alginate+ HNTs+ GS	422	16
Alginate+ CPC+/-Chitosan+ HNTs+ GS	998	11

The numbers of CFUs near the beads containing GS loaded HNTs were small compared to the number of CFUs growing on the agar plate away from the zone of inhibition as can be seen in the summarized results in Table 3. The number was not zero as the regions of interest selected also included the peripheries of the zone of inhibition where the boundaries are not sharply defined.

6.3.3 Release Profile Study of GS from HNTs and Hydrogels Enhanced with HNTs

The release profile study of GS-loaded HNTs and of hydrogel composites enhanced with GS-loaded HNTs was performed to estimate the amount of GS released from HNTs and hydrogels.

The release study for GS from HNTs was done for a period of 7 days. Figure 6-10 shows calibration curve for GS used to calculate the concentrations for GS released from HNTs for 7 days.

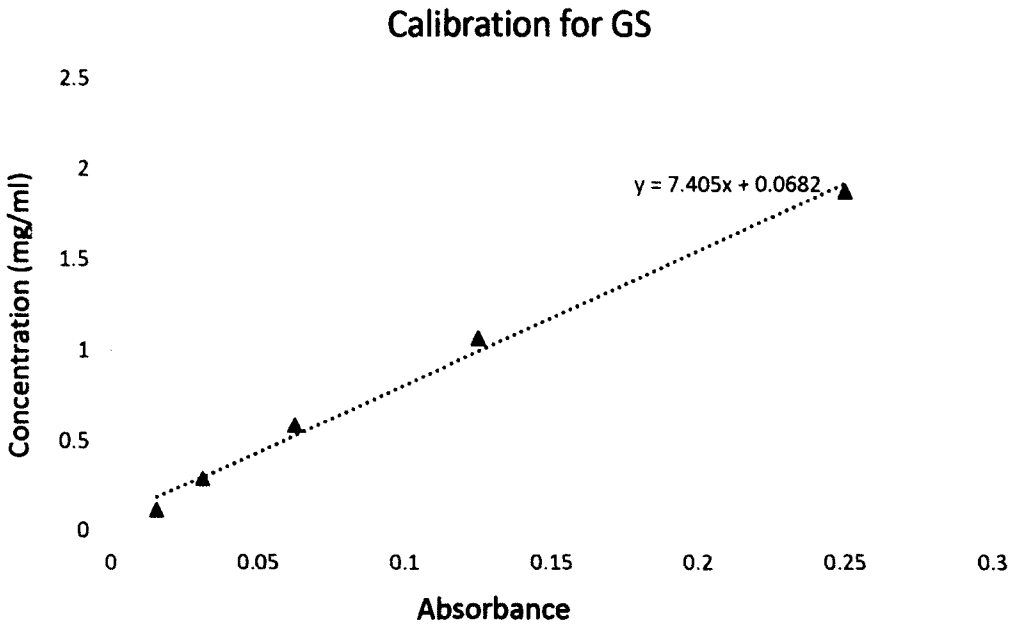

Figure 6-10. Calibration curve for GS used to calculate GS concentrations released from HNTs for 7 days (n=6).

Figure 6-10 shows a calibration graph of absorbance versus concentration (mg/ml). This graph gives the corresponding values for GS released from HNTs at a particular absorbance. Figure 6-11 shows the cumulative release of GS from HNTs for 7 days.

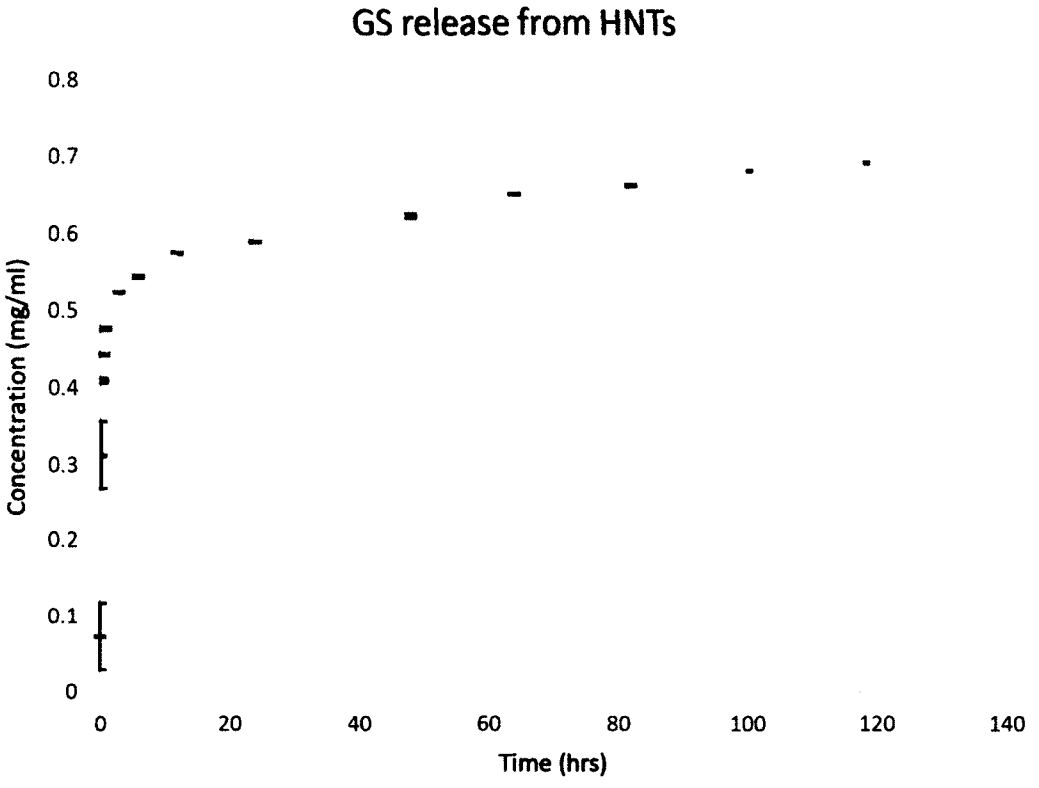

Figure 6-11. The cumulative release of GS from HNTs for 7 days.

Figure 6-11 shows the cumulative release of GS from HNTs for 7 days. The release for GS from HNTs was extended and sustained for a period of 72 hours and the points after 72 hours reach a plateau, as can be seen from the graph. The release study was repeated three times and each time the samples were collected in duplicates (n=6). The release profile of GS from the HNTs for a period of 7 days shows a release characterized by an initial high burst of release within the initial 24 hours and a later little additional release. The initial high burst of release within the initial 24 hours can be attributed to the drug being coated on the outer surface as well as the drug loaded in the lumen coming out as a high burst. The release of GS differs from that of the BMP 2 molecule discussed in the previous chapters because of the size difference of the molecules. BMP 2 is a protein and its molecular size is larger than Gentamicin sulfate

which is an aminoglycoside. As most of the drug comes off from the lumen within the period of initial 24 hours there is little drug coming out in the later stage of the study. The cumulative release profiles of GS from HNTs in hydrogel composites were obtained for a period of 7 days. Figure 6-12 shows the cumulative release profiles of GS from HNTs in hydrogel composites for 7 days. The error bars represent the standard deviation calculated by the standard deviation of the data point and the average of the triplicate samples (detailed process of calculation of the standard deviation described in Appendix B). [59]

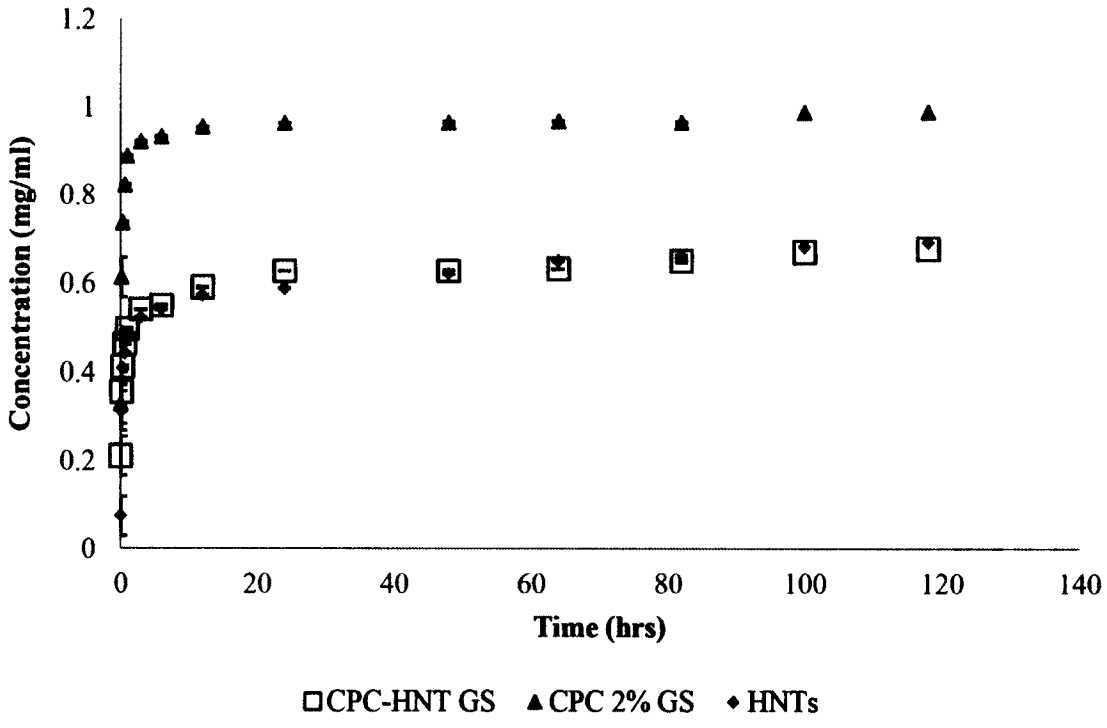

Figure 6-12. Cumulative graph of gentamicin sulfate release from hydrogels showing time (hours) vs. concentration (mg/ ml).

Figure 6-12 shows a cumulative release profile for GS from HNTs in hydrogel composites for 7 days. The graph shows time (hours) versus concentration (mg/l) of the GS released from the HNT enhanced hydrogel composite- alginate+CPC+HNTs+ GS

(green squares) and compared against alginate+CPC+ 2% v/v GS (blue triangles) and HNTs only (red rhombus). The calibration curve shown in Figure 6-10 was used to calculate the concentrations of GS released. The error bars represent the standard deviation calculated by the standard deviation of the data point and the average of the triplicate samples (detailed process of calculation of the standard deviation described in Appendix B). [59]

The comparative study of the cumulative release of GS from different constructs shows that all the release profiles are defined by a characteristic initial high burst of drug release in the initial 24 hours and a later small additional release. The initial high burst of release within the initial 24 hours can be attributed to the drug being coated on the outer surface as well as the drug loaded in the lumen coming out as a high burst. As most of the drug comes off from the lumen within the period of initial 24 hours there is little drug coming out in the later stage of the study.

A comparison of the initial high burst values of different constructs (CPC 2% GS v/s HNTs and CPC-HNT GS) reveals that loading GS in HNTs might reduce the amount of GS being released in the initial 24 hours, extending the release to 48 hours. This delayed release might be caused by the drug molecules being trapped in the inner lumen and the concentric layers of aluminosilicate and released in a slightly delayed manner.

For implants to be successful, formation of bacterial films on the surface of the implants has to be prevented. Usually, infection sets in within the first 24 hours. [38, 39, 40] For the prevention of infection, first 24 hours after implantation are crucial and an anti-infective needs to be supplied in a sustained manner over an extended period beyond 24 hours. The observations from Figures 6-7, 6-8, 6-9, 6-11, and 6-12 suggest that the

hydrogel composites enhanced with GS loaded HNTs would be a better anti-infective delivery system as the anti-infective GS would be released for an extended period of 48 hours which would prevent the bacterial growth on the implants.

CHAPTER 7

CONCLUSIONS AND FUTURE WORK

Chapters 4, 5, and 6, discussed three projects with interrelated concepts and novel application of hydrogels, nanoparticles and anodized titanium. The current chapter synthesizes the recorded observations and integrates them with concepts from Chapters 4, 5, and 6. A plan for the future direction of this work is also provided.

Chapter 4 discussed in detail the testing of the hypothesis that the addition of HNTs and growth factors to alginate hydrogels will improve the hydrogels' biological performance and material properties. The observations from the results suggest that the cells performed better in the alginate hydrogels with growth factor-loaded halloysites. Among the three growth factors used (BMP 2, 4, and 6), histochemical staining and analysis revealed that alginate hydrogels with BMP 6 and BMP 2+ 0.4M ascorbate medium performed better than the rest of the groups. BMP 2 is FDA approved for use in orthopedic and orthodontic applications. [13] Hence, it can be used in combination with 0.4 M ascorbate medium to yield best results with osteogenic response. The release of BMP 2 from halloysite was sustained and extended suggesting that the growth factor can be made available to the regenerating tissue throughout a seven day period, and at low amounts, which is crucial for cellular differentiation and maturation.

The release of BMP 4 and 6 could not be studied, as the customized kits for ELISA are not available commercially. In future studies, the release profiles of BMP 4

and 6 can be studied and compared to the release profile of BMP 2. These studies will reveal the pattern of release of these growth factors from halloysite and hydrogels. The behavior of the cells and the formation of hydroxyapatite crystals after mineralization can be studied by performing micro-CT (computational tomography) analysis on the hydrogels with osteoblasts encapsulated in them. This analysis would provide visualization of the three dimensional constructs, orientation of the cells and mineral deposits after cellular differentiation.

Chapter 5 discussed in detail the concept of "nanoseeds" or Nanoenhanced alginate hydrogel composites as potential chemoattractant materials. The primary hypothesis was to test if these constructs could attract the Osteoprogenitor cells towards them through molecular signaling by release of BMP 2. The histochemical analyses showed that the cells in the wells with growth factor-loaded HNT enhanced alginate hydrogel composites migrated towards the source of molecular signal, the hydrogel bead. It can be concluded from the observations that the "nanoseeds" can act as chemoattractants and can be used to accelerate the process of bone regeneration when used in combination with metal implant materials. The material testing also revealed that the material properties are altered by the addition of the composite materials (HNTs, CPC, and chitosan lactate).

NucBlue fluorescent staining results were not included as the stain faded after Day 3 of the migration study. The images for the NucBlue staining method were inconclusive but the same wells when stained with histochemical stains such as Alcian Blue and Von Kossa, showed that the cells had migrated from their site of seeding towards the molecular signal (the hydrogel composite beads with BMP 2). In future

studies, the modified behavior of the migrating cells can be studied at the molecular and genetic level by performing PCR and western blots to visualize the levels of osteogenic markers and gene segments expressed. To understand the material properties of the composite hydrogels and the interaction between the materials, Nanoindentation studies can be performed on the hydrogel constructs. Nanoindentation studies would quantify the surface roughness and other material features of the hydrogel constructs. The pilot study with the preosteoblasts being seeded directly on the composite hydrogel films can be extended into a full study.

Chapter 6 described the surface modification of the titanium by anodization and enhancing the alginate hydrogel composites with HNTs and GS (anti-infective agent). The primary hypothesis of the project was to improve the osteogenic properties of titanium making it more osteointegrative and prevent the growth of bacteria on its surface. The observations from the results showed that the osteogenic properties were improved upon anodization with 4 minutes of anodization producing the most modified surface and having the highest deposition of calcium phosphate (hydroxyapatite crystals). The bacterial inhibition studies showed that the alginate hydrogel composites with GS could prevent the growth of bacteria. It can be concluded from the observations that anodization of titanium and coating the surface of the metal with anti-infective hydrogels would prevent the bacterial growth and improve its osteogenic properties.

Mammalian cellular studies with co-culture of bacteria can be performed in the future, to assess the performance of anodized titanium coated with anti-infective hydrogel coatings in simulated internal environment. In the future, the *in vitro* studies can be extended to *in vivo* studies with animal models. Anodized titanium can be tested for

cellular response by seeding osteoblasts directly on the metal surface for an extended period of 28 days or more. Bacterial inhibition studies can also be extended beyond 24 hours if the bacteria can be cultured for an extended period. The bacterial studies can be done with other bacterial species like *Staphylococcus.*

All the above projects were tested *in vitro* due to time and resource constraints. Future studies can extend these projects to *in vivo* testing on animal models. The scope of all the projects in this dissertation was limited to the osteogenic aspect of bone regeneration. The skeletal regeneration has other aspects like angiogenesis and bone remodeling. These aspects can be studied in the future by selecting angiogenic growth factors and conducting the studies on co-cultures containing skeletal cell lines (e.g. myoblasts, osteoblasts, mesenchymal stem cells, and chondrocytes).

An investigative study on the effect of growth factors, nanoparticles and hydrogel composites on cell behavior with a comparison between murine bone cell lines and human bone cell lines can help to predict the behavior of these constructs in humans as implant materials. As with any research, the experimental design can be improved. The experiments can be extended to 28 days, more advanced imaging techniques, like micro-CT, or mechanical testing, like Nanoindentation, can be used to quantify the results that are discussed in this dissertation. The three projects indicate that the constructs hold promise as potential implant materials that can overcome some limitations of the current commercially available implant materials.

REFERENCES

[1] "Surface Area and Pore Size Analyzer." [Online]. Available: http://www.ifm.latech.edu/resources/equipment/nova.php.

[2] "Regenerative Medicine," *NIH Fact Sheets*. [Online]. Available: http://report.nih.gov/nihfactsheets/viewfactsheet.aspx?csid=62.

[3] "Phases of fracture healing." [Online]. Available: https://o.quizlet.com/KTNqsUFrrdpPmtsMI8N0Jg_m.png.

[4] "National Ambulatory Medical Care Survey: 2012 State and National Summary Tables." [Online]. Available: http://www.cdc.gov/nchs/data/ahcd/namcs_summary/2012_namcs_web_tables.pdf.

[5] "National Ambulatory Medical Care Survey," *National Ambulatory Medical Care Survey*. [Online]. Available: http://www.schwebel.com/userfiles/files/Fractures(1024).pdf.

[6] "NANODROP 2000." [Online]. Available: http://www.nanodrop.com/Productnd2000overview.aspx.

[7] "Halloysite Product Information." [Online]. Available: http://www.sigmaaldrich.com/catalog/product/aldrich/685445?lang=en&region=US.

[8] "Gentamicin Sulfate Data Sheet," *Gentamicin Sulfate, USP - PRODUCT DATA SHEET*. [Online]. Available: http://www.toku-e.com/Upload/Products/PDS/20120604005203.pdf.

[9] "Fractures," *MedLine*. [Online]. Available: https://www.nlm.nih.gov/medlineplus/fractures.html.

[10] "Fracture with implants image." [Online]. Available: http://www.dandalaw.com/wp-content/uploads/2015/06/broken_leg_collection_of_injury.png.

[11] "Fracture Image." [Online]. Available: http://orthoanswer.org/hip/femur-fractures/causes.html.

[12] "FE-SEM S4800 HITACHI." [Online]. Available: http://www.latech.edu/ifm/resources/equipment/hitachi_s-4800.php.

[13] "FDA- Sodium alginate." [Online]. Available: https://www.accessdata.fda.gov/scripts/cdrh/cfdocs/cfcfr/CFRSearch.cfm?fr=184.1724.

[14] "Broken Bone." [Online]. Available: http://www.medicinenet.com/broken_bone_types_of_bone_fractures/page8.htm#what_is_the_treatment_for_a_broken_bone.

[15] "Bone-Graft Substitutes: Facts, Fiction, and Applications." [Online]. Available: http://www.aaos.org/research/committee/biologic/BI_SE_2003-1.pdf.

[16] "Bone Morphology Description," *Introduction to Bone Biology: All About Our Bones*. [Online]. Available: http://www.iofbonehealth.org/introduction-bone-biology-all-about-our-bones.

[17] "Bone Health and Osteoporosis A Report of the Surgeon General," Bone Health and Osteoporosis A Report of the Surgeon General. [Online]. Available: http://www.ncbi.nlm.nih.gov/books/NBK45513/pdf/Bookshelf_NBK45513.pdf.

[18] "Bone Anatomy Image." [Online]. Available: http://www.apsubiology.org/anatomy/2010/2010_Exam_Reviews/Exam_2_Review/06-03_LongBone.JPG.

[19] "An Introduction to Biodegradable Polymers as Implant Materials." [Online]. Available: http://www.osteosynthesis.stryker.com/medias/pdf/introductiontopolymers_whitepaper.pdf.

[20] Z. Song, L.Borgwadt, and N. Hoiby, "Prosthesis Infections after Orthopedic Joint Replacement: The Possible Role of Bacterial Biofilms," *Orthopedic Review (Pavia)*, vol. 5, no. 2, 2013.

[21] William Arnould-Taylor, "A Textbook of Anatomy and physiology," in *A Textbook of Anatomy and physiology by William Arnould-Taylor*, 3rd ed., Nelson Thornes, pp. 11–24.

[22] W. Wei, "Halloysite nanotube composites for sustained release of antimocrobial agents (antiseptics and antibiotics)," Louisiana Tech University, Ruston, 2013.

[23] Victor P. Eroschenko, "Di Fiore's Atlas of histology with functional relationships," 10th ed., Lippincott Williams And Wilkis, 2008.

[24] V. Galkowski, B. Petrisor, B. Drew, and D. Dick, "Bone Stimulation for Fracture Healing: What's All the Fuss?," vol. 43, no. 2, pp. 117–120.

[25] U. Jammalamadaka and K. Tappa, "Osteoinductive calcium phosphate clay nanoparticle bone cements (CPCs) with enhanced mechanical properties.," in *Conf Proc IEEE Eng Med Biol Soc*, Chicago, IL, 2014, pp. 3917–3920.

[26] T. Sakimura, S. Kajiyama, and S. Adachi, "Biofilm-Forming Staphylococcus Epidermidis Expressing Vancomycin Resistance Early after Adhesion to a Metal Surface," *Biomed Research International*, vol. 2015, p. 8, 2015.

[27] T. Kalteis, C. Luring, and G. Gugler, "Acute tissue toxicity of PMMA bone cements," *Zeitschrift fur Orthopadie und Ihre Grenzgebiete*, vol. 142, no. 6, pp. 666–672, 2004.

[28] T. Albrektsson and M. Jacobson, "Bone-metal interface in osseointegration," *Journal of Prosthetic Dentistry*, vol. 57, no. 5, pp. 597–607, 1987.

[29] S. Karnik, "Bioactive Hydrogels for TMJ Repair," Louisiana Tech University, Ruston, 2012.

[30] S. I. Abd Razak, N. F. Ahmad Sharif, and W. A. W. Abdul Rahman, "Biodegradable Polymers and their Bone Applications: A Review," *International Journal of Basic & Applied Sciences*, vol. 12, no. 1, pp. 31–49, 2012.

[31] S. Brunauer, P. H. Emmett, and E. Turner, "Adsorption of Gases in Multimolecular Layers," *Journal of the American Chemical Society*, vol. 60, no. 2, pp. 309–319, 1938.

[32] R. Langer and J. P. Vacanti, "Tissue Engineering," *Science*, vol. 260, no. 5110, pp. 920–926, 1993.

[33] R. E. Marx and M. J. Morales, "Morbidity from bone harvest in major jaw reconstruction: a randomized trial comparing the lateral anterior and posterior approaches to the ilium," *J. of Oral Maxillofacial Surgery*, vol. 46, no. 3, pp. 196–203, 1988.

[34] Patrick W. Tank and Thomas R. Gest, "Atlas of Anatomy," in *Atlas of Anatomy*, 1st ed., Lippincott Williams And Wilkis, 2015.

[35] N. Hallab, K. Merritt, and J. J. Jacobs, "Metal Sensitivity in Patients with Orthopaedic Implants," *The Journal of Bone and Joint Surgery*, vol. 83, no. 3, p. 428, 2001.

[36] Michael G. Newman, Henry H. Takei, and Fermin A. Carranza, "Carranza's Clinical Periodontology, Volume 1," in *Carranza's Clinical Periodontology, Volume 1*, 9th ed., vol. 1, Saunders Company, 2002, pp. 907–908.

[37] M. Ribeiro, F. J. Monteiro, and M. P. Ferraz, "Infection of Orthopedic Implants with Emphasis on Bacterial Adhesion Process and Techniques Used in Studying Bacterial-Material Interactions," *Biomatter*, vol. 2, no. 4, pp. 176–194, 2012.

[38] M. J. Weinstein, G. M. Lauedemann, and E. M. Oden, "Gentamicin, A New Antibiotic Complex from Micromonospora," *Journal of Medical Chemistry*, vol. 6, pp. 463–464, 1963.

[39] L. Zhou, P. Chu, and Y. Zhang, "Antibacterial coatings on titanium implants," *Journal of Biomedical Materials Research Part B: Applied Biomaterials*, vol. 91 B, no. 1, pp. 470–480, 2009.

[40] K.S.W. Sing, "Adsorption methods for the characterization of porous materials," *Advances in Colloid and Interface Science*, vol. 76–77, pp. 3–11, 1998.

[41] K. Y. Lee and D. J. Mooney, "Hydrogels for Tissue Engineering," *Chemical Review*, vol. 101, no. 7, pp. 1869–1880, 2001.

[42] J. M. Bemmelen, "The hydrogel and the crystalline hydrate of cupric oxide," *Journal of Chemical Industry and the Colloids*, vol. 1, no. 7, pp. 213–214, 1907.

[43] J. C. Middleton and A. J. Tipton, "Synthetic biodegradable polymers as orthopedic devices," *Biomaterials*, vol. 21, no. 23, pp. 2335–2346, 2000.

[44] Inderbir Singh, "A Textbook of Anatomy with Color Atlas," in *A Textbook of Anatomy with Color Atlas*, 4th ed., Jaypee, pp. 6–10.

[45] H. Lodish, A. Berk, and S. L. Zipursky, "Collagen: The Fibrous Proteins of the Matrix," in *Molecular Cell Biology*, 4th ed., W. H. Freeman, 2000.

[46] E. Jimi and S. Hirata, "The Current and Future Therapies of Bone Regeneration to Repair Bone Defects," *International Journal of Dentistry*, vol. 2012, pp. 1–7, 2012.

[47] E. J. Applegate, "The Anatomy and Physiology Learning System," in *The Anatomy and Physiology Learning System*, Saunders Company, 1995, pp. 43–69, 109–139.

[48] E. B. Taddei, V. A. R. Henriques, and C. R. M. Silva, "Production of new titanium alloy for orthopedic implants," *Materials Science and Engineering: C*, vol. 24, no. 5, pp. 683–687, 2004.

[49] D.Campoccia, L. Montanaro, and C. R. Arciola, "The significance of infection related to orthopedic devices and issues of antibiotic resistance," *Biomaterials*, vol. 27, no. 11, pp. 2331–2339, 2006.

[50] D. Wang, K. Christenssen, and K. Chawla, "Isolation and characterization of MC3T3-E1 preosteoblast subclones with distinct in vitro and in vivo differentiation/mineralization potential," *Journal of Bone and Mineral Research*, vol. 14, no. 6, pp. 893–903, 1999.

[51] Courtney M. Townsend Jr., R. Daniel Beauchamp, B. Mark Evers, and Kenneth L. Mattox, "Sabiston textbook of surgery: the biological basis of modern surgical practice," *Sabiston textbook of surgery: the biological basis of modern surgical practice*, 19th ed., Elsevier Health Sciences, pp. 480–520, 2012.

[52] C. L. Romano, S. Scarponi, and E. Gallazzi, "Antibacterial Coating of Implants in Orthopaedics and Trauma: A Classification Proposal in an Evolving Panorama," *Journal of Orthopedic Surgery and Research*, vol. 10, no. 157, 2015.

[53] C. A. St. Pierre, M. Chan, and Y. Iwakura, "Periprosthetic Osteolysis: Characterizing the innate immune response to titanium wear-particles," *Journal of orthopaedic research : official publication of the Orthopaedic Research Society*, vol. 28, no. 11, pp. 1418–1424, 2010.

[54] B. P. Chan and K. W. Leong, "Scaffolding in Tissue Engineering: General Approaches and Tissue-Specific Considerations," *European Spine Journal*, vol. 17, no. 4, pp. 467–479, 2008.

[55] A. S. Hoffman, "Applications of thermally reversible polymers and hydrogels in therapeutics and diagnostics," *Journal of Controlled Release*, vol. 6, no. 1, pp. 297–305, 1987.

[56] A. R. Amini, C. T. Laurencin, and S. P. Nukavarapu, "Bone Tissue Engineering: Recent Advances and Challenges," *Critical reviews in biomedical engineering*, vol. 40, no. 5, pp. 363–408, 2012.

[57] A. H. Reddi, "Bone morphogenetic proteins: An unconventional approach to isolation of first mammalian morphogens," *Cytokine Growth Factor Review*, vol. 8, no. 1, pp. 11–20, 1997.

[58] A. D. Augst, H. J. Kong, and D. J. Mooney, "Alginate Hydrogels as Biomaterials," *Macromolecular Bioscience*, vol. 6, no. 8, pp. 623–633, 2006.

[59] L. Zheng, L. An, and X. Wu, "ModelingDrug-CarrierInteractionintheDrug ReleasefromNanocarriers," *Journal of Drug Delivery*, vol. 2011, p. 15, 2011.

APPENDIX A

IMAGE ANALYSIS

IMAGE ANALYSIS

For quantifying the values of the intensities of RGB colors in the histochemically stained hydrogel sections we used Image J© software. The software plotted graphs for RGB peaks and grayscale intensity values. This image analysis was used to substantiate the observations and inferences drawn in the histological staining images in Sections 4.3.1.1, 4.3.1.2, and 4.3.1.3.

The method used in this dissertation for Image J image analysis can be summarized as follows:

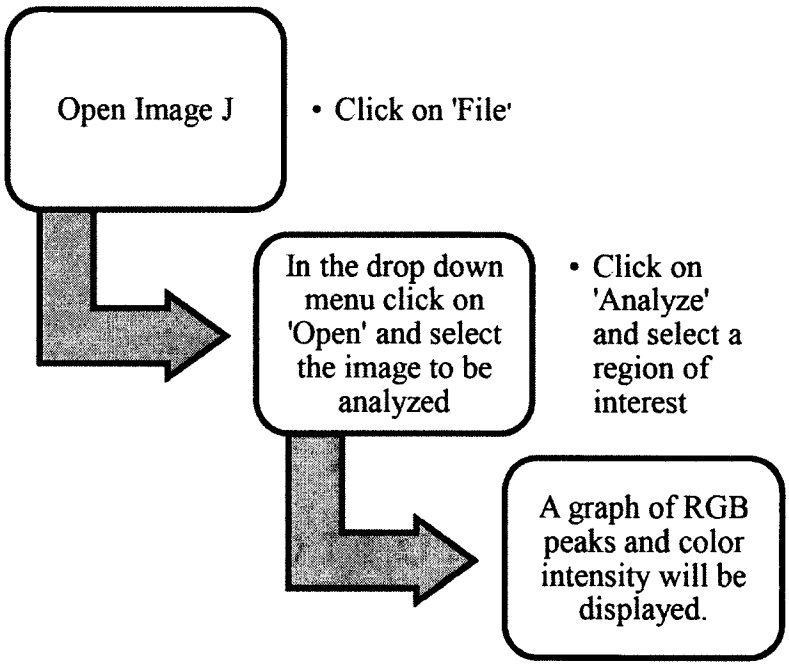

APPENDIX B

RELEASE STUDY PLOT AND ERROR BARS

RELEASE STUDY PLOT AND ERROR BARS

The process of release study and plotting the graphs can be summarized as

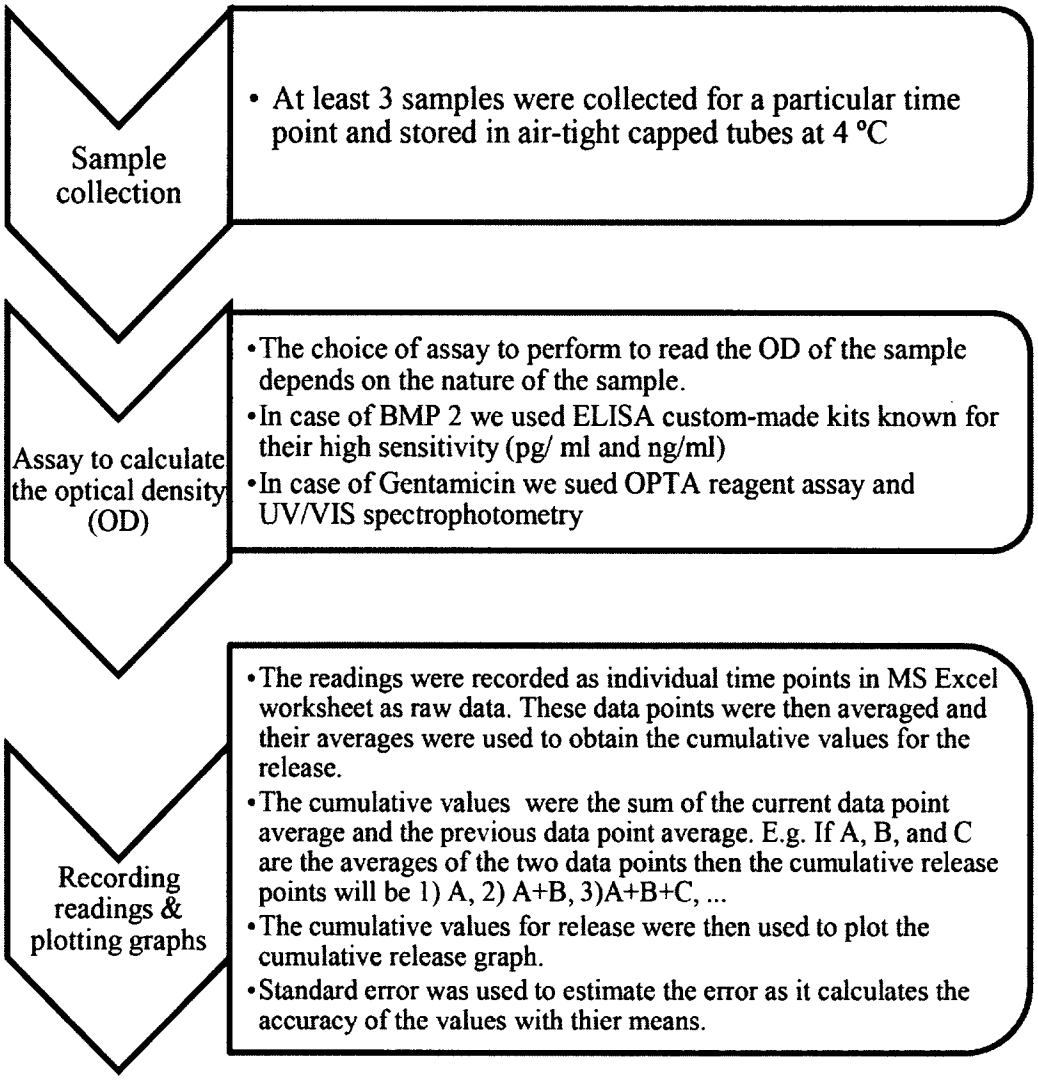

follows:

In the article by Zheng et al., 2011 in the Journal of Drug Delivery, the authors describe four types of release profiles and describe the curve as either having initial high/ low burst release or late little/ extended release. In this dissertation, we used

this model to describe the release profiles of the growth factor BMP 2 and antibiotic Gentamicin.

We chose to use standard deviation bars to represent the deviation from the average of each point. The author uses averages and standard deviation for each point to plot the error bars for the cumulative plot. The standard deviation is calculated as

$$S.D. = \sqrt{\frac{\varepsilon(x - \bar{x})^2}{N - 1}}.$$

where $S.D.$ is the standard deviation of that point, x is the data point, $\bar{x}$ is the average of the readings and N is the number of samples taken for that point.

For calculating the concentrations we plotted a calibration curve for the respective bioactive molecule by using known standards and their corresponding absorbance values. The absorbance values shown by the experimental samples were then plotted using the equations mentioned in the calibration curves to find the concentrations. The final graph was the plot of the concentrations calculated from the calibration curves and the corresponding time points. For the BMP 2 plot, the graph is not a cumulative plot but the plot of individual data points and shows a general representation of the concentrations for the particular time point.

APPENDIX C

EXPERIMENTS WITH INCONCLUSIVE

RESULTS AND FAILURES

EXPERIMENTS WITH INCONCLUSIVE RESULTS AND FAILURES

The following is the list and a brief description of the experiments that were conducted on the hydrogel constructs to investigate either their biological or material properties which had inconclusive results or failed to perform in the given conditions.

1. **NucBlue© fluorescent staining assay.**

   The NucBlue© fluorescent staining assay was performed to visualize the cells in collagen gel matrix for the Nanoseeds project. The cells were first stained with the protocol provided by the manufacturers and then seeded on the collagen gel matrices. The study was to be carried out for 7 days and with samples imaged on days 0, 3, and 7. The NucBlue© stain is a vital stain and helps in visualization of the cells without requiring sample processing and fixing. The stain faded out after Day 3 and the results were inconclusive as the migration of the cells towards the chemoattractant hydrogel beads could not be visualized.

   We had to rely on the histochemical staining (Alcian Blue and Von Kossa stains) which had better visualization of the cells along with ECM materials and minerals to study the cellular migration.

2. **Nanoindentation of the hydrogel constructs.**

   The hydrogel composite samples were sent to University of Wisconsin, Milwaukee to quantify and analyze their material properties like surface roughness, elasticity, and

pore distribution by Nanoindentation technique. It was courtesy of Dr. Lobat Tayebi who referred Dr. Steve Hardcastle as the point of contact and testing of the samples. Dr. Hardcastle encountered difficulties in performing the Nanoindentation technique on the hydrogels as the samples kept rupturing and the tip was not suitable to be used on our samples. We were advised to obtain diamond tips and the study had to be kept on hold due to the high cost of the tips and the tests.

1. **Gradient Tech© cell migration study.**

   To study the cell migration of the preosteoblast towards the loaded and unloaded HNTs, we tried using Gradient Tech© cell migration 2D construct. The study was inconclusive as it required the use of fluorescent microscope for 48 hours. The results obtained for a period of 8 hours were inconclusive and we had to settle for the histological staining of the cells seeded on the collagen gel matrices.